SWECLIM
SWEDISH REGIONAL CLIMATE MODELLING PROGRAMME

SMHI

No. 83, Nov 1998

Reports Meteorology and Climatology

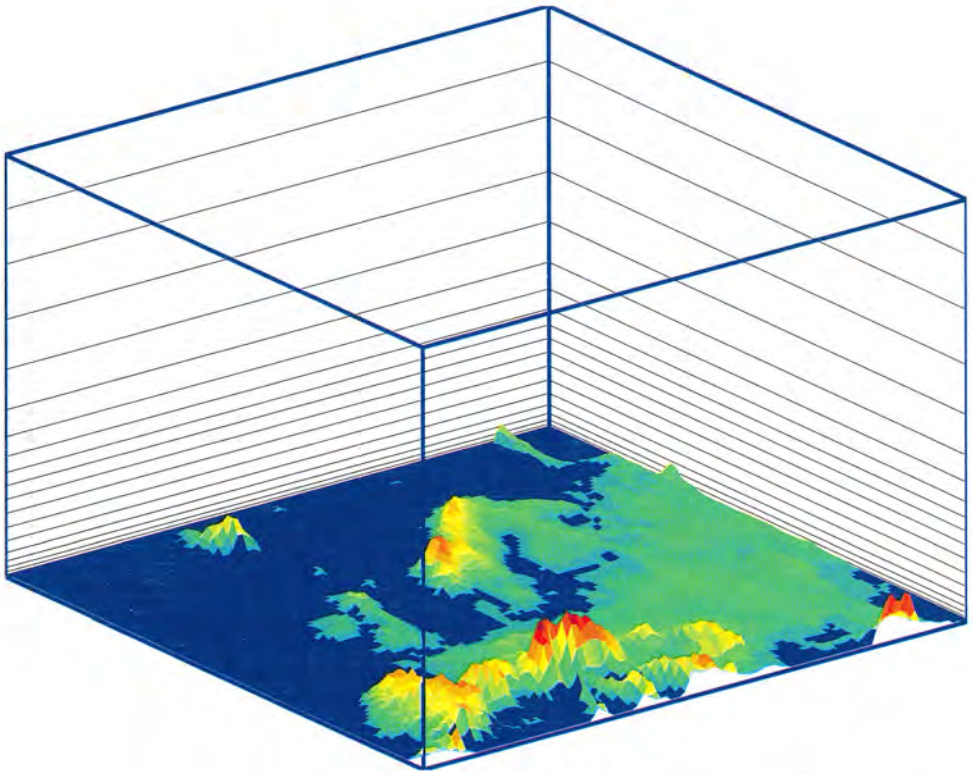

RCA – Rossby Centre regional Atmospheric climate model:
model description and results from the first multi-year simulation

Markku Rummukainen, Jouni Räisänen, Anders Ullerstig, Björn Bringfelt, Ulf Hansson, Phil Graham and Ulrika Willén
Rossby Centre, SMHI

Cover illustration: A descriptive view of the present geographical set-up of the regional model (RCA): domain, land-sea distribution, orography and resolution. The depcited vertical levels are for the model half levels and the horizontal grid is illustrated as the mesh at the top of the figure.

RMK
No. 83, Nov 1998

RCA – Rossby Centre regional Atmospheric climate model:
model description and results from the first multi-year simulation

Markku Rummukainen, Jouni Räisänen, Anders Ullerstig, Björn Bringfelt, Ulf Hansson, Phil Graham and Ulrika Willén

Report Summary / Rapportsammanfattning

Issuing Agency/Utgivare	Report number/Publikation
Swedish Meteorological and Hydrological Institute S-601 76 NORRKÖPING Sweden	RMK No. 83
	Report date/Utgivningsdatum November 1998

Author (s)/Författare

Markku Rummukainen, Jouni Räisänen, Anders Ullerstig, Björn Bringfelt, Ulf Hansson, Phil Graham and Ulrika Willén

Title (and Subtitle/Titel

RCA – Rossby Centre regional Atmospheric climate model: model description and results from the first multi-year simulation

Abstract/Sammandrag

The first version of the Rossby Centre regional climate model (RCA) has now been developed. The RCA model is based on a parallel coding of the operational weather forecast model HIRLAM. Some modifications have been done on the model formulation, especially in its surface/snow/soil scheme, in an attempt to include the regional and local scale climate-modifying forcing up to time scales of several years. The physical parameterization choices in HIRLAM and in RCA are discussed in some detail. One of the notable features in RCA is that the regional sea ice climate, as well as ice on the numerous lakes in the region, has been included in a crude, but time-efficient fashion. It appears that realistic modeling of the sea/lake ice is most important for modeling the regional climate in the Nordic region.

The RCA model has been run for a ten-year period, focusing on the Nordic region, using results from a coupled ocean-atmosphere general circulation model. In this first multi-year simulation, the regional resolution was 44 km. Several results are illustrated from this regional simulation and they are compared to the driving global model data, to analyzed observations and to Swedish station data for the 1961-90 period. The apparent model development needs are also discussed briefly.

Key words/sök-, nyckelord

Dynamical downscaling, regional climate modeling, model parameterizations

Supplementary notes/Tillägg	Number of pages/Antal sidor	Language/Språk
This work is a part of the SWECLIM programme.	76	English

ISSN and title/ISSN och titel

0347-2116 SMHI Reports Meteorology Climatology

Report available from/Rapporten kan köpas från:

SMHI
S-601 76 NORRKÖPING
Sweden

Contents

1 Introduction

This report is a description of the first version of the regional climate model at Rossby Centre. The Rossby Centre performs regional climate modeling within the new Swedish SWECLIM program, focusing on the Nordic region. Several components of the regional climate are addressed in the program: the atmosphere, the Baltic Sea, Kattegat and Skagerrak, the land surface and hydrological processes. The atmospheric regional climate model (RCA) is built on a parallellized version of a high resolution limited area model (HIRLAM) which is in operation use in weather forecasting. RCA features some modifications to the HIRLAM-code, prompted by the first experiences at Rossby Centre. The driving for the regional modeling is obtained from coupled general circulation model (GCM) integrations. The present RCA choices on the model domain, the grid and the nesting strategy are preliminary. This first version of RCA aims to lay the technical-practical foundation for future scenario-production runs. Testing with meteorological analyses as forcing (see e.g. Sass and Christensen, 1995) is also being done as a part of the model development effort. The regional ocean model and the tools for hydrological interpretation are presently under development and they will be reported on elsewhere.

RCA is used in SWECLIM to produce regional interpretation of climate change scenarios calculated with coarse global models. The targeted time horizon extends 50-100 years into the future. The basic experiment set-up is to perform two multi-year integrations with RCA. The first integration is the *control run*. It gives the baseline against which the results of the second integration, the *scenario run*, are compared. The control run should be thought of as a state of the present-day climate or, more generally, a state of the climate before the change in climate forcing to be studied occurs. The scenario run incorporates this additional climate forcing, for example accumulation of greenhouse gases in the atmosphere. The *climate change* scenario is obtained as the difference between the scenario run and the control run. This difference can then be added to (present-day) climate statistics in order to project the model results into a practical form for end-users' applications.

It is not evident that the model designed for short-range (weather) prediction would be successful also in extended (climate) calculations. These two modeling endeavors target different scales and combine a different driving data to the regional model. Some reasons why problems might arise in the climate calculations are:

- the length of the simulations increases from few days up to 1-2 decades
- the spatial scale of the lateral forcing data is coarsened from the order of 100 km and 31 vertical layers (e.g. ECMWF T213L31) to a typical GCM resolution (around 3° in the horizontal and 19 layers in the vertical or in spectral resolution: T42L19)
- the relation between the physical parameterization schemes in the driving model and in the regional model are different (HIRLAM is driven with ECMWF data, and RCA with GCM data. In addition, HIRLAM builds on an earlier version of the model at ECMWF, so their parameterizations have been similar for a long time).

There are different opinions whether it really is detrimental to have different physical parameterizations in a regional model and in the global model used to drive the regional

one. In some regional modeling work (e.g. Jones et al., 1995; Christensen et al., 1996), it is thought that such a combination is doubtful. In other works (e.g. Giorgi et al., 1993a) the regional model parameterizations have been successfully developed more or less independently of those in the driving model(s).

Why is it then that RCA builds on HIRLAM that is designed for short time scales and has quite different physics from those in climate models? Firstly, the physical parameterizations in HIRLAM have been tuned for computational efficiency. This implies that the performing of the regional integrations can become more efficient than what could be achieved with a regionalized version of a GCM. Secondly, interaction with the HIRLAM project adds to the research and development potential in SWECLIM.

The organization of the discussion in this report is as follows: the framework for RCA, the parallel form of the HIRLAM model is highlighted in Section 2. Some characteristics of the (first) driving GCM for RCA are listed in Section 3. The use of other GCMs for driving RCA will be considered in future work. The RCA-model is discussed in Section 4. The discussion is detailed only on the areas where changes to the HIRLAM seem to be needed, with respect to using it in modeling the regional climate. Results from the first long RCA simulation (the 10-year control run) are presented in Section 5. Finally, the main topics on the further development of the regional modeling are outlined in Section 6.

2 Parallel version of the HIRLAM2.5 model – the framework for RCA

RCA builds on a parallel coding of the operational high resolution limited area (weather forecast) model HIRLAM, version 2.5 (Källén, 1996; see also Machenhauer, 1988 and Gustafsson, 1993. Up-to-date information on the HIRLAM project can be read from http://www.knmi.nl/hirlam/). Some features from HIRLAM version 2.7 have been adopted in addition. The parallellization has been developed by the Swedish, Spanish and Finnish Meteorological institutes and the Cray Research Inc. (Eerola et al., 1997). RCA is run on the Cray T3E at the National Supercomputer Centre (NSC) in Linköping, Sweden, using typically 12-52 processors and the Cray shared memory message-passing library (shmem). The coding allows for a safe use of the stream buffers (streams) on the T3E. Streams are used to improve the flow of information between the main memory and the secondary cache (there is a separate secondary cache on each processor). If the streams feature is switched on, they become operational when repeating cache misses start to occur. In such a case, new data are pre-fetched into the stream buffers while the earlier data are being operated on.

An important detail in the HIRLAM/RCA parallellization is the concept of "halo zones". Spatial information is required over the processor boundaries in the calculation of horizontal derivatives. The halo zones are the means of providing for this. Each processor, in addition to its main body of grid points (these points from all processors sum up into the geographical domain and they cover it without overlap), has additional points at all sides. These extra points make up the halo zones and they appear only in the calculations. The halo zones are overlapping so that the halo zone points on a particular processor are actual points on its neighbor processor. The halo zones are visualized in Figure 1. In the Eulerian scheme, the halo zones for most variables are one row/column wide. For surface pressure, the halo zones are two rows/columns wide, due to the layout of the (Arakawa C) horizontal grid staggering. Whenever there is a change in a field of the domain within a certain processor, the halo zones of its neighboring processors have to be updated as well by swapping information between the processors. In the distribution of the model domain to the processors, the total dimensions of the domain have to be taken into account for achieving numerical efficiency. If the dynamical load balancing (see below) is to be used, this is even more important.

The halo zones are used in the adiabatic part of the model. In the parameterized physics part, calculations are done for each vertical profile independently. Information does not need to be shared between different processors. In order to maintain a good performance also in vector computers, calculations over a number of profiles (a slab) are carried out in the physics part. The time taken by the physics part changes constantly, as the short-wave radiative processes are active only when the sun is up. When the sun is setting or rising in the model domain or when the polar night sets on the northern part of the model domain, the processors calculating nighttime conditions start waiting for the processors calculating daytime processes. Numerical efficiency can be increased by a dynamic redistribution of the workload on the processors. The redistribution works by timing of the physics calculation and by altering the number of vertical profiles assigned to each processor at regular intervals (every "n^{th}" time step).

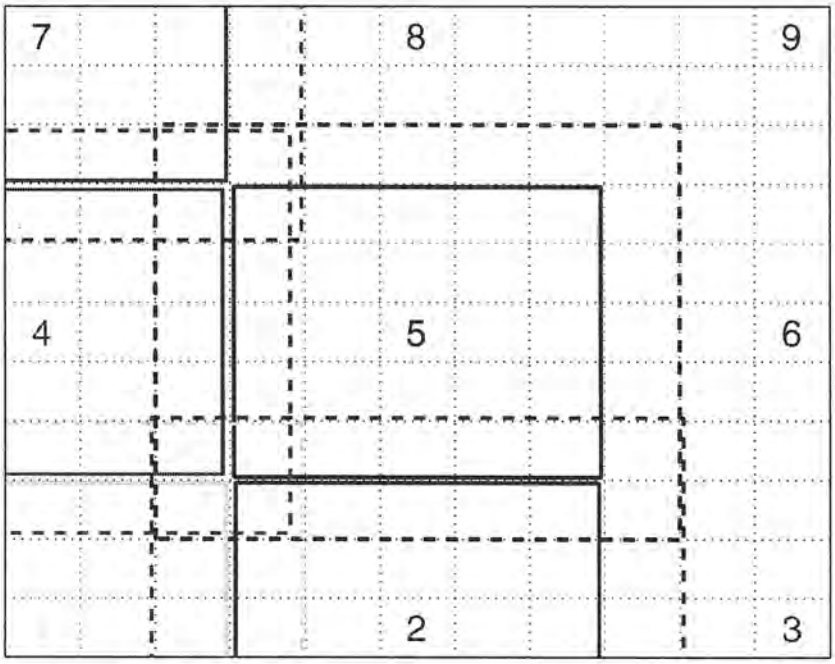

Figure 1. *Schematics of the halo zones. The solid lines border the actual domain at the processors (1-9). The dashed lines border their halo zones. The centermost processor (in black, here number 5) is drawn in full. The other processors extend outside the frame. The borders of the processors on the left and below the center one are also drawn, other processors have been numbered only. In RCA, the typical number of processors in use and the number of points each of them contains are much larger.*

The progress in the execution of the program on different processors has to be aligned with forced waiting (barriers) in the program flow before and after information is fetched from a single processor or written to a single processor (interprocessor communication). This makes the code more time-consuming as some processors will wait idle for the others to catch up. The semi-implicit solver, where global communication is required, has been implemented with data transposition technique.

The handling of input/output is a serious bottleneck in the model. At present, only one processor handles the I/O. This keeps the algorithms simple, but the performance is also degraded significantly. In RCA runs, there is massive I/O every six hours when new boundary data are read in and when the latest output are stored.

The scalability of the present RCA (82 by 114 points) degrades considerably when more than about 40 processors are used. This is partly because of the relatively small grid-point domain, but also due to the inefficient I/O. The scalability is illustrated in Figure 2, where the speed-up of the code is shown for four processor geometries. The speed-up of the non-linear dynamics part, the horizontal diffusion part, the semi-implicit part and the physics calculations are shown.

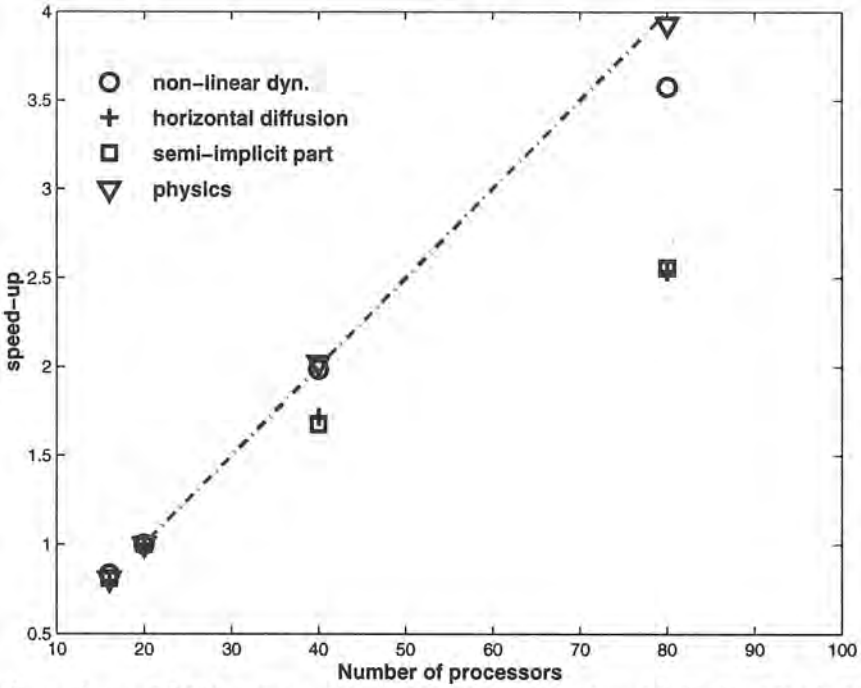

Figure 2. *Speed-up of RCA integration on Cray T3E, using 16 (2x8), 20 (2x10), 40 (2x20) or 80 (2x40) processors. The division of the processors in the x-direction and the y-direction of the domain is given in the parentheses. The model was run in its normal configuration (full I/O) for 24 hours in a September situation. The dash-dotted line gives the linear speed-up line, using the 20-processor integration as the reference. The total running times of the model with the runs (but excluding the normal mode initialization) with 16, 20, 40 and 80 processors were 216, 179, 105 and 66 seconds, respectively. The times were measured with the UNICOS timef utility.*

As shown in Figure 2, the physics part scales perfectly. Nevertheless, some components of the physics calculation are notably unbalanced, especially the surface/soil parameterization (calculations are done for land and ice points, not for the sea surface ones) and the cloud microphysics parameterization. Non-linear dynamics scales quite nicely as well, but the same is not true for the horizontal diffusion and the semi-implicit parts. The relative time-consumption of these main parts, and I/O, is given in Table 1.

Table 1. *Relative running times of the main parts of RCA.*

	16 proc.	**20 proc.**	**40 proc.**	**80 proc.**
Non-linear dynamics	9.7%	9.8%	8.8%	8.0%
Horizontal diffusion	3.7%	3.5%	3.7%	4.1%
Semi-implicit calculation	7.4%	7.2%	7.7%	8.3%
Physics	66.4%	65.0%	57.9%	48.5%
I/O	12.8%	14.5%	21.9%	31.1%

Of course, neither the non-linear dynamics nor the physics becomes more efficient with an increasing number of processors, even though their relative execution times get shorter. The single-processor I/O needs the same absolute amount of time regardless of how many processors are designated for the integration. Further calculations cannot go on before the I/O is done, so having more processors translates into more total idle time in the integration, thus resulting in the poor speed-up behavior.

3 The driving model – the Hadley Centre coupled GCM, HadCM2

The first GCM data to drive RCA have been imported from long simulations with the recent UKMO coupled ocean-atmosphere GCM HadCM2 (Johns et al., 1997). Some aspects of HadCM2 are listed in Table 2.

Table 2. *Some aspects of HadCM2. SW and LW specify short-wave and long-wave radiation. The climate sensitivity describes the equilibrated global mean surface temperature response to a doubling of CO_2.*

	HadCM2
Atmospheric resolution	2.5° x 3.75° Arakawa B. L19 in hybrid coordinates, top at 10 hPa.
Ocean resolution	Global 2.5° x 3.75°, congruent L20.
Spin-up	Coupled spinup of 510 years.
Radiation	4 bands in SW, 6 bands in LW (Slingo, 1989; Slingo and Wilderspin, 1986). Trace gases accounted for are H_2O, O_3 and CO_2.
Convection, convective clouds and precipitation	Penetrative convection scheme with explicit downdraught (Gregory and Rowntree, 1990; Gregory and Allen, 1991). Convective cloud amount as in Slingo et al. (1988).
Vertical diffusion	First-order scheme (Smith, 1990).
Layer clouds and prec.	Smith (1990).
Surface scheme(s)	4 layer soil temperatures with zero heat flux at the base. Snow, canopy and soil water included (see Johns et al., 1997 for references).
Time integration scheme	Split-explicit (Cullen and Davies, 1991). Advection with Heun (Mesinger, 1981).
Time steps	30 min atmosphere. 60 min ocean.
Explicit corrections applied during model integration	Atmospheric energy and mass are corrected for numerical loss. Any negative humidities are also fixed.
Flux adjustments	Seasonal averages of heat and fresh water are flux adjusted. The adjustments are calculated from 25 years of the coupled spin-up.
Prognostic variables	Surface pressure, horizontal wind, total water mixing ratio and liquid water potential temperature.
Climate sensitivity	2.5°C

HadCM2-simulated winds, temperatures, humidities and surface pressure are imported for RCA with a six-hour time resolution. HadCM2 sea surface temperatures and sea ice data are imported with a five-day time resolution. Layered soil temperatures and the one-layer soil moisture are imported as monthly means.

The manner in which the RCA experiments ride on HadCM2 results is illustrated in Figure 3. The RCA control run is forced with a time slice (the 2039-2049 portion of the longer global model run that extends from 1860 till 2100) from the HadCM2 control run with a pre-industrial level of the greenhouse gases in the atmosphere. The RCA scenario run is forced with the corresponding time slice from the HadCM2 scenario run (also run from 1860 to 2100) in which a gradual increase in greenhouse gases has been included. This increase has been prescribed according to measurements for the period of 1860-1990 and by applying a constant rate of increase of 1 % per year thereafter. In precise terms, the climate changes (scenario run - control run) obtained in this way tell *how the scenario climate would differ from the pre-industrial climate under the made assumptions on the changes in the atmospheric composition.*

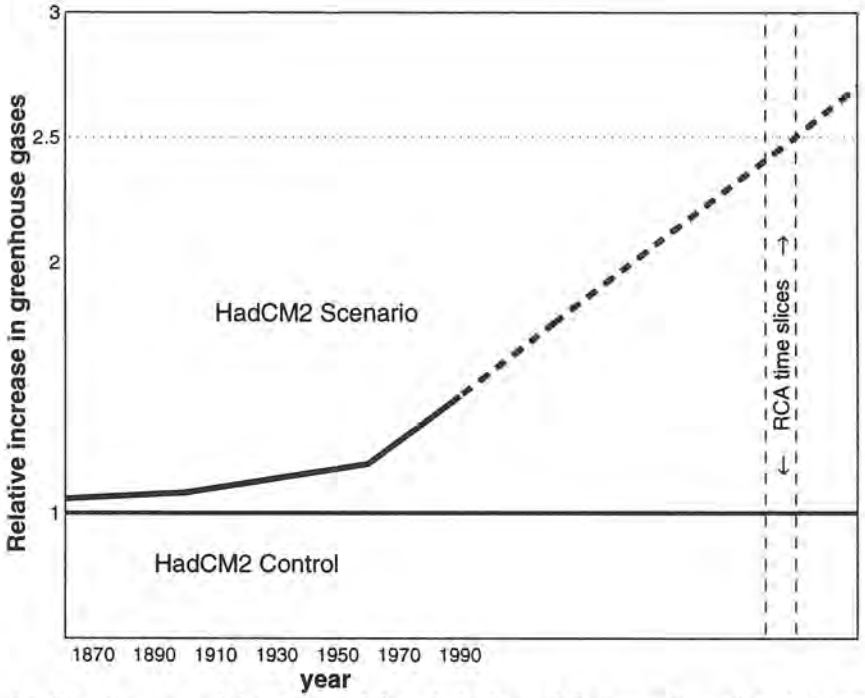

Figure 3. *An illustration of the idea of the global model time slices for driving the regional model. Note that in the scenario time slice, the impact of the accumulating gradual increase in greenhouse gases is being felt.*

If one wants to interpret the differences between the scenario run and the control run as climate changes from the present to some period in the future, this future period should be placed somewhere around the year 2100. This has two reasons:

1) The control run simulates nominally preindustrial rather than present climate. Between the pre-industrial time and the present, some climate changes have already occurred. In particular, the global mean temperature has risen by 0.5°C during the last century with the increases in greenhouse gases being the most probable main contributor.
2) The assumed 1 % per year increase in atmospheric greenhouse gases in the scenario run after 1990 is somewhat faster than in the central scenarios outlined by the IPCC (1996). This results into a level of greenhouse gases in the scenario time slice that is 2.5 times the preindustrial one.

The difference in global mean temperature between the scenario and the control run time slices in HadCM2 is 2.6°C. This is close to the best estimate of the IPCC (1996) for the greenhouse-gas-induced global mean warming between 1990 and 2100 (roughly 2.5°C). Assuming a substantial increase in the amount of anthropogenic sulfate aerosols, the global mean warming by 2100 would be less, of the order of 2°C. If, on the other hand, the amount of sulfate aerosols would decrease and/or there would be an even faster increase of greenhouse gases, the period described by the time slice could occur earlier than around year 2100. The future changes in aerosol concentrations are very difficult to predict as their atmospheric lifetime is very short. The longevities of the anthropogenic greenhouse gases ensure that their concentrations will continue to increase in the atmosphere even though the speed of the increases will depend on

several factors, like the success in the measures to limit the release of these greenhouse gases into the atmosphere.

These two HadCM2 reruns were given their initial conditions from the original HadCM2 control and greenhouse gas runs described by Mitchell and Johns (1997); the rerunning was necessary because the needed data had not been archived from the original run. However, as a result of nonlinear amplification of initially bit-level differences associated with the use of a different computer, the simulations giving the boundary conditions for the RCA model are not identical with the corresponding periods in the original simulations.

HadCM2 has been shown to behave in a very stable manner in a long control experiment, with virtually no drift in atmospheric temperatures (Tett et al., 1997). In addition, when run with gradually increasing equivalent CO_2 and a simple sulfate aerosol scheme, the simulated global mean surface air warming from 1860 to 1990 matches quite well with the observed one (Mitchell et al., 1995; Tett et al., 1997).

The climate in the HadCM2 control simulation has been compared to observations by Johns et al. (1997) and Tett et al. (1997). Many aspects of the present large-scale climate are simulated with considerable skill, and the model performance shows a general improvement over an earlier version of the UKMO climate model. In addition, Räisänen (1997) has calculated verification statistics for HadCM2 and a lower-resolution version of the Hamburg ECHAM3 GCM. HadCM2 has been found to correlate better with observed climatologies than ECHAM3. For example, the global spatial correlation between the observed and HadCM2-simulated fields of sea level pressure is as high as 0.96 in both the northern winter (December-February; DJF) and summer (June-August; JJA).

Among the deficiencies of HadCM2, Johns et al. (1997) note a general cold bias in tropospheric zonal mean temperatures in both DJF and JJA. In the lower troposphere north of 45°N, this is reversed to a warm zonal mean bias of 1-3°C in DJF. The wintertime Icelandic low is slightly too weak and slightly too far south, resulting in too weak time mean westerly winds in northern Europe in DJF. Consistent with this pressure field feature, the Atlantic storm track is located somewhat too far south and its strength (measured by the band-pass filtered 500 hPa height variance) is slightly lower than observed. The storm track is slightly too far south also in summer.

Comparison for the Scandinavian land area (the 25 HadCM2 land grid boxes at least partly within the borders of Finland, Sweden, Norway and Denmark; 56°-71°N, 5°-32°E) between the 240 years of the original HadCM2 control simulation and the CRU climatological analyses for 1961-90 (Hulme et al., 1995; CRU stands for the Climatic Research Unit at the University of East Anglia, UK) reveals a general cold model bias of 2-3°C in spring and in summer. In winter and in fall, the differences between the model and the observations vary spatially. For example, in winter, both the western and eastern parts of this region are somewhat cold, whereas the areas bordering to the Baltic Sea are too warm by 2-4°C. The HadCM2 10-year control run time slice features even unrealistically warm wintertime Baltic Sea surface temperatures (in particular in the Bothnian Bay region). In addition, the sea ice is persistently absent in the Baltic Sea area in these HadCM2 data.

Although these errors in the land area time mean temperature are not negligible, they are relatively small compared with the temperature biases found in many older GCM experiments (Räisänen, 1994). However, HadCM2 tends to overestimate the interannual variability of monthly mean temperatures in summer and autumn. This feature becomes more marked towards central and eastern Europe, and it has been noted

also by Tett et al. (1997). The overly strong interannual temperature variability is attributed to the tendency of the modeled soil moisture to diminish too much in summer.

Taking the Scandinavian land area as whole, the amount of precipitation in HadCM2 exceeds the CRU climatological values. The differences are smallest in September (10 %) and largest April (in excess of 50 %). However, as the CRU precipitation climatology is not corrected for measurement errors, the difference of the HadCM2 results to true precipitation is smaller. This applies especially in winter when much of the precipitation falls in solid form. Due to the relatively coarse resolution, HadCM2 is of course unable to capture the sharp maximum of precipitation along the western coast of Norway. Instead, a broader and weaker maximum of precipitation is simulated further east over the Scandinavian mountains.

Compared with the CRU climatology, the simulated total cloudiness in HadCM2 also appears too large in all seasons, the area mean difference being around 10 %.

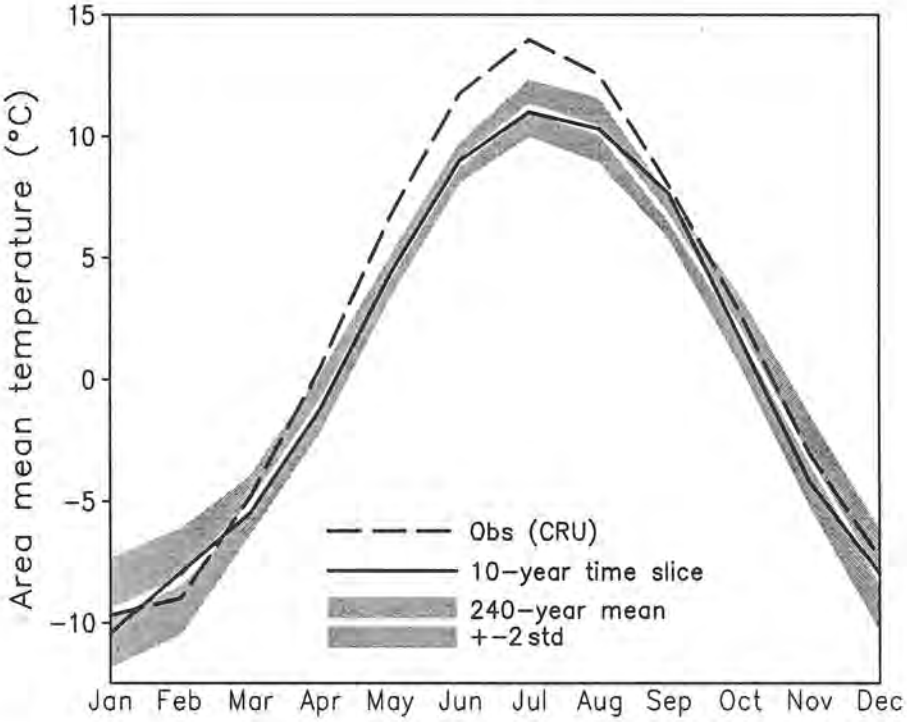

Figure 4. *Monthly mean temperatures averaged over the 25 HADCM2 land grid boxes at least partly within Finland, Norway, Sweden and Denmark. The solid line shows the monthly means in HadCM2 in the 10-year time slice used for the RCA control experiment, and the dashed line those obtained from the CRU climatology. The white streak between the grey bands gives the 240-year monthly means in the original HadCM2 control run. The gray bands indicate the approximate 95 % probability interval of natural variability for 10-year means (mean ±2 interdecadal standard deviations calculated from the 240-year run).*

As a result of unforced internal variability in HadCM2, the climate statistics for the time slices used to for RCA are not identical with those from the original 240-year control run. An example of this is shown in Figure 4. Averaged over the Nordic area (excluding Iceland), the annual mean temperature in the 10-year time slice coincides almost exactly

with the 240-year mean. However, differences up to almost 1°C occur in individual months. The differences between the 10-year and 240-year means vary somewhat within the Nordic area.

For another illustration of the variability within the HadCM2 control run, the simulated wintertime North Atlantic Oscillation (NAO) index during the period 2039-2049 (i.e. the HadCM2 period used to drive RCA) is shown in the upper part of Figure 5. The NAO is basically an irregular variation in the pressure gradient between the Icelandic low and the Atlantic subtropical high (e.g. Hurrel and Van Loon, 1997). Several aspects of the regional climate in Scandinavia have been shown to correlate with it (Johansson et al., 1998; Chen and Hellström, 1998). In particular, the positive (negative) phases of the oscillation are usually associated with warmer (colder) than average winter temperatures in Northern Europe. For Figure 5, the index was derived from the DJF mean pressure difference between the grid box closest to Lisbon, Portugal (7.5°W, 40°N) and the grid box closest to Akureyri, Iceland (22.5°W, 65°N). This pressure difference was normalized by subtracting the 240-year mean wintertime pressure difference in the original control run and by dividing by the corresponding interannual standard deviation.

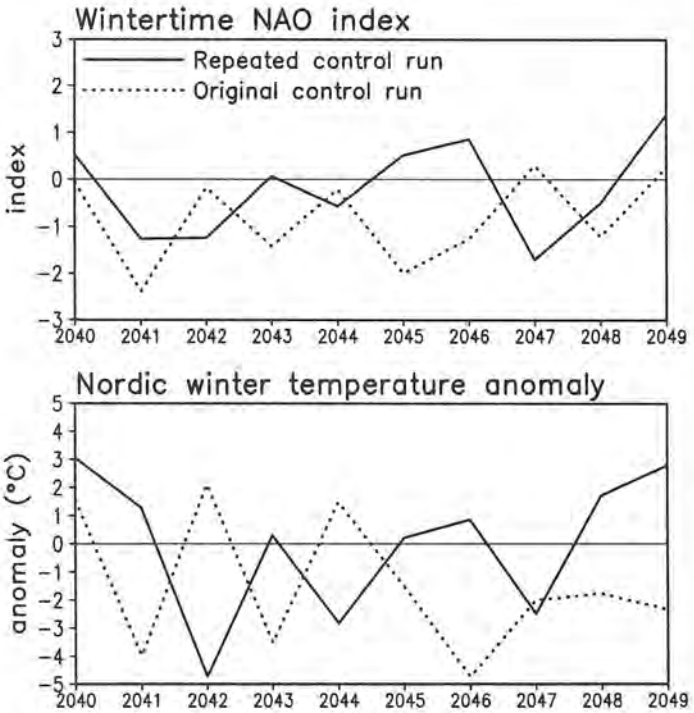

Figure 5. *Interannual wintertime variations of the North Atlantic Oscillation index (above) and the Nordic land area mean temperature anomaly (below) in the repeated (solid) and in the original HadCM2 control run (dotted). A winter begins from the beginning of December, preceding the year given on the horizontal axis, and extends to the end of February.*

It is of interest to note how the behavior of the NAO differs between the rerun 10-year time slice and the same period in the original 240-year run. The original run is strongly dominated by a negative phase (the 10-winter mean index is -0.81), but in the rerun time slice the positive and negative phases are in a closer balance (mean index -0.19). In

addition, in accordance with the difference in NAO, the original 10-year period is characterized by generally colder winters in northern Europe than the rerun (see the lower panel). The 10-winter Nordic mean temperature anomaly relative to the 240-year mean in the original control run is clearly negative (-1.5°C) in the original run, but slightly positive (+0.2°C) in the rerun. Thus, at least in this respect, the rerun time slice is (fortuitously!) closer to the long-term mean climate of HadCM2 than the same period in the original control run.

4 Regional model setup

4.1 Domain and resolution

If a regional climate model is to provide high-resolution results for impact studies, a resolution of the order of 20 km is desirable. Especially the simulation of the regional hydrological balance requires such detail. When input to the regional model is taken from a (relatively) low-resolution global climate model, special techniques are needed to achieve a suitable scale-transition in time and space. An established technique is the so-called double nesting, i.e. performing the regional model simulation in two stages. The first stage is done by forcing a relatively large regional domain with a relatively coarse resolution with the global model data (i.e. the regional domain is nested into the global one). In the second stage, the results from the first stage are used to force a smaller regional domain with the intended high resolution (the second regional domain is nested to the first one).

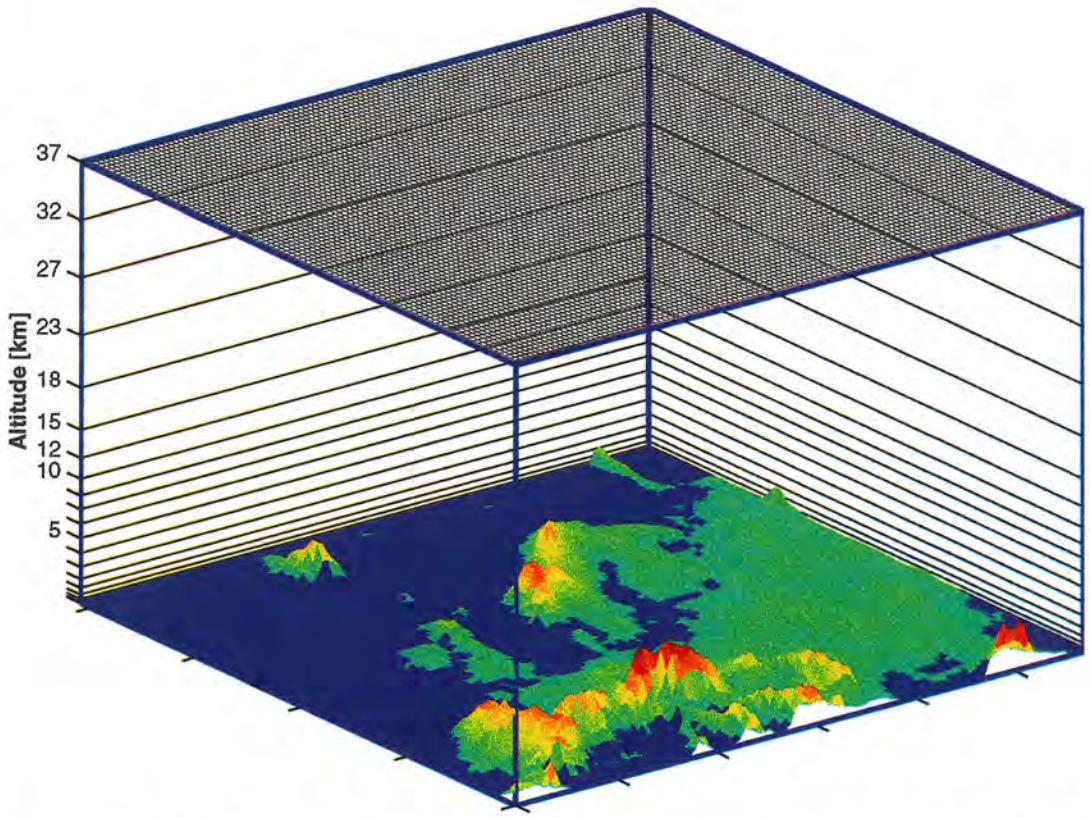

Figure 6. *The RCA domain, illustrative topography and half levels (the latter define the bottom and the top of the layers). The 44-km grid is drawn at the top of the figure, though it is almost too fine to be seen. The layers are labeled in approximate altitude in kilometers. With a surface pressure of 1000 hPa, the half levels are at altitudes of 0,0.04, 0.3, 0.7, 1.3, 2.0, 3.0, 4.2, 5.4, 6.7, 7.9, 9.0, 10.4, 12.2, 14.6, 18.1, 22.5, 27.4, 32.2, 37.1 km. The lower level labels have been omitted from the figure for clarity.*

The model domain is set with a rotated latitude/longitude grid with south pole at 32°S, 35°E. The horizontal grid (0.4°, i.e. 44 km) in this first RCA version reflects a compromise between the computational load of model runs (the load increases as the resolution gets higher) and the demand for a high (enough) resolution to capture the regional climate forcing aspects. The model domain is shown in Figure 6, including the land-sea distribution and a qualitative representation of the orography. The present horizontal dimensions of the model grid are 82 points (latitude) by 114 points (longitude). The grid itself is Arakawa's C-grid. Thus, pressure, temperature and humidity are calculated at the center of the grid boxes and the wind components at the middle of the top and the bottom edges in the case of the meridional component and at the middle of the side edges in the case of the zonal component. The nineteen vertical levels in RCA are the same as in the driving GCM. The first four levels are in σ-coordinates, the top three are in pure pressure coordinates and the levels in between are in hybrid coordinates. Horizontal wind, temperature and humidity are integrated at the full levels and the vertical velocity at half levels.

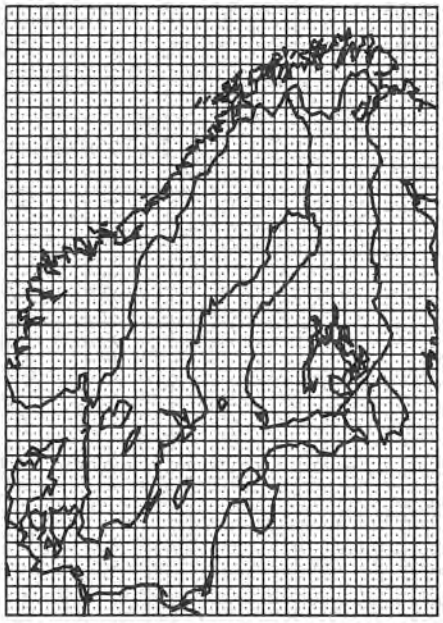

Figure 7. *RCA grid for the Nordic countries and the Baltic Sea area.*

How the 0.4° horizontal resolution covers the the Baltic Sea area is illustrated in Figure 7. Eventually, methods for reaching the targeted high resolution (a resolution of the order 20 km is aimed for) will be evaluated for use in RCA. At least three approaches are to be considered in more detail. The first is the double nesting approach. The second is to leap directly from the GCM resolution to the target one in RCA. The third is to use some form of variable resolution in the regional domain.

4.2 The model

HIRLAM/RCA is formulated with primitive equations and the hydrostatic assumption. The six prognostic variables are surface pressure, horizontal wind components, temperature, specific humidity and (total) cloud water content. Only a short description is given here on the adiabatic part of the model, as it is described in detail elsewhere. As changes seem to be needed in the physics parameterizations in the climate simulations, the physics in the model is described in more detail.

4.2.1 Initialization

Initialization is done with an implicit non-linear normal mode scheme (after Machenhauer, 1977; see also Källén, 1996) with three vertical modes. Whether the procedure is necessary in the extended climate integrations has not been addressed.

4.2.2 Model dynamics, integration scheme and the program flow

Two choices of advective transport are available, an Eulerian scheme and a semi-Lagrangian scheme (McDonald, 1994). The latter basically allows for a longer integration time step than the former. However, the present implementation of the semi-Lagrangian scheme hosts numerical problems and it has been unsuitable for long integrations with RCA. These problems have been noted also in the HIRLAM project (see e.g. HIRLAM Newsletter, 30, February 1998). Consequently, RCA has been run with the Eulerian scheme (with a 5 minute time step) for the time being.

Time integration is performed with a three time-level semi-implicit scheme (after Simmons and Burridge, 1981). The explicit dynamical part (advection, horizontal diffusion) is computed with a leap-frog scheme for horizontal wind, temperature and specific humidity and with an upstream scheme for cloud water. Vertical advection is done on temperature and specific humidity, but not on cloud water. After the explicit part of the integration, the implicit part is added as a correction term. The tendencies due to the parameterized physics are thereafter computed and added to the dynamical tendencies. This is followed by the boundary relaxation and, finally, by (Asselin) time-filtering for the leap-frogged variables.

4.2.3 Convection and condensation

There are two convection-condensation schemes available in HIRLAM. The schemes include a modified Kuo-type (1965, 1974) convection routine and condensation routines for calculating the microphysical processes. In the older scheme, cloud water is a diagnostic variable. In the newer scheme (Sundqvist et al., 1989; Sundqvist, 1993), cloud water is a prognostic variable. The present coding of the scheme hosts some problems, like "water bombs" (intensive grid-point precipitation in situations where no precipitation should occur). For this reason, the convective precipitation is monitored on-line in RCA integrations, flagging large precipitation events for off-line analysis.

The convection/condensation operates columnwise in the model. The first step is to check whether convective condensation occurs. The conditions are that the temperature should be below the moist adiabatic value in two or more layers above the lifting condensation level (LCL) of surface air and that there is a convergence of water vapor in the column, without including surface evaporation. The LCL is located only for the air at the lowest model level, so convection is never started by lability at higher levels. In such cases, vertical diffusion can still account for some transport.

If the conditions for convective condensation are not met, the possibility of stratiform condensation is checked for. Stratiform condensation starts in a cloud free grid box if relative humidity exceeds a given threshold value U_{00}. U_{00} increases with decreasing altitude from its bulk tropospheric value in the three lowest layers. In the lowest two layers, U_{00} is depends also on stability (U_{00} becomes larger with increasing stability) and it increases with decreasing temperature below the threshold temperature of 238 K. This is said to be done to suppress ice cloud formation. Finally, U_{00} is given a somewhat lower value over land than over ocean. The threshold values re less than 100 % everywhere, so stratiform condensation is considered to be a sub-grid scale process in the horizontal.

The microphysical processes are formulated similarly in both the convective and in the stratiform case, albeit with different parameter values. Solid forms of cloud water are diagnostic (Sundqvist, 1993) and based on the local temperature.

For the most part, the HIRLAM convection/condensation routines are used as such in RCA. As the performance of the parameterized convection/condensation processes is in general sensitive to other model details (like resolution), tuning of the HIRLAM routines should be done anew for RCA.

A number of the parameters in the microphysics parameterization are suitable for tuning as neither theory nor observations fix definite values for them. The parameters that have been identified for eventual tuning are listed in Table 3. The threshold relative humidity values for condensation to start affect the balance between specific humidity and cloud water. Some temperature-related control on the microphysics is available with modifications to the coalescence factor (affects cloud water at temperatures above zero degrees Centigrade) and to the Bergeron-Findeisen parameter (has effect in colder temperatures). Increases in the cloud-water-to-precipitation conversion rates have a strong control on the amount of water residing in the clouds. In addition, the way cloud composition is partitioned between water and ice and the way the fractional cloud cover is diagnosed can also be used for tuning.

At the moment, the only change in RCA, compared to HIRLAM2.5, is that the way the saturation water vapor pressure is calculated is different. In HIRLAM at temperatures above 0°C the saturation vapor pressure is calculated with respect to water, at temperatures below -15°C, the calculation is done with respect to ice and in the intermediate temperature range, a linear combination of values with respect to water and ice are used. As there is also a diagnostic partitioning between liquid cloud water and cloud ice, it is more attractive to use the same temperature-dependency for the saturation vapor pressure when it is used in cloud microphysics calculations. This is implemented in RCA. Basically, the saturation vapor pressures, calculated with respect to water and ice surfaces in the given temperature are summed after weighting them with the probability for liquid cloud water and the probability for cloud ice, respectively.

Table 3. *Microphysics parameters that can suit for tuning in RCA.*

Name	Role	Value
hu_{00}	Threshold RH for stratiform condensation to start over land	0.85
hu_{00}max	Maximum hu_{00}	0.975
duoorl	Land-sea difference in hu_{00}	0.10
huoorl	Level-dependency of duoorl	No change in the vertical
coales	Coalescence factor	100
hccu	Basic conversion rate of cloud water into precipitation in cumulus clouds	$2 \cdot 10^{-4}$ s^{-1}
hcst	Basic conversion rate of cloud water into precipitation in stratiform clouds	$1 \cdot 10^{-4}$ s^{-1}
cbfeff	Bergeron-Findeisen parameter	4

4.2.4 Horizontal diffusion

The Eulerian advection is run with the explicit, fourth order horizontal diffusion operating on model levels for the wind components. Temperature and specific humidity are diffused horizontally on reference pressure surfaces, to be able to model their transport better over steep orography. In the case of excessive orographic precipitation, horizontal diffusion for moisture and temperature over steep terrain could also be switched off entirely as in Christensen et al. (1996). In RCA with the 0.4° grid and the 5 min time step, the fourth order scheme diffusion coefficient has been set to $7 \cdot 10^{13}$. There is no diffusion of cloud water.

In the semi-Lagrangian scheme, an implicit horizontal diffusion formulation would be used instead of the explicit scheme.

4.2.5 Vertical diffusion

Momentum, sensible heat (actually, the dry static energy) and moisture are transported by vertical diffusion in the surface layer and in the free troposphere.

The vertical diffusion in HIRLAM2.5 is based on the Monin-Obukhov similarity theory (the strength of the exchange depends on static stability and roughness length) in the surface layer (lowest model level which is at a height of appr. 25 m). Above the surface layer, vertical diffusion follows the so-called K-model (the exchange depends on static stability and mixing length), modified from Louis (1979) and Louis et al. (1981). This scheme is often called the "Louis scheme". A form of shallow convection is included in the scheme (Geleyn, 1987) to modify diffusion in moist air (moist boundary layer and in clouds!). The modifications are done through changes in the (analytical) stability functions (as described in Källén, 1996). Shallow convection is switched on when specific humidity becomes larger than a threshold value, set at 95% of the local specific humidity at saturation. Shallow convection corrects for the underestimation of the vertical exchange of sensible heat and moisture in unstable situations (in the whole of the troposphere!).

Another vertical diffusion scheme (after Holtslag and Boville, 1993; Woetmann-Nielsen and Amstrup, 1997) has also been considered within the HIRLAM project. This other scheme is called the "Holtslag scheme". It aims to improve the simulation of unstable/convective situations with the size of the mixing eddies becoming comparable to the height of the boundary layer. The Holtslag scheme includes a modification to the local gradient of the diffused quantity and to the calculation of the exchange coefficients (see also Perov and Gollvik, 1996). The modification of the local gradient is done with a countergradient term that is presently non-zero only for heat. A preliminary shallow convection parameterization is also included in the Holtslag scheme. Inclusion of vertical diffusion of cloud water has also been tested (Sass, 1995; Woetmann-Nielsen, 1996), but without concluding it to have been a major improvement.

The (local) exchange coefficients for momentum, dry static energy and specific humidity are calculated in both schemes with:

$$K_{u,v,q,s} = l^2 \left| \frac{\partial \vec{V}}{\partial z} \right| f_{u,v,q,s}$$

with l as the mixing length and f as an analytical formula (Louis et al., 1981) depending on stability (stable, neutral, unstable), gradient Richardson number and height above the surface. In the Holtslag scheme, however, other analytical formulae f than those in the Louis scheme are used in calculating the Ks. The expression with the || is the magnitude of the local vertical velocity shear. The exchange coefficients for dry static energy (index $_s$) and specific humidity ($_q$) are equal. A height-dependency of the free tropospheric asymptotic mixing length (λ) is added to the Blackadar (1962) formulation. The boundary layer λ is set to 300 m and above 1000 m altitude, it falls exponentially towards its upper tropospheric value of 30 m. In the Holtslag scheme, the (local) exchange coefficients are replaced, if the situation calls for it (c.f. the discussion above). New exchange coefficients are calculated according to Holtslag and Boville (1993):

$$K_{u,v,q,s} = kw_t z\left(1-\frac{z}{h}\right)^2$$

where k is the von Karman's constant, w_t is a turbulent velocity scale (a function of the static stability parameter), z is height and h is the boundary layer height.

The distribution of roughness length is prescribed for land points in the local scheme, without taking into account snow cover or other time-varying features. Over sea, the Charnock (1955) formula is used in both the local and the non-local scheme, with the Charnock constant set to 0.018. Somewhat lower values might be more appropriate for the open sea whereas higher values have been proposed for coastal areas. At present, there is only one roughness length and it is used for each of the diffused quantities.

The latent heat flux at the surface responds to surface wetness so that the saturated specific humidity at the surface temperature, q_s, is reduced with respect to soil moisture deficiency over land. This is done using a soil wetness parameter G:

$$q_{ssurface} = Gq_s + (1-G)q_n, \quad G = 0.05 + 0.95(w_s / w_{s\max})^8$$

where q_n is specific humidity at the lowest model level. In HIRLAM, the presence of snow allows the snow-covered fraction of the grid box to evaporate at the potential rate (G equal to unity). This feature is removed in RCA to restrict evaporation from snow cover (which is very small in reality). The soil wetness parameter can be likened to the ratio of the aerodynamic resistance to the sum of the aerodynamic and surface resistances. A G equal to unity equals to zero surface resistance on surface evaporation.

The modifications suggested by Makin and Perov (1997) on the sensible and latent heat exchange coefficients over sea are considered in RCA. These changes reduce the wind-speed-dependencies of the sensible and latent heat surface exchange coefficients but leave the one for momentum unchanged.

The surface fluxes for momentum, moisture and dry static energy are parameterized with bulk formulae:

$$F_{u,v,q,s} = \rho C_{u,v,q,s}\left|\vec{V}_z - \vec{V}_{sfc}\right|((u,v,q,s)_z - (u,v,q,s)_{sfc})$$

with the Cs, the bulk transfer coefficients (alt. drag coefficient), derived from an expression akin to that for the Ks.

Both the Louis and the Holtslag schemes have been tried out in RCA. At least on the RCA monthly-to-seasonal time scales, the Holtslag scheme, in its present extent, was not found to perform better than the older scheme. Compared to the older scheme, water vapor was lifted somewhat higher from the surface and in general the tropospheric cloud water amount became larger.

4.2.6 Radiation

The parameterization of radiation in RCA is the very same scheme that is used in HIRLAM (Savijärvi, 1990; modified by Sass et al., 1994). The scheme has only two spectral intervals, one for the short-wave part and the other for the long-wave part. The scheme is highly parameterized and computationally effective. The basic calculated parameter is the vertical divergence of the net radiative flux, to which the temperature tendency is proportional.

In the short-wave part, both clear-sky and cloudy contributions to the absorption are calculated whenever there are clouds in the column in question. The total absorption is obtained using the maximum layer cloud cover in the column. The formulation includes crudely the contributions from O_2, CO_2, O_3 (without seasonal effects), H_2O (using the on-line specific humidity profile), aerosol absorption and aerosol scattering. Cloud absorption and transmissivity formulations have been simplified from more detailed results, and in HIRLAM/RCA they depend on cloud water.

The clear air short-wave heating rate ($_{sa}$) is given by:

$$\frac{\partial T}{\partial t_{sa}} = S \times \frac{q}{c_p} \times \frac{p}{p_0} \left[Y(u_s) + b_4 \alpha \cos\theta Y(u_*) \right] + b_5 (\cos\theta)^{0.3}$$

where S is the solar constant, q is specific humidity, θ is the solar zenith angle, p is pressure, p_0 is reference pressure, c_p is the specific heat, α is short-wave albedo at the surface, $Y(u_s)$ and $Y(u_*)$ express the dependence of short-wave absorption on water vapor (u_s and u_* are the linearly pressure-scaled slant water vapor paths for the direct and the ground-reflected (isotropic) beams). b_4 and b_5 are tuned constants.

The short-wave heating rate in clouds ($_{sc}$) with the top at p_Z, transmittance $\hat{S}$ and absorptance $\hat{A}$ is given by:

$$\frac{\partial T}{\partial t}_{sc} = \hat{S}(p_Z, p) \frac{\partial T}{\partial t}_{sa} + \frac{g}{c_p} F_{sZ} \frac{\partial}{\partial p} \hat{A}(p_Z, p)$$

The flux density at the top of the topmost cloud (F_{sZ}) in the above is given by:

$$F_{sZ} = S \times \cos\theta \left[1 - 0.024 \cos\theta^{-0.5} - b_8 0.11 u_s^{0.25} - b_9 \frac{p}{p_{00}} \left(\frac{0.28}{1 + 6.43 \cos\theta} - 0.07 \alpha_* \right) \right]$$

The first term in the brackets above is for absorption by stratospheric ozone. There is no seasonality for this term. Such a modification could be implemented quite simply (Savijärvi, 1990). The second term is for absorption by aerosols, H_2O, CO_2 and O_2 in the troposphere. The third term is for scattering effects with α_* as the clear-sky albedo above the cloud top. The b_8 and b_9 are constants giving the aerosol absorption and scattering. The contribution of the clear air (F_{s0a}) net solar flux density to the net SW flux at the surface (F_{s0}) is calculated with a similar expression. The F_{s0} includes also a cloudy contribution (F_{s0c}). The latter is essentially F_{sZ}, modified by in-cloud absorption and transmission, multiple reflections between the surface and the cloud as well as absorption in reflected beams. The surface short-wave albedo varies according to surface condition (water, ice, open land or forest) and it is modified in the presence of snow. Note that no aging effects for the snow are included at present. The instantaneous

grid-point albedo is calculated as a sum of the fractional contributions of the different surface covers. The albedo field is put through a nine-point smoothing to remove strong gradients (see Bringfelt et al., 1995). The surface-type -dependent albedos are listed in Table 4.

Table 4. *The surface-type -dependent albedos.*

Surface type	Albedo
Water, no ice	0.07
Ice, no snow	0.50
Ice with snow	0.70
Open land, no snow	0.20
Forest, no snow	0.10
Open land, snow	0.51
Forest, snow	0.18

The long-wave part is based on an empirical water vapor emissivity function E, which includes the effects of the H_2O line spectrum on radiative transfer:

$$E(p_{i-1/2}, p_{i+1/2}) = a_1 + a_2 X - a_3 X^2 - a_4 X^3$$

with X incorporating a formulation for the linearly pressure scaled water vapor path.

In all columns, the total radiative effect in the long-wave is combined from the clear sky contribution and from three different cloud configuration contributions. The contributions (see Sass et al., 1994 for additional details) are given as:

- No clouds in the box and no clouds above it: $W_1(R_1+R_2+R_3)$
- No clouds in the box and clouds above: $W_2 f_2(R_1+R_3)+(W_2-W_3)R_2$
- Clouds in the box and no clouds above: $W_4R_4+W_5R_5+W_6R_6$
- Clouds in the box and clouds above: $W_7R_7+W_8R_5+W_9R_6$

The W_i are weight functions which include the cloud overlap assumption. The R_i are the different net radiative flux divergence contributions to the local long-wave radiative budget. R_1 gives the cooling to space by H_2O line spectrum, R_2 is for the surface radiation which reaches the level, R_3 is for the cooling due to water vapor continuum and it includes also a constant for the cooling due to CO_2 and O_3. R_4 is for the net radiation balance at cloud top and the last three, R_5, R_6, R_7, define the radiative interaction between clouds and between surface and clouds. The empirical emissivity function appears in R_1-R_2 and R_4-R_5. f_2 is introduced to reduce the cooling below clouds.

The long-wave scheme thus explicitly incorporates the model-calculated water vapor distribution and cloudiness (and consequently any changes in these). The contributions to the long-wave radiation processes from other trace gases (CO_2, O_3) are taken into account as constants.

The downward long-wave surface flux from clear atmosphere F_{i0a} and the downward long-wave surface flux from cloudy atmosphere F_{i0c} are given by

$$F_{i0a} = \sum_{k=1}^{N} B(T_k)\left(E(p_{k-1/2}, p_s) - E(p_{k+1/2}, p_s)\right) + a_9 + a_{10} q_N$$

$$F_{i0c} = B(T_{h*})C_{Eh*}(N)\left[1 - F_{i0a}/(\sigma T_{Ef}^4)\right]T_{Ef} = T_N - a_{14}\left(\frac{\partial T}{\partial p}\right)_N$$

B is the Planck black body radiation function, C_{Eh*} is the maximum effective cloud cover, σ is the Stefan-Boltzman constant, N signifies the lowest model layer and a_9, a_{10} and a_{14} are tuned constants. T_{Ef} is the effective temperature close to the surface. Finally, the net long-wave radiation at ground level is given by

$$F_{i0} = \varepsilon_0\left(F_{i0a} + F_{i0c} - \sigma T_{E0}^4\right)$$

T_{E0} is the surface temperature. The long-wave surface emissivity ε_0 is constant (0.95).

It is noted that such a highly parameterized radiation scheme can not be straightforwardly considered as suitable for use in regional studies with increasing greenhouse gas forcing in the driving GCM data. This is due to the radiative role of CO_2 being put in as few constants (i.e. its radiative contribution is always the same, independent of the amount of CO_2 working in the driving GCM; the conditions in the GCM do enter the regional simulation, however, in the lateral boundary forcing, as the prescribed SSTs and as the prescribed deep-soil temperatures). The contribution of water vapor in the radiative processes, however, is calculated with the up-to-date water vapor in the model. The tuning constants and expressions that could be refit for the climate (scenario) runs are given in Table 5.

Table 5. *Radiation scheme constants incorporating the contribution of sulfate aerosols and greenhouse gases other than water vapor.*

constant/expression	Purpose	Oper. HIRLAM value/notes
$b_5\cos(\theta)^{0.3}$	SW absorption by CO_2, O_2 and O_3	$b_5=1.7\cdot10^{-6}$ K s^{-1}
$-0.024\cos(\theta)^{-0.5}$	SW by O_3 in the stratosphere	fit to results with 350 DU total O_3
$-b_8$	aerosol absorption	$b_8=1.20$
b_9	aerosol scattering	$b_9=1.25$
$a_6q_k^3$, $a_{10}q_{k-1}$	water vapor continuum effects in the LW	a_6=11.5 K s-1 a_{10}=3000 J m-2 s^{-1}
a_7	CO_2 and O3 LW cooling in the troposphere	$a_7=2.3\cdot10^{-6}$ K s^{-1}
a_9	downward radiation in the presence of clouds and due to aerosols and gases other than water vapor	a_9=35 J m^{-2} s^{-1}

4.2.7 Soil processes and snow

The HIRLAM/RCA soil scheme is a modified version of the old three-layer ECMWF scheme (evidently from cycle 28) for soil temperature and soil moisture (see e.g. Blondin, 1988). Some details in the snow parameterization appear to come from the ECMWF model cycle 29. The surface and mid-layer temperature and soil moisture equations trace back to Budyko (1956) and to Deardorff (1978).

The soil scheme is of the force-restore type and it is closed from below with prescribed values. The force for the soil temperatures is the net energy balance at the surface (i.e. the sum of net radiation, sensible heat and latent heat flux densities). For soil moisture, the force is the net of precipitation, evaporation and snowmelt. The restores are given by the prescribed monthly deep-soil temperature and moisture values,

against which the mid-layer and, subsequently, surface temperature and moisture are relaxed. The time scale is given by layer thicknesses and heat, respective soil water, conduction diffusivities. The denomination and characteristics of the layers in this scheme are shown in Figure 8.

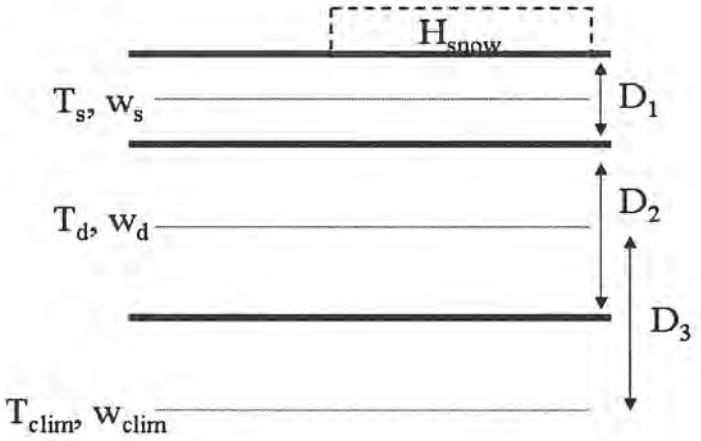

Figure 8. *The three soil layers and the (fractional) snow cover layout in RCA.*

The climatological deep-soil values influence the upper layers with time scales of the order of a month. The interaction time scales of the mid-layer with the surface layer above and the deep-soil layer below are of the order of a few days. The surface layer is characterized by a time scale of some hours, i.e. it responds within the diurnal cycle. There are alternatives to closing the soil scheme from below with prescribed deep-soil temperature and moisture as in HIRLAM. An alternative would be to prescribe the heat and moisture fluxes through the lower boundary or to impose zero-flux lower boundary conditions. The latter implies that the deep-soil layer is at such a depth as not to be affected by forcing from above during the simulation period.

The scheme in HIRLAM has been adopted for RCA with the climatological deep-soil temperature and moisture constructed from the driving GCM soil data. Some modifications have been done to improve the behavior of surface temperatures and snow cover (some deficiencies in the short time scale response in the HIRLAM surface scheme have been discussed by Sass and McDonald (1995), Rontu (1995), Sass and Järvenoja (1996) and McDonald (1996)). These modifications were prompted for after the first tests with long integrations with RCA showed that the surface-soil-snow scheme did not perform well enough. Especially the snow cover tended to respond too fast to above-freezing temperatures and the deep-soil driving of the mid-layer and the surface temperatures was too strong.

The bare soil heat capacity values and the heat diffusivity in the soil temperature equations are now explicitly modified to account for snow above. The equations for the upper soil layer temperature (T_s) and the intermediate soil layer temperature (T_d) are written in RCA:

$$\frac{\partial T_s}{\partial t} = \frac{1}{\left[(1-F_{snow})c_{soil}\rho_{soil} + F_{snow}c_{snow}\rho_{snow}\right]D_1}\sum_i \Phi_i + \frac{\left[\kappa_{soil}(1-F_{snow}) + \kappa_{snow}F_{snow}\right](T_d - T_s)}{0.5D_1(D_1+D_2)}$$

$$\frac{\partial T_d}{\partial t} = -\frac{\left[\kappa_{soil}(1-F_{snow}) + \kappa_{snow}F_{snow}\right](T_d - T_s)}{0.5D_2(D_1+D_2)} + \frac{(T_{clim} - T_d)\kappa_{soil}}{D_2 D_3}$$

ρ_{soil} and c_{soil} are the soil density and specific heat capacity, ρ_{snow} and c_{snow} are the same for snow. Φ_i span the net radiative, sensible heat and latent heat flux densities at the surface, F_{snow} is the fraction of snow cover in the grid point. κ_{snow} is the heat diffusivity of the snow. D_1-D_3 are the three layer thicknesses and κ_{soil} is the bare soil heat diffusivity. Note that the middle and the deep layer overlap in the scheme (see Figure 8). T_{clim} is the prescribed deep-soil temperature (it is also called the "climatological temperature").

The time evolution of the snow density is prescribed in RCA (see Table 6.), interpolating in time from tabulated monthly values in Eerola (1996). These values are based on conditions typical for southern Fennoscandia and they should be understood as approximative only when applied throughout the RCA domain. For c_{snow}, the value for ice is used, complemented with a formula for temperature-dependency (see Gray and Male, 1981, p. 294):

$$c_{snow} = (2.115 + 0.00779T) * 1000$$

with T in degrees Celsius so c_{snow} is given in [J kg^{-1} K^{-1}]. When the density and the specific heat capacity of the snow are set, its heat diffusivity parameter is obtained using the heat conductivity (λ) for ice (2.22 W m^{-1} K^{-1}) as in Douville et al. (1995):

$$\lambda_{snow} = \lambda_{ice}\left(\frac{\rho_{snow}}{\rho_{water}}\right)^{1.88}, \quad \kappa_{snow} = \frac{\lambda_{snow}}{\rho_{snow} c_{snow}}$$

Table 6. *Monthly snow density (Eerola, 1996).*

	Jan	Feb	Mar	Apr	May	June	July	Aug	Sep	Oct	Nov	Dec
kg m^{-3}	220	230	240	280	320	320	320	320	100	160	180	210

The equations for the upper soil layer moisture (w_s) and the intermediate soil layer moisture (w_d) are:

$$\frac{\partial w_s}{\partial t} = (1 - F_{snow})\Phi_q + P_{rain} + M_{snow} + \frac{(w_d - w_s)\lambda}{0.5D_1(D_1 + D_2)}$$

$$\frac{\partial w_d}{\partial t} = -\frac{(w_d - w_s)\lambda}{0.5D_2(D_1 + D_2)} + \frac{(w_{clim} - w_d)\lambda}{D_2 D_3}$$

The three atmospheric forcing terms (water flux terms) affecting w_s are the latent heat flux density, rainfall density and snow melt rate. λ is the water conduction diffusivity in the soil and w_{clim} is the prescribed ("climatological") deep-soil moisture field. The amount of soil water is constrained to stay positive but not to exceed the maximum value set as 0.02 m (of water) in a thickness equal to D_1. Thus, the maximum soil water contents (in meters of water) in w_s and w_{clim} are $0.02 \cdot D_2/D_1$ and $0.02 \cdot D_3/D_1$, respectively. Should more soil water become available, the excess is removed as point runoff in the topmost and in the mid-level layer and thus lost from the model. In case of soil water reduction in the mid-layer due to the relaxation (relaxation to w_{clim}) term, water is lost from the model without runoff.

In nature, the thermal and hydraulic soil characteristics vary from one soil type to another as well as with soil moisture content. To take these variations into account in RCA, the single HIRLAM soil type has for the time being been replaced with nine FAO-Unesco (1981) soil types (Bringfelt et al., 1995), as digitized by the German Weather Service. The availability of other (Nordic) databases for soil types is being investigated. It is also noted, however, that to include vegetation effects (interception, transpiration) is likely a more important topic than to have a detailed soil types in improving the model description of processes at the surface and in the soil. The inclusion of vegetation effects is, indeed, being investigated at present as well.

The nine FAO-Unesco soil types are:

(1) sand	(2) loam	(3) clay
(4) sand and loam	(5) loam and clay	(6) sand and clay
(7) peat	(8) ice	(9) rocks

Type nine, rocks, is not present in the digitized data within the RCA domain. Type (6), which also hardly appears in the domain, is treated with the characteristics of type (2). To use published values, type (4) is associated with sandy loam and type (5) with silt loam. The distribution of these soil types in the RCA domain is shown in Figure 9. The digitization of the data does not extend all the way to the southeastern and the northeastern corners, which have been filled in from the closest points with data.

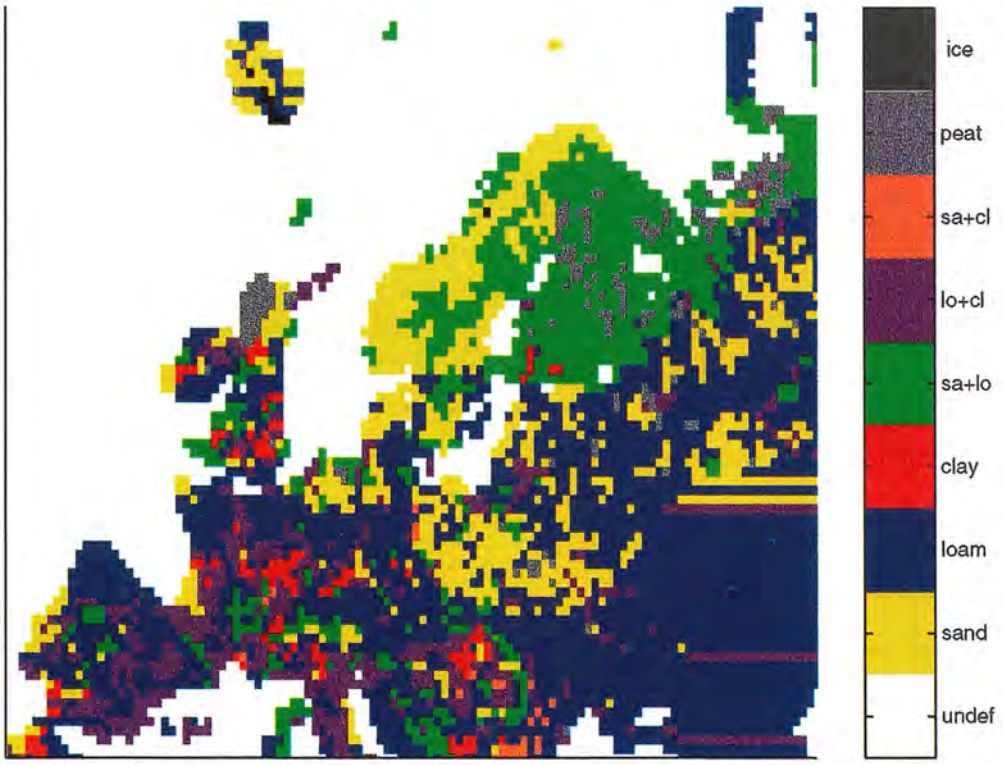

Figure 9. *The distribution of the FAO soil texture types in the RCA domain.*

With the addition of soil texture variability, the soil heat capacities (volumetric, i.e. in [J m^{-3} K^{-1}]), heat diffusivities (in [m^2 s^{-1}]) and hydraulic diffusivities (in [m^2 s^{-1}]) have been redefined. Their dependencies on soil moisture have been added. The heat capacity is now a linear combination of the dry soil value and the value for water, and different

soil types have different values. The amount of water is given by the volumetric soil moisture content, calculated according to:

$$\theta = \frac{w_d}{0.02} \cdot \left(\theta_{fc} - \frac{\theta_{wp}}{\alpha} \right) + \frac{\theta_{wp}}{\alpha}$$

w_d is the scaled (as explained earlier) mid-layer soil moisture content, the θ_s indicate volumetric moisture with the indices $_{wc}$ and $_{fc}$ specifying the wilting point and field capacity conditions, respectively. The constant of 0.02 scales soil moisture to its maximum allowed value in the model. An optional scaling parameter (α) to the volumetric moisture content at the wilting point is provided. It can be used in tuning the parameterization to give a reasonable behavior of the soil, with respect to both tabulated properties and the modeled time scales in the soil. At the moment, a is set to unity. An α larger than unity would cause the thermal and hydraulic soil properties to fall more rapidly with increasing dryness and the values at the wilting point would become very small. The α should never be set to too large of a value, as should the mid-layer dry out at some point, the interaction time constants between the layers would grow into years and the mid-layer soil moisture would have a very difficult time to recover.

Heat diffusivities are calculated from the volumetric heat capacity and the heat conductivity. The latter is derived with an expression as in Viterbo (1996; based on McCumber and Pielke,1981):

$$\lambda_{heat} = a \left| \Psi_{sat} \right|^{\frac{-1}{\ln 10}} \left(\frac{\theta_{sat}}{\theta} \right)^{\frac{-b}{\ln 10}}$$

a (=3.8) is a constant which converts the original units (McCumber and Pielke, 1981) to SI, ψ_s is the saturation matric potential, θ is the volumetric soil moisture content (with the index $_{sat}$ to indicate the value at saturation) and b is an empirical exponent from Clapp and Hornberger (1978). At soil moistures at or less than the wilting point values, the calculated heat diffusivity at the wilting point is used (as can be seen by substituting calculated θ at zero soil moisture content w_d). The dry soil value becomes somewhat too high (but in practice the soil never dries out totally in the model). The thermal diffusivity is then:

$$\kappa_{soil} = \frac{\lambda_{soil}}{c_{soil} \rho_{soil}}$$

With respect to the hydraulic diffusivity (λ_{water}), the first idea was to follow McCumber and Pielke (1982). Their expression can also be written as in Viterbo (1996), to illustrate the dependency on saturated conditions:

$$\lambda_{ate} = -\frac{b \gamma_{sat} \Psi_{sat}}{\theta} \cdot \left(\frac{\theta}{\theta_{sat}} \right)^{(b+3)} = -\frac{b \gamma_{sat} \Psi_{sat}}{\theta_{sat}} \cdot \left(\frac{\theta}{\theta_{sat}} \right)^{(b+2)}$$

The b and the ψ_s are as in the heat diffusivity expression and γ_{sat} is the saturation hydraulic conductivity value. Both the heat and hydraulic diffusivities are calculated

using θ/θ_{sat}, i.e. scaling to the saturated volumetric soil moisture (which corresponds to the total porosity of the soil). The maximum allowed volumetric soil moisture occurs at the field capacity case. The McCumber and Pielke formulation, in connection with the current layer thicknesses, runoff formulation and soil moisture initialization, led in test runs into leaky soil in RCA. In other words, following snow melt or rain episodes, the top soil layer lost moisture fast downwards and surface runoff was cut off (too) fast. Runoff did not have time to occur in the mid-layer either, as its moisture was lost fast in the restore process. If the model's runoff were defined as the net of precipitation and evaporation (and changes in the snow cover and soil moisture, to be more precise), the results would still have been realistic. This would have accounted for the changes due to the relaxation to the climatological layer (which caused mainly loss of water from the model). However, in order to produce more realistic runoff data in RCA, and to keep some of the McCumber and Pielke soil moisture feedback in the scheme, the hydraulic diffusivities in RCA are treated as in HIRLAM2.5 (where they are taken proportional to the thermal diffusivities). Further tuning of the scheme is needed before applying the McCumber and Pielke formulation.

The thermal and hydraulic characteristics of the different soil types, for soil moistures between wilting point and field capacity, are shown in Figure 10.

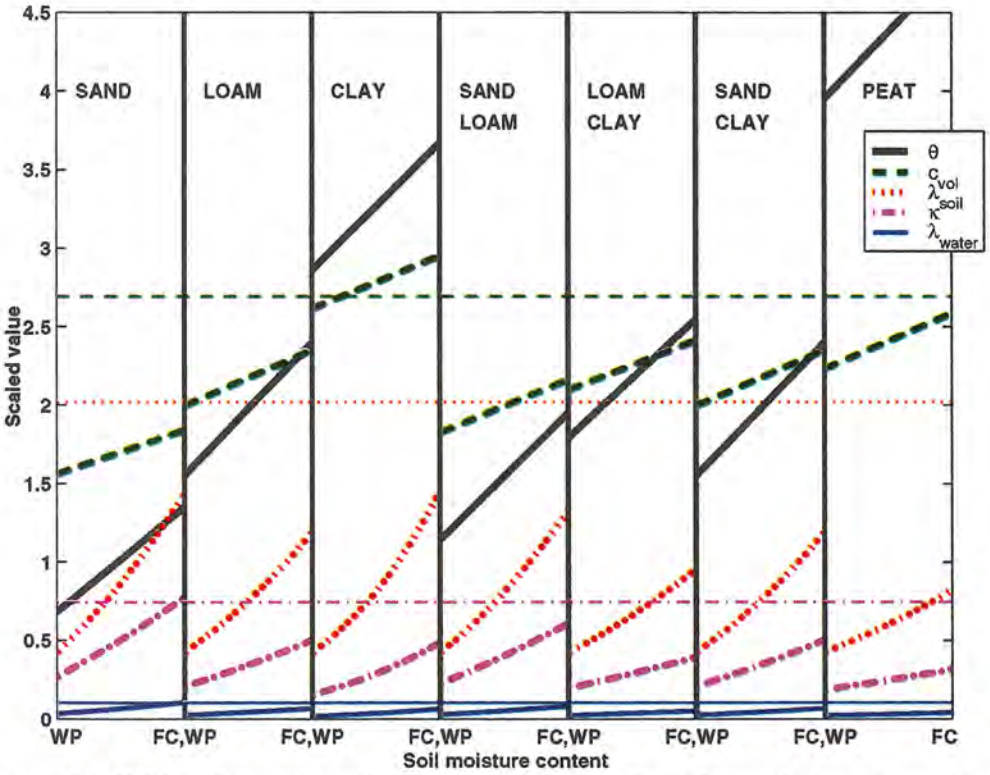

Figure 10. *RCA volumetric soil moisture (θ [$m^3\ m^{-3}$]), volumetric heat capacity (c_{vol} [$10^6\ J\ m^{-3}\ K^{-1}$]), thermal conductivity (λ_{soil} [$W\ m^{-1}\ K^{-1}$]), thermal diffusivity (κ_{soil} [$10^{-6}\ m^2\ s^{-1}$]) and hydraulic diffusivity (λ_{water} [$10^{-6}\ m^2\ s^{-1}$]) for seven of the FAO-Unesco soil types and as a function of soil moisture between wilting point (WP) and field capacity (FC). The horizontal lines show the HIRLAM2.5 values for c_{vol} ($2.7 \cdot 10^6$), λ_{soil} (2.025), κ_{soil} ($0.75 \cdot 10^{-6}$), λ_{water} ($0.11 \cdot 10^{-6}$).*

The volumetric heat capacities now show variation with soil moisture but in principal they agree with the earlier HIRLAM value as well as the constant value ($2.19 \cdot 10^6$) in Viterbo (1996). Note that the values in Viterbo (1996) refer to a single "representative soil type for the world", obtained by averaging a selection of tabulated characteristics for silt loam, loam, silty clay loam and clay loam.

The new thermal diffusivities are lower than the standard HIRLAM constant value. On the other hand, they are somewhat higher than the values also suggested for use in HIRLAM by Sass and Järvenoja (1996). They suggested values in the range of $0.1 \cdot 10^{-6}$-$0.2 \cdot 10^{-6}$. Viterbo's (1996) thermal conductivity ranges from 0.4 at wilting point (agrees well with the RCA values) to 2.25 at field capacity (i.e., a larger thermal conductivity than in RCA). His corresponding thermal diffusivities are $0.2 \cdot 10^{-6}$ and $1 \cdot 10^{-6}$, which also show a larger spread than is the case in RCA.

To compare the McCumber and Pielke (1982) hydraulic properties with Maidment (1992), the hydraulic conductivity (not shown) is calculated according to:

$$\gamma = \gamma_{sat} \left(\frac{\theta}{\theta_{sat}} \right)^{(2b+3)}$$

At field capacity, γ is about $1 \cdot 10^{-9}$ (in [m s^{-1}]) for the pure soil types sand, loam and clay. The γ-values in Maidment (Figure 5.3.2) for sand at 34 % saturation (which corresponds to the ratio of the RCA volumetric soil moisture content at field capacity to the RCA volumetric soil moisture content at saturation, c.f. Table 7), for loam at 53 % saturation (ditto) and for clay at 76 % saturation (ditto) are around to $1 \cdot 10^{-8}$. On the other hand, compared to e.g. Cosby et al. (1984), the Maidment γ-values are about an order of magnitude larger at saturation. In general, soil properties vary considerably in literature. Soil is inherently a heterogeneous medium and difficult to sample representatively.

The McCumber and Pielke values (not shown in Figure 10) trace a concave curve around the HIRLAM2.5 constant value. The differences grow towards soil moisture extremes for all soil types except for peat. The peat hydraulic diffusivity approaches the HIRLAM value with increasing soil moisture. When the hydraulic diffusivities are related to the new thermal properties with the same proportionality factor as in HIRLAM, a moderate dependency of hydraulic diffusivity on soil moisture is resolved. As is seen in Figure soilchar, the new values are almost always lower than the old HIRLAM ones, the two approaching each other at field capacity.

The heat capacity of ice is calculated as discussed earlier. Its heat diffusivity and soil water diffusivity are set as constants. These and the other parameterization constants in the surface/soil/snow scheme are listed in Table 7.

Snow and ice are treated as fractional snow cover and fractional ice cover. For snow, the thickness, in meters of water, is also considered. These can be converted into snow depth in centimeters by considering the typical snow density during the winter. Early in the winter, snow density is the least (around 160-210 kg m^{-3}) and it can increase into more than 300 kg m^{-3} by late spring. This gives a monthly conversion factor varying from 600 to 300 (snow thickness in equivalent water in [m] to snow depth in [cm]). Snow covers the entire grid box whenever the snow is deeper than 0.015 m (of water). Below this threshold, the fractional coverage is given by the ratio of snow thickness to the threshold depth. Snow thickness (H_{snow}) is affected by precipitation in the solid phase, the latent heat flux density and melting of snow. Snow melt occurs whenever surface temperature rises above 273.16 K.

Table 7. Surface/soil/snow parameterization constants in HIRLAM and in RCA.

Constant	Soil type (RCA	HIRLAM	RCA
ρ_{soil} – density of the soil [kg m^{-3}]		Const: $1.3 \cdot 10^3$	Comb. w heat cap.
c_{soil} – soil spec. heat cap. [J $kg^{-1}K^{-1}$]		Const: ½·$4.18 \cdot 10^3$	Comb. w density
$c_{soil}\rho_{soil}$ – dry soil vol. heat cap. [$Jm^{-3}K^{-1}$]		Const: $2.7 \cdot 10^6$	
	1-sand	-	$1.28 \cdot 10^6$
	2-loam	-	$1.35 \cdot 10^6$
	3-clay	-	$1.42 \cdot 10^6$
	4-sand/loam	-	$1.35 \cdot 10^6$
	5-loam/clay	-	$1.35 \cdot 10^6$
	6-sand/clay	-	$1.35 \cdot 10^6$
	7-peat	-	$0.58 \cdot 10^6$
	8-ice	-	T-dep.
κ_{soil} – heat diffusivity of soil [m^2 s^{-1}]		Const: $7.5 \cdot 10^{-7}$	Calculated
ψ_s – matric potential at saturation [m]		Not in use	
	1-sand	-	-0.121
	2-loam	-	-0.478
	3-clay	-	-0.405
	4-sand/loam	-	-0.218
	5-loam/clay	-	-0.786
	6-sand/clay	-	-0.478
	7-peat	-	-0.356
	8-ice	-	-
θ_{sat}, θ_{can}, θ_{wp} – volumetric soil moist. sat./field cap./wilt. point		Not in use	
	1-sand	-	0.395,0.135,0.068
	2-loam	-	0.451,0.240,0,155
	3-clay	-	0.482,0.367,0.286
	4-sand/loam	-	0.435,0.195,0.114
	5-loam/clay	-	0.485,0.255,0.179
	6-sand/clay	-	0.451,0.240,0.155
	7-peat	-	0.863,0.480,0.395
	8-ice	-	-
ρ_{snow} - density of snow [kg m^{-3}]		Not in use	Interp. Table 6.
c_{snow}– snow specifc heat cap. [J $kg^{-1}K^{-1}$]		Not in use	c_{ice} + T-dep.
κ_{snow} – snow heat diffusivity [m^2 s^{-1}]		Not in use	From λ_{ice} and ρ_{snow}
k_{snow} – reduction of κ_0 wrt snow		Const: 2/3	Not needed
zfact – empirical scaling for snow melt		Const: 0.1	Const: 0.3
D_1, D_2, D_3 –layer thicknesses [m], h=heat, w=water	Surface	$7.2 \cdot 10^{-2}$,	$7.2 \cdot 10^{-2}$,
	Middle	$43.2 \cdot 10^{-2}$, (=6·D_1)	6·D_1,
	Deep-soil	$43.2 \cdot 10^{-2}$ (=6·D_1)	9·D_1 (h). 6·D_1 (w).
λ_{water}– soil water cond. diff. [m^2 s^{-1}]		1/7 of κ_{soil} ⇒const.	1/7 of κ_{soil} ⇒ calc.
b – Clapp and Hornberger exponent		Not in use	
	1-sand	-	4.05
	2-loam	-	5.39
	3-clay	-	11.4
	4-sand/loam	-	4.9
	5-loam/clay	-	5.3
	6-sand/clay	-	5.39
	7-peat	-	7.75
	8-ice	-	-
γ_s – hydr. conduc. at saturat. [m s^{-1}]		Not in use	
	1-sand	-	$176 \cdot 10^6$
	2-loam	-	$6.95 \cdot 10^6$
	3-clay	-	$1.28 \cdot 10^6$
	4-sand/loam	-	$34.7 \cdot 10^6$
	5-loam/clay	-	$7.2 \cdot 10^6$
	6-sand/clay	-	$6.95 \cdot 10^6$
	7-peat	-	$8 \cdot 10^6$
	8-ice	-	-

The solving for the surface temperature and moisture in the presence of snow is done in two steps. In the first step, preliminary values for surface temperature and H_{snow} are calculated. The snow thickness obeys the following equation:

$$\frac{\partial H_{snow}}{\partial t} = \frac{F_{snow}\Phi_q}{\rho_{H_2O}} + P_{snow} - M_{snow}$$

The suggestion on precipitation reaching the surface in the solid phase (P_{snow}) by Sigg and Kjellstöm (1995) is included in RCA, i.e. instead of deciding on the phase of precipitation at the surface using surface temperature, the amount of snowfall is given explicitly by the microphysics of precipitation. The snow cover is affected by latent heat flux density, and snow melt (M_{snow}). In the first step, zero snow melt is used. In the second step, the preliminary values of the surface temperature and the snow thickness are then used to calculate the actual snow melt. It is the smaller of the preliminary value for the snow thickness (H_{snow}) and the result of:

$$M_{snow} = \frac{\rho_{snow} c_{snow} D_1 \left(\tilde{T}_s - T_{melt}\right)}{L_i \rho_{H_2O}} \times zfact$$

L_i is the latent heat of fusion. The snow melting point temperature, T_{melt}, is 273.16 K. Note that instead of using the soil density and heat capacity in the snow melt equation (as in HIRLAM2.5), values specific for snow are now used. An empirical correction, *zfact*, to the snow melt rate has been kept also in RCA. Its value in HIRLAM has been set with comparisons to hydrological model results and observations. In RCA, the correction has been reset so that the snow melt rate in the revised scheme would be comparable to empirical data in the Nordic area, i.e. 1-4 cm per day (see Brandt et al., 1987). After calculating the snow melt, the final snow thickness is recalculated and the snow melt is also used to correct the surface layer moisture. The grid average surface temperature is allowed to exceed the snowmelt temperature if snow is melting, as this can well occur when the snow cover is only partial. On ice, however, the surface air temperature is not allowed to exceed the water freezing temperature before all of the ice is gone.

In the land-covered grid points, snow cover and thickness, soil moisture and temperature at the two topmost layers are calculated every time step. T_s, T_d, w_s and w_d are all solved with an implicit time stepping method.

4.3 Surface and soil fields

4.3.1 Surface fields

In the operative HIRLAM, there are both constant and monthly-changing land surface/soil fields (Bringfelt et al., 1995). In weather forecasting over a few days, the following fields are kept constant:

- Fraction of land and water (sea/lakes)
- Fraction of forest
- Surface roughness over land
- Orography
- Ice cover and surface temperature for oceans and lakes

In RCA, the first four fields from the list above are kept constant in the multiyear simulations. Variation of surface roughness over land (with respect to snow cover) is to be introduced at a later stage. For specification of the water surface temperatures and ice cover, different alternatives have been considered.

The original idea was to use the GCM sea surface temperature and sea ice coverage as such. However, due to their horizontal coarseness, GCMs do not tend to include Nordic lakes or a well-represented Baltic Sea either. In the HadCM2 control climate time slice that provides forcing data for RCA, ice never develops on the Baltic Sea. The wintertime north-south temperature gradient is also reversed, with a warmer northern part of the Gulf of Bothnia than the Baltic Sea south of Åland. In the test runs, the use of these GCM data for the regional water bodies caused severe problems in reproducing a reasonable Nordic surface climate, mainly by keeping the near-surface temperature up to 10°C too warm over especially eastern Fennoscandia. For the North Atlantic and Arctic Sea, the HadCM2 sea surface data are better.

This problem with the regional sea (and lake) surface data has led to the construction of proxies for the lake ice cover and for the Baltic Sea ice cover from the closest GCM monthly mean soil layer temperatures. Using different combinations of the soil layers for the sea ice proxy and for the lake ice proxy, different time lags for the ice to form and melt could be designed. At present, the lake ice proxy follows the average of the first and second soil layer temperatures and the Baltic Sea ice proxy follows the average of the second and the third soil layer temperatures. The temperature thresholds for ice and no ice have been set to 272 and 274.5 K for the lake and the sea ice, respectively. The lake ice threshold was fitted into the snow cover climatology in the time slice and the sea ice threshold to the climatological ice extent in the Baltic Sea (Omstedt and Nyberg, 1996). Some examples of the Baltic Sea ice during the 10-year period are shown in Figure 11. The proxies are used only in the Nordic area. For the Atlantic, the HadCM2 ice data are used.

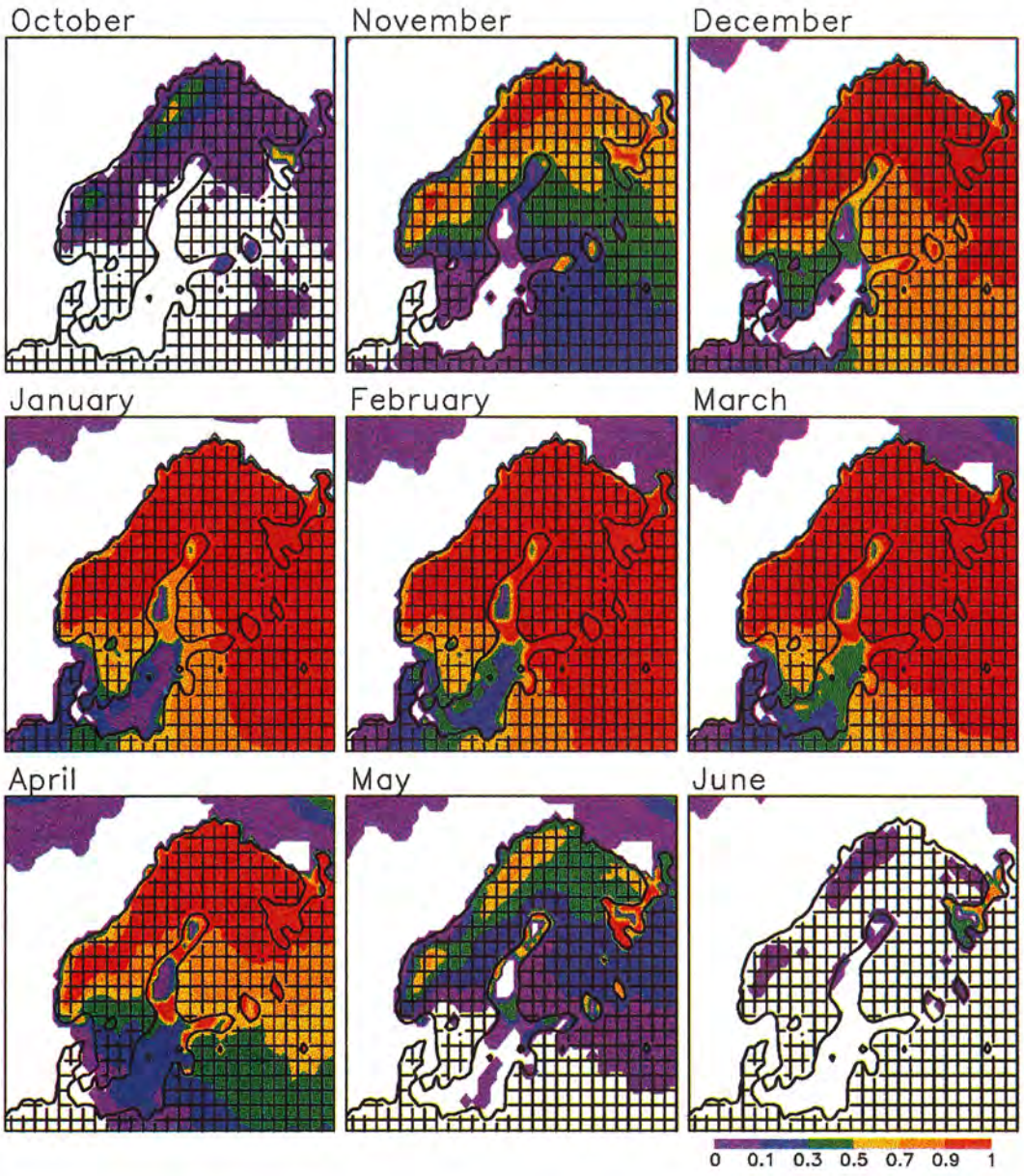

Figure 11. *Nordic region sea/lake ice cover summary for the 2039-2049 HadCM2 control simulation time slice as given by the constructed proxy. The colors show the ice probability in the 10-year time slice (i.e. the number of years (out of the total of ten) during the time slice when there is ice at mid-month. On land areas (hatched part of the region), ice forms only in the water-covered fractions, i.e. the lakes.*

There are some clear deficiencies in the definition of the sea ice proxy. For example, the persistently open spots in the Gulf of Bothnia and the long ice season at the White Sea are not too realistic. However, detailed tuning of the ice proxies was felt to lead into too much subjective tailoring in model domain, especially as the whole ice proxy approach is so approximate. The use of these proxies in climate scenario runs is not straight-forward, either.

The surface albedos are calculated using the snow cover and the fractions of ice, land and forest, as mentioned earlier. Variations with soil moisture or soil type are not considered. Incorporation of vegetation effects and either replacing the soil scheme or

refining the soil properties in the present scheme are important topics in the further development of RCA.

4.3.2 Climatological (deep-soil) fields

The so-called climatological deep-soil temperature and deep-soil moisture are prescribed as monthly means. In RCA, the monthly means are derived from monthly mean data for soil temperatures and soil moistures in the driving GCM time slice. These data are different for different years. Two different ways of constructing the regional model deep-soil temperatures from HadCM2 monthly mean soil layer temperatures have been considered. The first alternative is to match the soil-layer geometry (layer depths and thicknesses) in HadCM2 to that in RCA and to assign a suitable combination of the former data to RCA. The second way is to use the same method as in the old ECMWF soil model, starting from monthly and annual mean surface temperatures and apply suitable phase lag and amplitude damping parameters to obtain the deep-soil temperature (see e.g. ECMWF, 1991). I.e., the monthly mean climatological temperature is calculated from the annual mean, the current monthly mean and the previous monthly mean surface temperature:

$$T_{c\lim}^{month} = (1-c)T_{sfc}^{year} + c\left(aT_{sfc}^{month} + bT_{sfc}^{month-1}\right)$$

In the above, c (=0.77) is the amplitude damping parameter and a (=0.5) and b (=0.5) are the phase lag parameters. This second alternative would have enhanced the cold Nordic bias present in HadCM2. Consequently, the first alternative has been adopted for now. At present, the RCA deep-soil temperature is taken as the average of HadCM2 soil layers 2-3. The temperatures are corrected for differences in orography between the two models. The RCA middle layer soil temperature is initialized with the average of HadCM2 soil layers 1-2. After initialization, the mid-layer temperature is forced by the surface and restored by the deep-soil temperatures, as described earlier. In HadCM2 there are in total four soil temperature layers. Their thicknesses vary somewhat geographically and with the four soil types (ice, fine, medium and coarse).

The RCA climatological deep-soil moisture is also constructed from the HadCM2 data. The relative wetness in RCA deep-soil is defined as the ratio of the monthly mean HadCM2 soil moisture to the monthly mean HadCM2 maximum soil moisture at the same location. To obtain the actual soil moisture content in RCA, this relative wetness is then multiplied by the specified maximum soil moisture value. In HadCM2, the maximum soil moisture content varies geographically through three soil-type-dependent parameters; the volumetric soil moisture content at saturation, the volumetric soil moisture content at wilting point and the rootdepth. Instead of using the maximum soil moisture content distribution from the GCM the largest value which occurs at each point in the time slice(s) is used in the scaling, to represent the field capacity value.

The monthly values for mean deep-soil temperatures and deep-soil moistures derived from the GCM are interpolated in time in the regional model to give a smoother evolution from one day to the next.

4.4 Setting up the RCA simulations

4.4.1 Vertical and horizontal interpolations from GCM to RCA

As RCA is set to have the same vertical levels as the driving GCM, vertical interpolations are kept to a minimum. Due to the different orography and land-sea distribution in the GCM and in RCA, the large-scale surface pressure first in the initialization and then in the boundary zones during RCA integration are matched using the HIRLAM routines.

Otherwise, the interpolation of scalar large-scale fields is done bilinearly in the horizontal. The large-scale u- and v-components are interpolated as scalars to the two points for wind staggering in the Arakawa C-grid and they are then rotated from the HadCM2 regular latitude/longitude-grid to the latitude/longitude-grid in RCA.

4.4.2 Boundary relaxation

As in HIRLAM, the lateral boundary relaxation is performed according to the flow relaxation scheme of Davies (1976). Boundary data are interpolated linearly in time between two consecutive large-scale sets of fields, six hours apart, and applied over a narrow zone just inside the outer boundary of the regional domain. The relaxation has the form of

$$X_i = (1-\alpha_i)X_i + \alpha_i X_i^b$$

where X is the relaxed variable (horizontal wind component, surface pressure, specific humidity or temperature), α is the relaxation weight, i counts the grid-point distance from the outer edge of the boundary zone (where i=1) and b designates a value from the driving model. With the Eulerian advection, the form for α by Kållberg (1977) is used:

$$\alpha_i = 1 - \tanh\left(\frac{2(i-1)}{N-4}\right)$$

N is the width of the relaxation zone in grid-point units (at present in RCA, N = 8). In the normal mode initialization (N = 4) and in the case of semi-Lagrangian advection (N = 8), a cosine form for α is typically used instead:

$$\alpha_i = \frac{1}{2}\left[1+\cos\left(\frac{\pi(i-1)}{N}\right)\right]$$

The form of these two relaxation profiles is shown in Figure 12 over an eight-point boundary zone. Point number one is at the outer boundary, where full weight is given to the large-scale data.

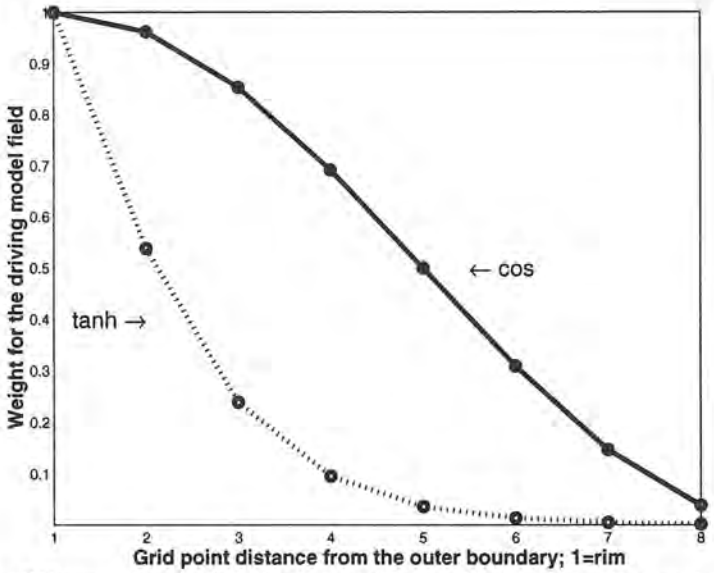

Figure 12. *Two different forms for the lateral boundary relaxation weights.*

The Davies-type lateral relaxation of specific humidity and cloud water can be replaced in RCA with an optional inflow-outflow condition (see Giorgi et al., 1993b). According to it, whenever flow is directed out of the regional model domain, the outermost boundary zone specific humidity and cloud water values are extrapolated from the closest four upstream grid box values. With a flow into the regional domain, the time-interpolated driving model values are used throughout the boundary zone. The idea is to allow moisture to flow out of the regional model without hindrance and to avoid spuriously large amounts of precipitation occurring in the boundary zone.

Another option in the lateral relaxation is to relax (to the driving model) even the orography using the same weights as for surface pressure. To avoid a mismatch between the very first two boundary data sets, the relaxation of orography would have to be made the for an eight-point boundary zone even in the normal mode phase.

Finally, the formulation of the deep-soil processes, as explained earlier, is also a form of boundary relaxation, this time at the lower boundary in the model domain. In the same manner, the GCM sea surface state serves as the final boundary condition for RCA. The large-scale SSTs and sea-ice coverage, at the appropriate RCA grid points, are used as the lower boundary condition for the atmospheric calculations. Regionally, though, corrections are made to the ice cover, as explained earlier. It is noted that when the ice proxies prescribe an ice cover for a particular grid box, the SST information is not used (after the ice melts, the SST information is used, of course).

4.4.3 Restart utility

In long model runs, it is practical to be able to stop and restart the run, without the stop/restart affecting the results. In other words, the result from a stopped and restarted run should be exactly the same as from a continuous run. To do this, enough information has to be stored. Restarts allow for more flexible long integrations, as a, say, ten-year run can be run in many parts, between which the latest results can be scanned for eventual errors in the model. The archiving of restart data allows also for interesting periods to be studied in more detail, for example the sensitivity to new parameterizations can be tested, and for obtaining extended output from a desired

period. Restarts can also be utilized to simplify studying unexpected problems at a lower computational cost in the case of a run crashing without a clear reason.

The RCA integrations are dynamically backed up with the NQE checkpointing utility at T3E/NSC. However, each checkpoint requires too much storage to be a practical means for longer-term archiving, so also explicit "dumps" are done at regular intervals. These "dumps" define the full state of the model. They include two time-levels of the prognosed variables (u, v, T, q, surface pressure and cloud water, top and mid-layer soil temperature and moisture, snow depth, sea surface roughness, total cloudiness) and some of the tendencies. The necessary housekeeping variables are also stored. If the semi-Lagrangian scheme is used, then vertical velocities and trajectory data have to be included as well. The dumps are done at the full machine-defined precision.

4.4.4 On-line statistics

The progress and performance of RCA is monitored on-line during model runs by calculating some statistics every time step. These include the area mean surface pressure, temperature, specific humidity, cloud water and the area mean absolute surface pressure tendency. The maximum wind speed and its location are also recorded. The regular output of model level data and post-processed data (see next section) is also used for monitoring purposes.

4.5 Model output

The produced output can be divided into four parts. The first two, the on-line statistics and model dumps, were already mentioned. The other two are the regular output of variables on model levels and the regular output of postprocessed variables at the surface, near the surface and on some pressure levels. Model level data are saved in the long integrations only from the topmost and lowest model level, to allow for monitoring of the upper and lower boundaries of the atmospheric domain. If the integration is to be followed by another nesting step, the prognosed variables have to be stored at all model levels. The archiving in model level data files is done for horizontal wind components, temperature, specific humidity, cloud water, cloud cover, surface pressure and roughness lengths. The postprocessed output is richer and it is given in Table 8. These latter data are for the scientific evaluation of the model performance as well as for the end-use of the results in scenario construction and impact studies. Thus, they must be specified accordingly. Note that the surface energy fluxes at every location are calculated and post-processed taking into account the fractions of land and water. If land (water) covers less than 1 % of the grid point area, only the value for water (land) is post-processed.

Table 8. Postprocessed model output, done at all horizontal grid points.

Variable	Output at level/layer	Output interval
Temperature	Deep soil layer	Every six hours
Temperature	Intermediate soil layer	Every six hours
Temperature	Surface	Every six hours
Temperature max	Surface	Every six hours
Temperature min	Surface	Every six hours
Temperature	2 m	Every six hours
Temperature max	2 m	Over six hours
Temperature min	2 m	Over six hours
Temperature	850, 700, 500, 300, 100 hPa	Every six hours
Soil moisture	Deep soil layer	Every six hours
Soil moisture	Intermediate soil layer	Every six hours
Soil moisture	Surface	Every six hours
Specific humidity	2 m	Every six hours
Relative humidity	850, 700, 500, 300, 100 hPa	Every six hours
Wind components (u,v)	10 m	Every six hours
Wind speed max	10 m	Over six hours
Wind components (u,v)	850, 700, 500, 300, 100 hPa	Every six hours
Vertical velocity	850, 700, 500, 300, 100 hPa	Every six hours
Geopotential height	850, 700, 500, 300, 100 hPa	Every six hours
Mean Sea Level Pressure		Every six hours
Total cloud cover	Surface	Every six hours
Sunshine hours	Surface	Accumulated for six hours
Convective precipitation	Surface	Accumulated for six hours
Large-scale precipitation	Surface	Accumulated for six hours
Snow depth	Surface	Every six hours
Ice cover	Surface	Every six hours
Latent heat flux	Surface	Six hour average
Sensible heat flux	Surface	Six hour average
Momentum flux	Surface	Six hour average
Net short-wave radiation	Surface	Six hour average
Net long-wave radiation	Surface	Six hour average
Net short-wave radiation	Model top	Six hour average
Net long-wave radiation	Model top	Six hour average
Albedo	Surface	Every six hours
Surface roughness	Surface	Every six hours
Runoff	Surface	Six hour average
Deep-soil runoff	Soil mid-layer	Six hour average
Vertically integrated cloud water	Total column	Six hour average
Vertically integrated water vapor	Total column	Six hour average
Profiles of u,v,T,q and cloud wat.	At 23 locations	Every six hours

Vertical profiles are stored from 23 locations (see Figure 13). Some of the locations coincide with Nordic meteorological sounding sites and the rest are locations where the driving GCM grid and the RCA grid coincide closely.

Figure 13. *Locations for which vertical profiles are saved in RCA.*

4.6 Summary of the main changes to the HIRLAM2.5 code

A number of modfications to HIRLAM2.5 have been tested for use in RCA, mainly to improve the model performance when running it over several years. Many of the modifications have been discussed earlier in this report. Here a summary is made of the main ones:

- The calculation of the solar declination and the solar constant is done daily in RCA (done only in the beginning of HIRLAM runs). A 360-day year (with twelve 30-day months) is used, as in the driving GCM.
- The boundary relaxation scheme has been complemented with an optional inflow/outflow condition for moisture and with a possibility for including also orography in the relaxation.
- In the condensation scheme, the calculation of saturation specific humidity is done with the same temperature dependency as the cloud ice content diagnosis (in HIRLAM this is not true). The output relative humidity is calculated with respect to a water surface.
- Some details have been added to the ice-snow-surface-soil scheme. The single HIRLAM2.5 soil type with constant thermal and hydraulic properties has been replaced by eight FAO-Unesco soil types. These new soil types have each been given their individual thermal and hydraulic properties which also depend on soil moisture. The sea and lake ice are treated with proxies generated from the driving GCM data. The soil and snow equations have been revised so that the heat capacities and heat diffusivities entering in the surface and mid-layer temperature equations are now explicitly combined from the bare soil values and the snow values. The snow has been given more realistic thermal properties than those in HIRLAM2.5 and in RCA there is a crude accounting for aging of snow by altering the snow density over winter. Evaporation from the snow cover has been reduced in RCA compared to that in HIRLAM2.5.
- The standard HIRLAM output has been complemented with additional variables, including accumulated and averaged quantities.

- Other differences in RCA from the HIRLAM2.5 include changes to the vertical structure (RCA uses the driving GCM layers, including the specification of the half levels) and the climatological deep-soil data.

Some of these changes might be considered to be relevant also in the operational use of HIRLAM in weather forecasting on a time scale of few days. The changes that reflect processes and formulations having effect or varying on longer time scales are not relevant for the operational use of HIRLAM.

5 Results from the first extended simulation

5.1 Introduction

In the first 10-year RCA simulation the following set-up has been used (the modifications with respect to HIRLAM2.5 were listed in the previous section):

- model domain as shown in Figure 6 (82 by 114 point grid, 0.4° horizontal resolution, 19 levels in the vertical, 5 minute time step)
- the Eulerian transport scheme, the 4th order horizontal diffusion scheme (not switched off at steep orography) and the Louis vertical diffusion scheme with the oceanic heat and moisture surface drag coefficients as in Makin and Perov (1997)
- a 10-year time slice from the HadCM2 control run (September 2039 – November 2049 in HadCM2 model time) for the lateral driving data as well as for constructing the deep-soil climatological fields (these data are from a control climate simulation, i.e. run with unperturbed greenhouse gases!).
- the lake and Baltic Sea ice cover as explained in Section 4.3 with the HadCM2 SSTs for ice-free water surfaces, including the lakes
- lateral relaxation is applied to u, v, T, q, surface pressure and cloud water with the tanh-shape relaxation weights in an eight-point wide boundary zone (neither the inflow/outflow formulation for moisture nor the relaxation of orography are in use)

In this chapter, the focus is on a general evaluation of the RCA performance. The emphasis is on the Nordic region. The regional model results are compared to the driving global model data to see if the regional climate simulation improves in the regional model. In some cases, the regional model results are also compared to observations and analyzed observations from the 1961-90 period (gridded monthly means and some station data). *Note that rather than presenting results variable by variable, the discussion is organized so that it starts with a view on large scale time mean results, continues then with a look at results on the regional and local scales, eventually ending in a presentation of basic measures of temporal variability.*

Much of the discussion focuses on 10-year mean statistics from the regional model control run and the driving global model data. The very first three months of the simulation have been omitted to avoid obvious spin-up effects in soil moisture. The large-scale atmospheric circulation and surface climate are considered first, comparing the RCA results and the driving HadCM2 results in the whole regional model domain. Then, a closer look is taken on some aspects in Northern Europe. The ability of RCA to reproduce the local temperature and precipitation statistics at Swedish meteorological stations is considered next. Finally, some remarks are made on the variability of the regional model climate at daily and interannual time scales.

5.2 Large-scale climate in RCA and differences to HadCM2

5.2.1 Seasonal mean sea level pressure, 500 hPa height, 850 hPa temperature and 300 hPa zonal wind in RCA and HadCM2

The RCA 10-year mean winter (DJF) and summer (JJA) mean sea level pressure, 500 hPa height, 850 hPa temperature and 300 hPa zonal wind component are shown in Figure 14. The differences between RCA and HadCM2 simulation are also indicated (with thin solid lines where the difference RCA-HadCM2 is positive, stippled lines for zero difference and dashed lines for negative difference). For calculating the differences, the HadCM2 data were bilinearly interpolated to the RCA grid.

The large-scale circulation of the driving GCM is maintained to a large degree in RCA. One of the differences is a persistent turning of the MSLP isobars in the boundary relaxation zones, in particular at the main inflow zone in the west and at the main outflow zone in the east. This turning is seen best when the flow is perpendicular to the lateral boundary, and is suggestive of a problem in the boundary forcing process (the boundary relaxation is not tuned well in RCA or maybe the scale transition between the driving model and the regional model is too large). Although the boundary relaxation zones are excluded from Figure 14, this feature is still visible e.g. by the positive RCA-HadCM2 difference in MSLP in the western/northwestern part of the figure domain. In addition, the MSLP difference field has a lot of structure over high topography in RCA, which is associated with the method of reduction of the actual surface pressure to the mean sea level is done in the two models.

The RCA-HadCM2 differences in the 500 hPa height are, like those in MSLP, positive over the northern Atlantic. Further east in the model domain, in particular over central Europe, the sign of the difference is reversed. The negative height biases in RCA compared with HadCM2 reflect a predominant cold bias in the lower tropospheric temperatures, seen from the maps for the 850 hPa temperature. The cold bias is largest over Central Europe, up to 1.5°C in summer. This results in an increased meridional height gradient and strengthened zonal winds in the middle and upper troposphere in the southern part of the domain. Over southern Scandinavia, on the other hand, the time-averaged zonal wind is slightly reduced.

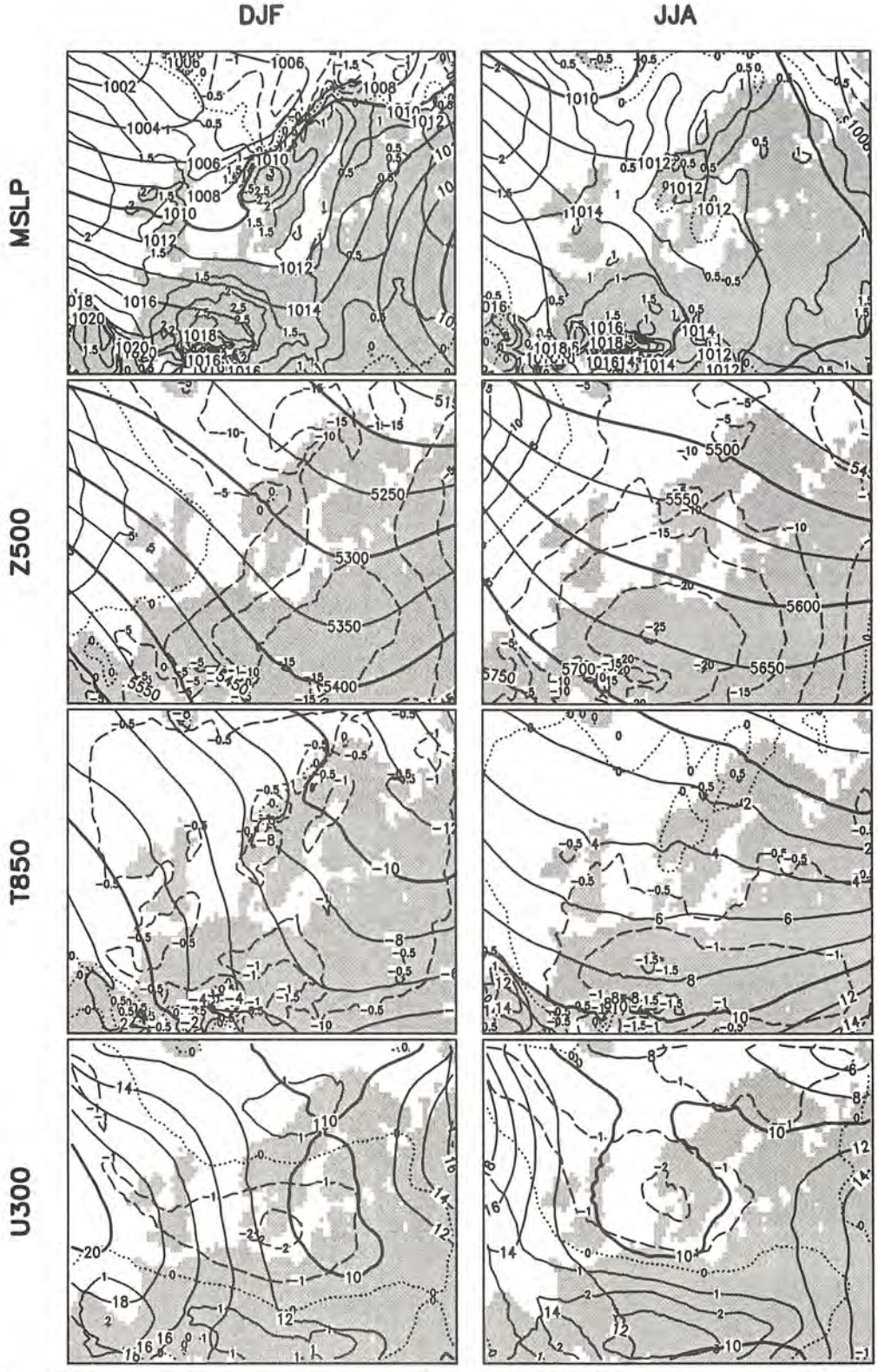

Figure 14. *Aspects of large-scale climate from the RCA 10-year downscaling for the winter (DJF) on the left and for the summer (JJA) on the right. From the top: 1) mean sea level pressure [hPa]; 2) 500 hPa height [m]; 3) 850 hPa temperature [°C]; 4) 300 hPa zonal wind [m s^{-1}]. The fields from RCA are shown with the lines with the large labels, and the differences between RCA and HadCM2 with the lines with small labels. The boundary relaxation zones are excluded.*

5.2.2 Sea level pressure variability in RCA and HadCM2

As an indicator of the daily variability in the atmospheric circulation, the total intraseasonal variances in sea level pressure in the two models in winter and in summer are compared in Figure 15. To avoid biases associated with the smoothening of pressure fields in horizontal interpolation, the standard deviations for HadCM2 were first calculated in the HadCM2 grid and then interpolated to the RCA grid.

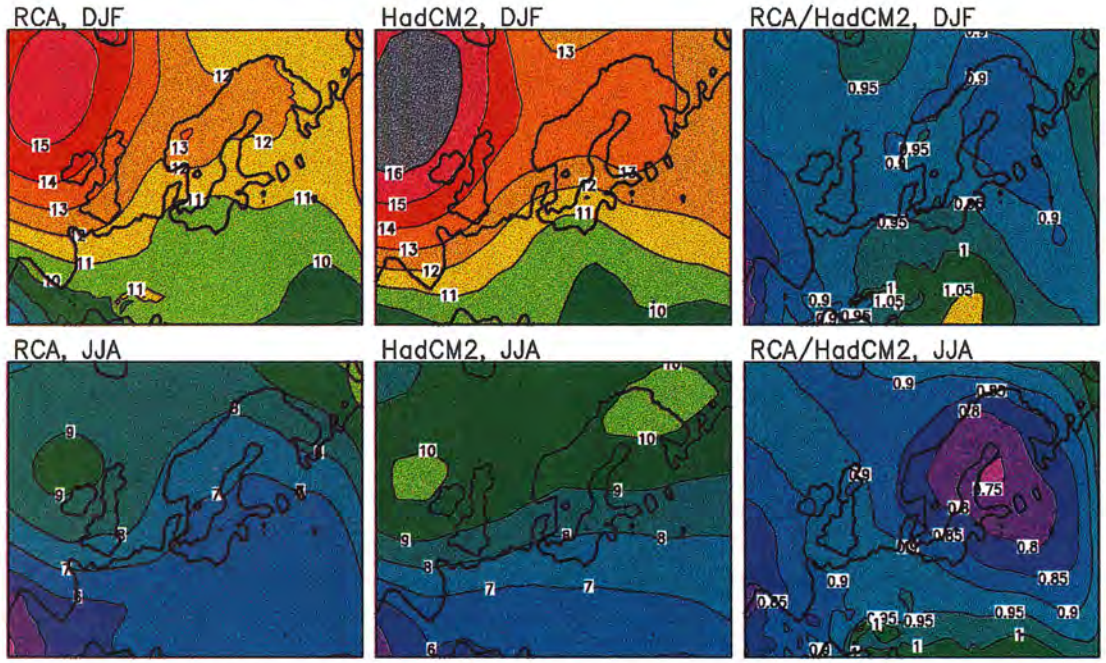

Figure 15. *Total 10-year intraseasonal standard deviation [hPa] of sea level pressure in winter and in summer in RCA and in HadCM2, and the ratio between RCA and HadCM2.*

The overall spatial distribution of variability in the two models is closely similar (in particular in winter), as is the seasonal contrast with more variability in winter than in summer. However, excluding the southern and easternmost parts of the RCA domain, the variability in RCA is somewhat smaller than that in HadCM2. This is actually true for all seasons, even though the difference is in relative terms largest in summer. Probable contributors to these differences are the slight intermodel differences in the time mean circulation. For example, the general southward shift in variability in RCA coincides with the strengthening of the upper tropospheric zonal winds in the southern part of the model domain with weakened winds further north (c.f. Figure 14). In addition, differences in boundary layer frictional damping and other physical parameterizations may play a role, as well boundary relaxation problems.

Another way of comparing the pressure variability in the two models is applied in Table 9.

Table 9. *10-year annual and area mean frequency [%] of different values of sea level pressure [hPa] in RCA and HadCM2.*

	< 960	**960-970**	**970-980**	**980-990**	**990-1000**	**1000-1010**	**1010-1020**	**1020-1030**	**1030-1040**	**1040-1050**	**>1050**
RCA	0.006	0.064	0.53	2.4	9.4	26.0	38.2	20.0	3.2	0.15	0.008
HadCM2	0.011	0.130	0.79	3.3	11.0	26.3	34.4	19.5	4.3	0.27	0.006

Here, the frequencies of different values in sea level pressure in both the HadCM2 and the RCA simulation are shown. The frequencies are averaged over the whole RCA domain, excluding the boundary relaxation zones and high orography (surface height over 1000 m in RCA. The statistics include all seasons, but very high and low pressure values are naturally most frequent in winter when the variability is largest. The differences are as expected from the smaller standard deviation and the generally slightly higher time mean pressures in RCA than in HadCM2. Both strong highs (> 1030 hPa, with the exception of the very rare class of > 1050 hPa) and deep lows are less common in RCA than in HadCM2. The difference is more marked in the deep lows, though. Pressure values below 970 hPa are 50 % less frequent in RCA than in HadCM2. Together with the fact that the frequencies in this part of the distribution fall quasi-logarithmically by a factor of roughly 10 for each 10 hPa pressure decrease, this suggests that the deepest cyclones are about 3 hPa shallower in RCA than in HadCM2.

5.2.3 Area mean differences in RCA and HadCM2

A selection of monthly area mean differences RCA-HadCM2 (biases) is listed in Table 10. Again, the RCA boundary relaxation zones have been excluded. For surface air (two-meter) temperature and precipitation, area means for land grid boxes only are also given. The interannual standard deviations are also shown to characterize the stability of these differences.

The small cold bias in RCA, compared with HadCM2, is in the winter restricted to the lower troposphere. In summer and early fall it extends well up to 500 hPa. At 300 hPa, systematic differences are in all months small. Area mean differences in surface air temperature are similar to those in 850 hPa temperature. They are much larger over land than over sea, where the use of the HadCM2 SSTs strongly constrains the temperature evolution except in the presence of ice. The domain-average land-area cold bias approaches 1.5°C in August and September, but it is negligible in May and June.

In terms of the domain-averaged precipitation, the totals are relatively close during all seasons, although there is generally slightly more precipitation in RCA. The difference is more systematic over sea areas. Over land RCA simulates somewhat less summer precipitation than HadCM2. However, there is a marked difference in the partitioning of precipitation between the large-scale and convective components. This is the case in particular over land areas, where RCA simulates much more large-scale precipitation but substantially less convective precipitation than HadCM2. Although the partitioning between large-scale and convective precipitation is somewhat ambiguous, one interpretation of this is that RCA would underestimate convective precipitation over land (alternatively the fraction of convective precipitation in HadCM2 is too large). Over sea, the precipitation is partitioned in a more similar manner in the two models, but there is an excess of precipitation in RCA compared with HadCM2. This stems in the winter from the convective and in the summer from the large-scale component.

Table 10. *10-year monthly means and interannual standard deviations of area mean differences between the downscaling and the driving (RCA-HadCM2) simulation. The two-meter temperatures in the two models are reduced to the same height with a lapse rate of 5.5°C km^{-1}.*

	Jan	Feb	Mar	Apr	May	June	July	Aug	Sep	Oct	Nov	Dec
T (300 hPa)	0.3±	0.1±	0.2±	0.1±	0.0±	-0.2±	-0.3±	0.0±	0.0±	0.1±	0.1±	0.1±
	0.2	0.2	0.2	0.2	0.3	0.2	0.4	0.3	0.2	0.2	0.2	0.2
T (500 hPa)	0.2±	0.0±	0.2±	-0.1±	-0.2±	-0.6±	-0.7±	-0.6±	-0.6±	-0.2±	-0.1±	-0.1±
	0.3	0.3	0.3	0.3	0.3	0.4	0.5	0.3	0.4	0.3	0.5	0.4
T (850 hPa)	-0.5±	-0.7±	-0.4±	-0.5±	-0.2±	-0.2±	-0.4±	-0.6±	-0.8±	-0.4±	-0.5±	-0.7±
	0.4	0.3	0.4	0.4	0.4	0.4	0.5	0.4	0.4	0.3	0.4	0.4
T (2 m)	-0.3±	-0.6±	-0.4±	-0.2±	0.0±	-0.1±	-0.4±	-0.8±	-0.7±	-0.2±	-0.3±	-0.3±
	0.4	0.4	0.3	0.4	0.3	0.2	0.4	0.3	0.4	0.2	0.4	0.4
T (2 m, land)	-0.7±	-1.0±	-0.7±	-0.4±	0.0±	-0.1±	-0.9±	-1.5±	-1.4±	-0.6±	-0.8±	-0.6±
	0.6	0.6	0.5	0.7	0.5	0.4	0.8	0.6	0.7	0.4	0.6	0.6
T (2 m, sea)	0.2±	0.1±	0.1±	0.2±	0.1±	0.0±	0.1±	0.0±	0.0±	0.2±	0.3±	0.3±
	0.2	0.2	0.2	0.1	0.1	0.1	0.1	0.1	0.1	0.1	0.2	0.1
Large-scale Prec	6±	4±	8±	11±	16±	15±	13±	11±	12±	11±	6±	6±
[mm month^{-1}]	4	3	6	3	3	3	3	4	4	4	7	6
Large-scale Prec	9±	8±	12±	17±	23±	21±	17±	15±	18±	18±	10±	10±
(land)]	5	4	9	6	5	4	6	6	7	7	7	6
Large-scale Prec	1±	-1±	2±	4±	9±	9±	9±	7±	6±	3±	2±	1±
(sea)]	6	5	3	5	4	4	4	4	5	5	10	7
Conv Prec	3±	3±	2±	-3±	-10±	-16±	-13±	-8±	-4±	-1±	0.6±	1.9±
[mm month^{-1}]	3	3	2	2	3	2	4	3	2	3	4	4
Conv Prec	-7±	-6±	-4±	-10±	-20±	-28±	-23±	-16±	-14±	-12±	-11±	-9±
(land)	2	3	2	2	4	4	6	5	4	4	3	3
Conv Prec	13±	12±	9±	5±	1±	-2±	-3±	-1±	5±	9±	11±	14±
(sea)	4	5	4	5	2	3	6	3	5	5	6	6
Total Prec	8±	7±	10±	8±	7±	-0±	0±	3±	8±	10±	7±	7±
[mm month^{-1}]	3	3	5	3	4	3	5	4	3	4	5	3
Total Prec	2±	3±	7±	7±	3±	-7±	-6±	-1±	3±	7±	0±	1±
(land)	4	3	7	5	6	5	7	5	5	5	6	5
Total Prec	14±	11±	11±	9±	11±	7±	6±	5±	10±	11±	14±	15±
(sea)	5	5	5	4	4	5	4	4	4	3	8	4

The near-surface temperature differences between HadCM2 and RCA, the differences in accumulated precipitation as well as other surface climate factors are considered further in the next section.

5.3 European surface climate in RCA and differences to HadCM2 – Seasonal mean two-meter temperatures and precipitation

In the previous section, it was indicated that in the domain- and time-averaged sense, the differences in the free troposphere climate in RCA compared to HadCM2 are relatively small. At the surface, the significance of having a different model resolution and different parameterizations increases and the differences between the two models grow more pronounced.

The 10-year seasonal mean RCA two-meter temperatures and their differences to those in HadCM2 are shown in Figure 16. The mean 10-year seasonal (three-month) total precipitation averages are shown in Figure 17. The RCA data have been reduced to the HadCM2 orography[1]. In addition, the grid points in which the land-sea distributions differ significantly have been left blank in the figure[2].

Differences in the two-meter temperature are smallest over the Atlantic Ocean, where the surface air temperatures are largely determined by the SSTs taken directly from the HadCM2 simulation. Over most of the land area in the model domain, RCA exhibits a slightly cooler climate than HadCM2. The largest difference in this direction occurs in summer and fall in Central Europe. In the Nordic area, the RCA summer temperatures are slightly warmer than HadCM2's and in the other seasons, differences occur in both directions. The RCA winter climate in most parts of Sweden, and especially in the Baltic Sea area is colder than in HadCM2 (see Figure 16). By contrast, parts of the northern Fennoscandia are warmer in winter in RCA than in HadCM2. As will be discussed, this is due to the existence (lack) of sea ice in RCA (HadCM2). In spring, the differences between the models are small over land, but the prescribed ice cover in RCA still forces its near-surface temperatures over the Baltic Sea a few degrees lower. In summer, RCA slightly reduces the cold bias in HadCM2, up to 1-2°C in central and northern Sweden. In fall, western Fennoscandia is colder and eastern Fennoscandia is warmer in RCA than in HadCM2. Some of these differences indicate an improvement over the HadCM2 simulation, but this is not true in all cases. In addition to the use of the prescribed ice cover in RCA, which has a very marked local effect on the temperatures, the differences between RCA and HadCM2 may be affected by the specified soil characteristics and the chosen snow cover parameterization. Of course, the model resolution plays a role as well in whipping up local-to-regional scale differences.

It is important to recall that HadCM2 does not produce a perfect simulation of the present-day Nordic climate. With respect to observations made during 1961-1990 (Hulme et al., 1995), HadCM2 suffers from a cold summer bias of up to 2-4°C over the Nordic Countries (Räisänen (manuscript); see also Section 3 in this report). There is a slight cold bias in some parts of the Nordic area in winter, but also a warm bias of 2-4°C around the Bothnian Bay, which is unrealistically lacking sea ice in HadCM2. In the intermediate seasons, cold biases dominate but are not as large (and in the fall not as spatially uniform) as in summer.

In precipitation, the largest differences are found over the Alps, the Pyrenees and the Scandinavian mountains, which are all resolved much better in RCA than in HadCM2. Another difference to HadCM2, which is apparently not explained by the finer resolution alone, is a decrease of summer precipitation in Central Europe.

---

[1] Using a lapse rate of 5.5°C km^{-1}. This value is close to the "European mean" lapse rates used by Hulme et al. (1995). Most likely, however, it is not very representative in Northern Europe in winter when temperature frequently increases with height in individual weather situations.

[2] For the RCA grid points in which the fraction of land cover in RCA is over (below) 50 %, the differences from HadCM2 are shown only if the bilinearly interpolated HadCM2 fraction of land is over (below) 50 % as well.

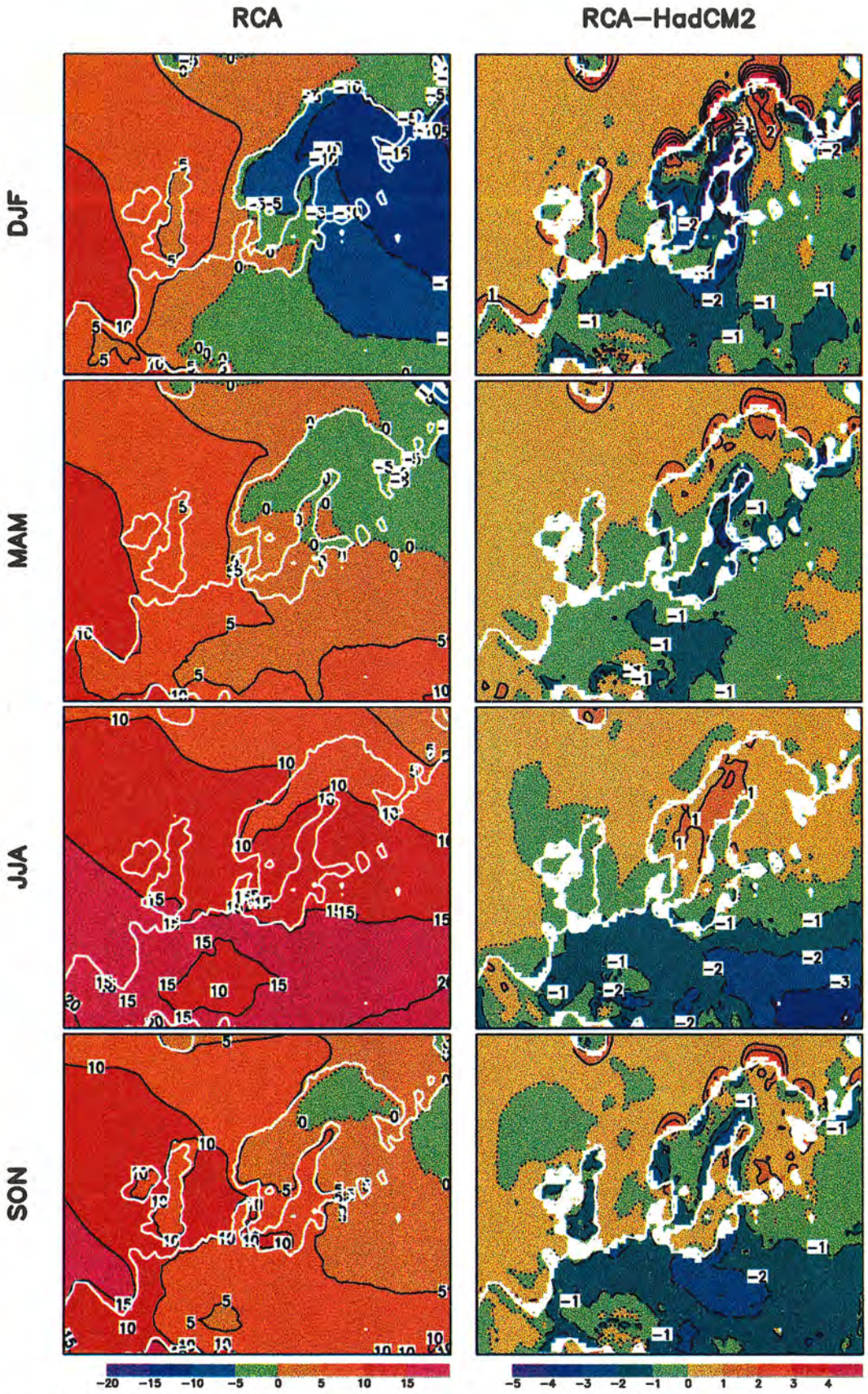

Figure 16. *The 10-year mean seasonal RCA temperatures [°C] are on the left and the RCA-HadCM2 differences on the right. The seasons are, from the top down: 1) DJF; 2) MAM; 3) JJA; 4) SON.*

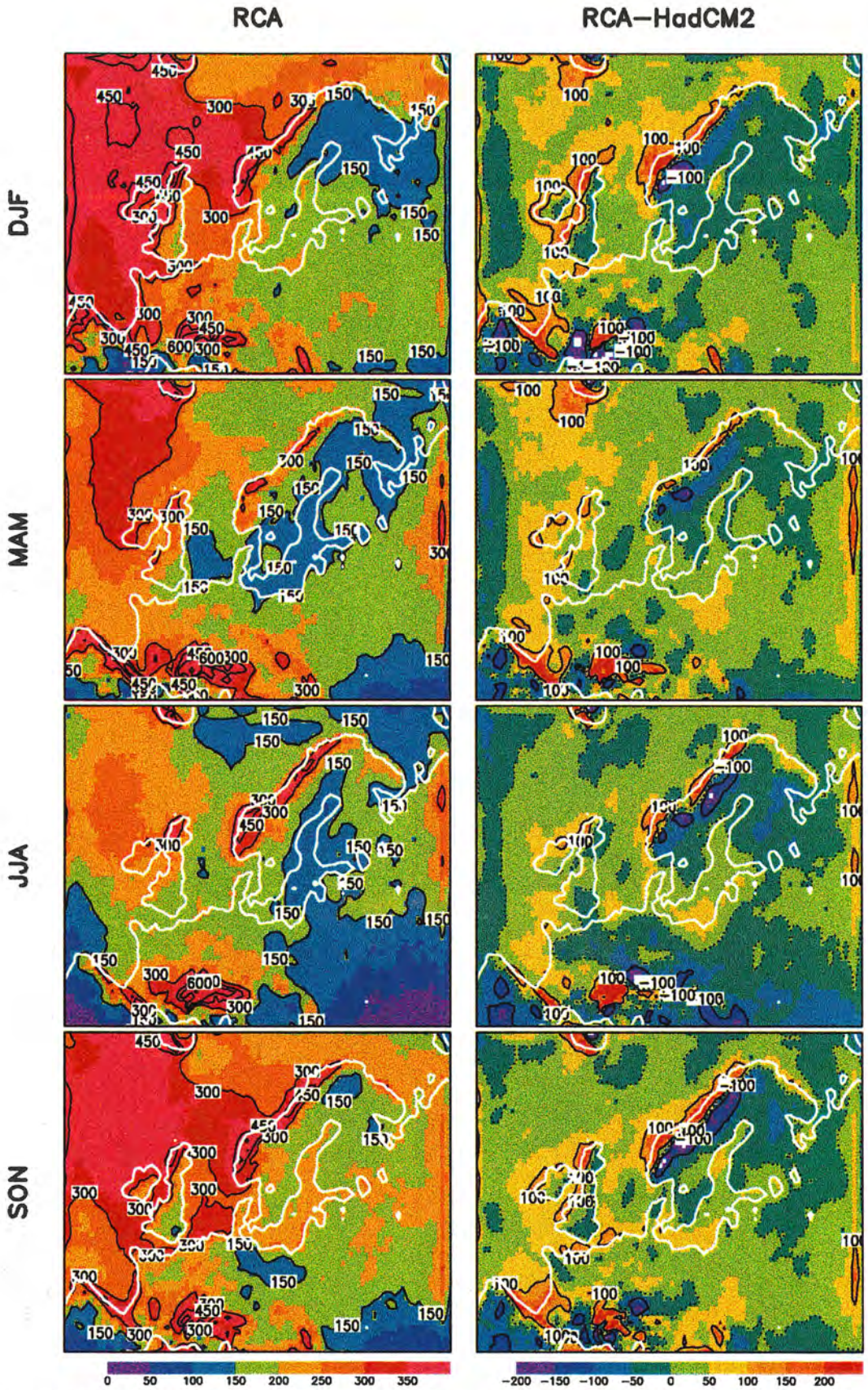

Figure 17. *The 10-year mean RCA seasonal precipitation [mm in 3 months] is on the left and the RCA-HadCM2 differences are on the right.*

In the Nordic area, a dominant feature in the RCA-HadCM2 precipitation difference is the two-pole pattern at the Scandinavian mountain chain. Precipitation is larger (smaller) in RCA at the western edge of the mountains (at the lee of the mountains) than in HadCM2. The precipitation maximum along the Norwegian coast is sharper in RCA than in HadCM2. The general decrease of precipitation in RCA, with respect to that in HadCM2, extends to Finland in the east and indicates a strengthened shadowing effect due to the sharper and higher appearance of the mountain range with the higher resolution. While there are deficiencies even in the RCA simulated precipitation, it represents a general improvement over that of HadCM2. More discussion on the precipitation follows later in this report.

There are interesting features in the climate simulated by RCA in different parts of the domain that could be discussed in much more length. However, the focus is now turned on the simulation of the regional and local climate in the Nordic area.

5.4 Nordic surface climate in RCA and differences to HadCM2

For a first more detailed look at the RCA control climate in the Nordic area, the 10-year annual mean values of various components of the hydrological cycle are shown in Figure 18. The 10-year Nordic two-meter temperature distribution is also shown.

5.4.1 Two-meter temperature

The modeled two-meter temperature distribution follows well the observed conditions in the Nordic area. In agreement with observations, the model simulation exhibits the south-north temperature gradient in Sweden. In the north, the west-east temperature gradient (it is colder close to the Scandinavian mountains and warmer at the coast of the Gulf of Bothnia) is also captured, as well as the feature that in the south the inland is slightly colder than the east and west coasts. There is a general cold bias of about 1°C (compared to the 1961-90 climate, see e.g. Raab and Vedin, 1995) over Sweden in RCA, though. For example, the simulated annual mean temperature at the southern tip of Sweden is +7°C in RCA. The observed annual mean is +8°C. Another example is that the 0°C isotherm rounds the end of the Bothnian Bay in RCA, whereas in observations it is about one hundred kilometers further to the north. It should be added that the simplified ice treatment in RCA shows through in the two-meter temperatures over the Gulf of Bothnia. The two minima in the ice cover proxy show up as local warm spots (c.f. Figure 11 in Section 4).

5.4.2 Evaporation

RCA simulates somewhat less evaporation than what observational data indicate in Sweden. The estimated 1961-90 mean annual evaporation was 400-500 mm in southern Sweden, with local maxima at the large lakes Vänern and Vättern, and in an area a bit north of the southern tip of the country (Raab and Vedin, 1995). In the central and northern parts of the country, the spatial distribution of the 1961-90 estimated evaporation has a gradient from the coast in the east (up to 400 mm evaporation) to the mountains along the western border (100-200 mm). These south-north and east-west contrasts are reproduced in RCA and even the local maxima in southern Sweden are

captured. However, the amount of evaporation is generally underestimated by about 20-25 % in the model, compared to the values in Raab and Vedin (1995).

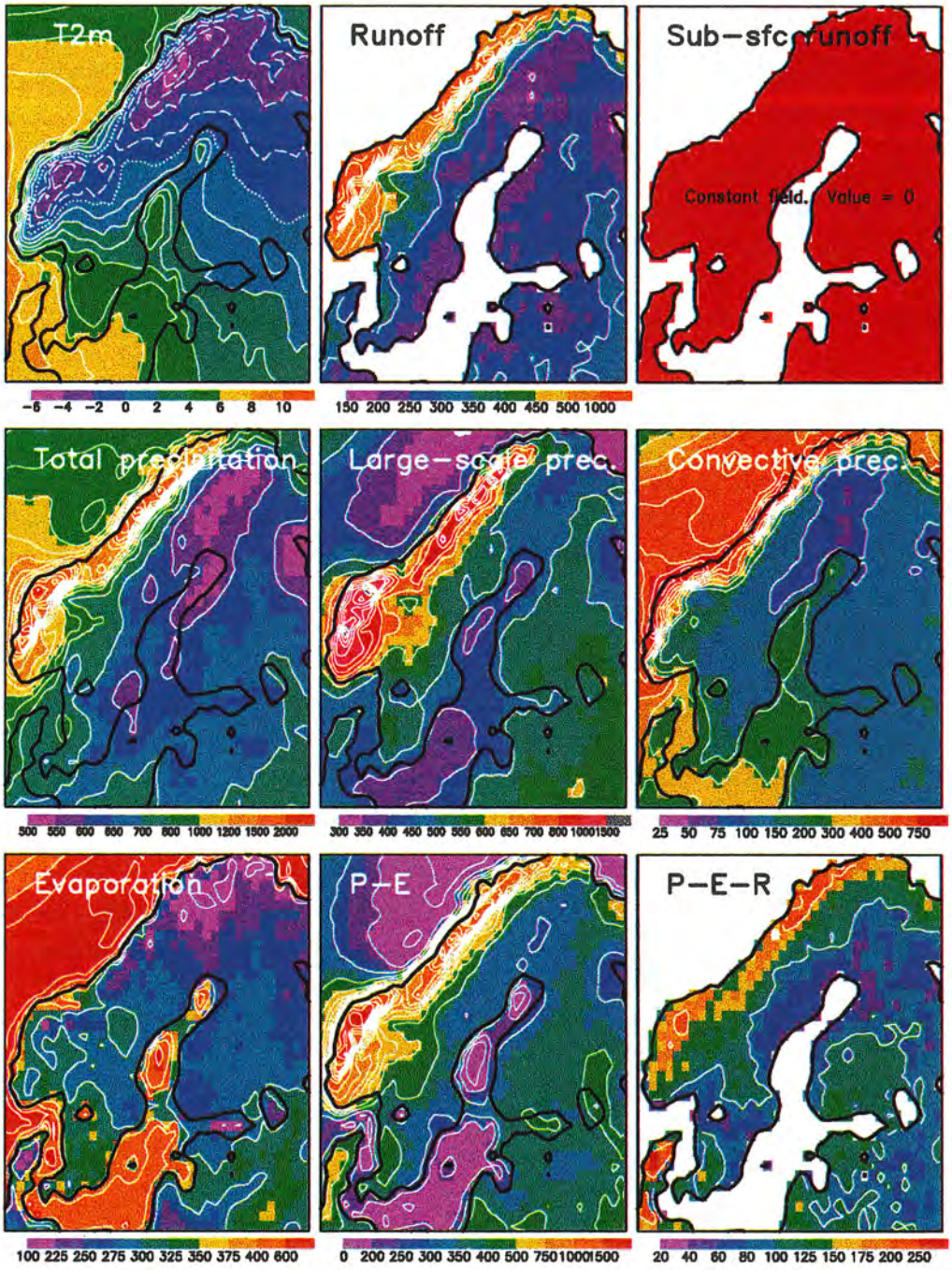

Figure 18. *Top row from left to right: 10-year annual means of two-meter temperature [°C], surface runoff [mm] and sub-surface runoff [mm]. Middle row from left to right: 10-year annual means of total precipitation [mm], large-scale precipitation [mm] and convective precipitation [mm]. Bottom row from left to right: 10-year annual means of evaporation [mm], the difference between precipitation and evaporation (P-E) [mm] and the residual of precipitation, evaporation and runoff (P-E-R) [mm]. Note that the scales differ. Isolines are drawn every 1°C for the two-meter temperature and every 100 mm for the other parameters.*

5.4.3 Runoff

In addition to the lack of evaporation in RCA, also the point runoff seems to be underestimated. The "point runoff" occurs locally, when the soil in the grid box reaches field capacity, i.e. how the runoff finds its way to the rivers and to the sea is not considered. The simulated surface runoff has a realistic spatial distribution in the area of Sweden (showing the eastern and inland minima, the maxima at the west coast and along the western mountain chain). In the southeast of Sweden, even the amount of runoff is not too bad, being 200-250 mm per year in the model. In other parts of the country, the underestimation in point runoff is of the order of 20-40 %. Note that no sub-surface runoff occurs in the model. The 1961-90 estimated (using meteorological observations and hydrological modeling) annual point runoff (Raab and Vedin, 1995) largely mirrors the precipitation distribution in Sweden. There is a general west-east gradient with the largest values at the mountains in the west (500-1500 mm per year) and in the south-western part (300-600 mm per year). The driest parts of the country, with respect to runoff, are the central and southern inland (200-400 mm per year) as well as the southeastern coastal and near-coastal regions (100-300 mm per year).

The underestimation of runoff and its seasonality in RCA can be illustrated by summing up the point results for totals in the five main Baltic Sea drainage basins. These basins are shown in Figure 19.

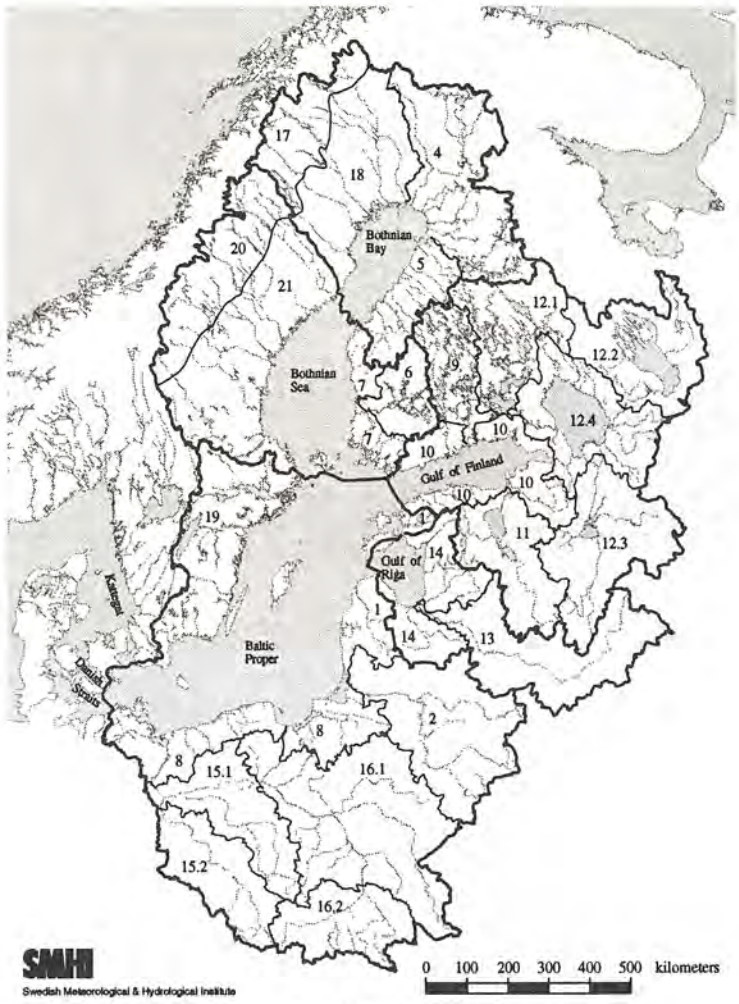

Figure 19. *The five main Baltic Sea drainage basins.*

The RCA results for the Baltic Sea drainage basins and results from the calibrated hydrological model, HBV-Baltic (Graham, 1998) are shown in Figure 20. The hydrological model was run with gridded time series of observed temperature and precipitation (1980-1994), to calculate soil moisture, snow dynamics, evaporation, river runoff and, of course, the point runoff.

RCA underestimates especially the seasonal maxima. The seasonal dynamics are captured for all the basins, though with a somewhat large winter runoff and a somewhat small summer runoff. The annual cycle in runoff in the region reflects the snow climate, but also the seasonal precipitation. These will be discussed later in this report.

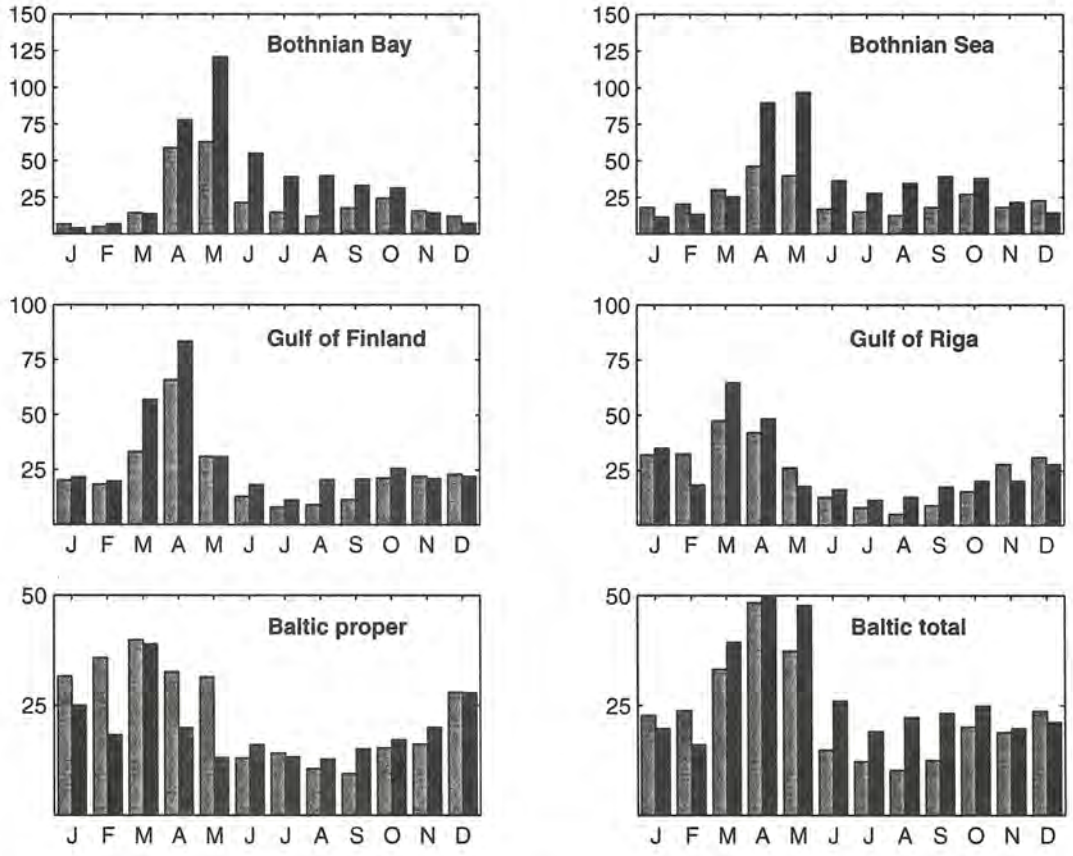

Figure 20. *Modeled point runoff in RCA and from the calibrated hydrological model HBV-Baltic for 1980-1994 (see Graham, 1998). The RCA runoff is drawn in gray and the hydrological model runoff is drawn in black. The vertical axis is for the average point runoff [mm month^{-1}] in each of the five drainage basins. The Baltic Sea total (average point runoff over all of the five basins) is also shown.*

5.4.4 Soil moisture

As a consequence of the simultaneous underestimation of evaporation and runoff, the total moisture balance of the ground (P-E-R) over Sweden and in Northern Europe in general is substantially positive, of the order of 100 mm per year. This does not happen in nature. In the model, the imbalance is able to arise due to the use of the fixed deep-soil ("climatological") moisture field. As the moisture content of the deep-soil layer is

not modified by the soil moisture changes in the layers above, the deep-soil layer can act as an artificial and infinite source or sink of moisture. Thus, soil moisture accounting in the model is not conservative and the water balance is not closed. One may note that the RCA residual runoff (the P-E balance) is better in agreement with the 1961-90 annual runoff conditions in Sweden than the RCA formal runoff (R).

5.4.5 Snow

The RCA simulated 10-year mean snow depths and frequencies in the middle of each calendar month are shown in Figure 21. The period July-September when the Nordic area is snow-free apart from a few mountain grid points is excluded.

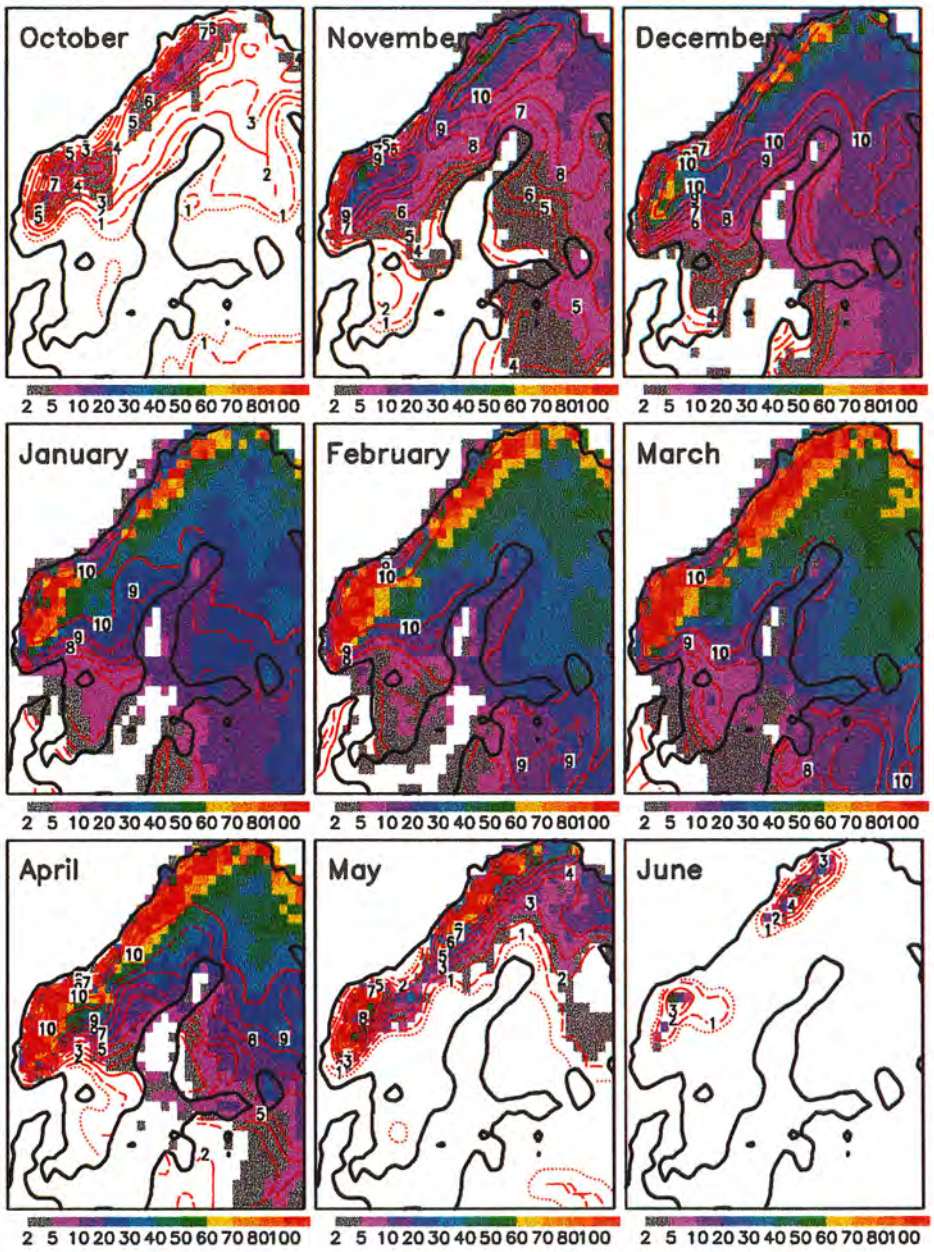

Figure 21. *RCA 10-year mean snow depth on the 15th of each month (Oct-June) color in [cm of snow], derived from the modeled snow water equivalents. The contours specify the number of winters in which the snow water equivalent exceeded 1 mm.*

The snow builds up reasonably in RCA during late fall. By the middle of December, Finland, Norway and the central and northern parts of Sweden are already snow-covered in most winters. The large snow depths in middle and late winter are simulated over the Scandinavian mountains and in eastern and northern Finland (the maximum snow water equivalents [kg m^{-2}] compare also well with observations). However, snow amounts in southern Sweden appear to be somewhat underestimated (this might be explained by the shortness of the simulation). For example, the average snow depth in the RCA simulation in mid-February is below 10 cm throughout this area, whereas the observed mean snow cover in 1961-1990 (Raab and Vedin, 1995) has a local maximum of 30 cm in the southern highlands. In addition, although the retreat of snow during the spring appears in the model pretty much as what has been observed, this may be partly fortuitous because (as discussed later) the simulated spring temperatures are generally below the observed means. Thus, there are some hints that snow would melt somewhat too effectively in the model.

5.4.6 Precipitation

Precipitation is the driving force of surface hydrology. The overall, annually averaged precipitation distribution over the Nordic area is at first glance realistic (see Figure 18). The well-known maximum along the Norwegian coast and over the Scandinavian mountains is well-developed, and it is of the right magnitude (from 1200 mm up to 2000 mm per year). The observed maximum along the Swedish west coast is also reproduced, although its magnitude is smaller in RCA (800-900 mm/year) than in the 1961-90 observations (900-1100 mm/year). The characteristic precipitation minima at the south-eastern coast of Sweden and along the border of Finland and Sweden in the north are also reproduced in RCA. However, the secondary precipitation maximum along the Swedish Bothnian Bay coast is essentially absent from RCA.

To show how the Nordic precipitation climate in RCA differs from that in HadCM2, the mean 10-year annual precipitation from HadCM2 and the difference between the two models are shown in Figure 22 (the RCA absolute values were provided in Figure 18). In addition to the total amount, the partitioning to large-scale and to convective precipitation is shown.

The role of the Scandinavian mountain range in triggering precipitation is evident even in HadCM2, but the maximum is weaker, broader and further from the Norwegian coast than in RCA. Several finer-scale details simulated by RCA are totally lacking from HadCM2 (as expected from its coarse resolution). Compared to HadCM2, RCA features also less convective precipitation (over land) and more large-scale precipitation in the Nordic region. Keeping in mind that the division between large-scale and convective precipitation is strongly model-dependent (and very difficult to analyze from observations as well), some additional remarks are now made on the differences between RCA and HadCM2. The 10-year Nordic seasonal mean (see Figure 18 for the domain) large-scale, convective and total precipitation statistics from RCA and HadCM2 are shown in Figure 23.

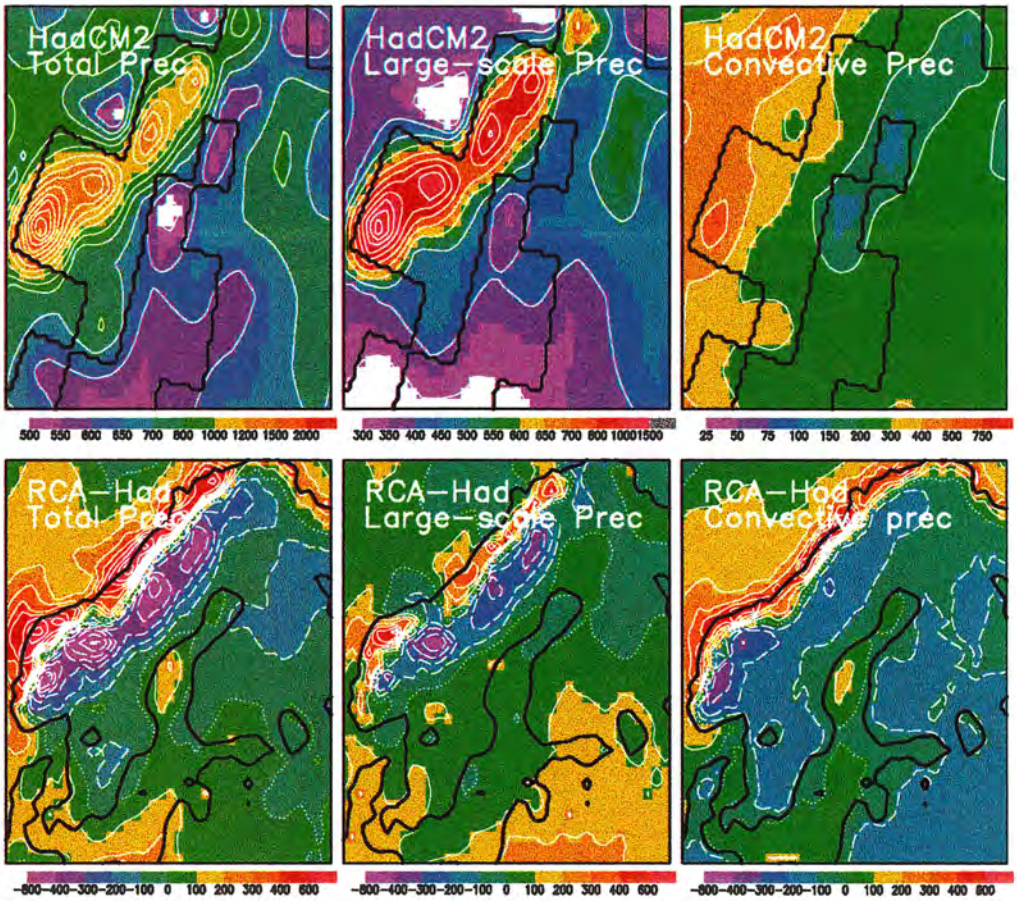

Figure 22. *Top row: Annual mean accumulated precipitation in the HadCM2 10-year control run time slice. The color scale is the same as in Figure 18. In some small areas, the HadCM2 precipitation is below this scale (giving white areas in the total and large-scale precipitation panels). The coastal lines in the top row are drawn at the HadCM2 grid resolution. Bottom row: the RCA-HadCM2 differences in the accumulated precipitation.*

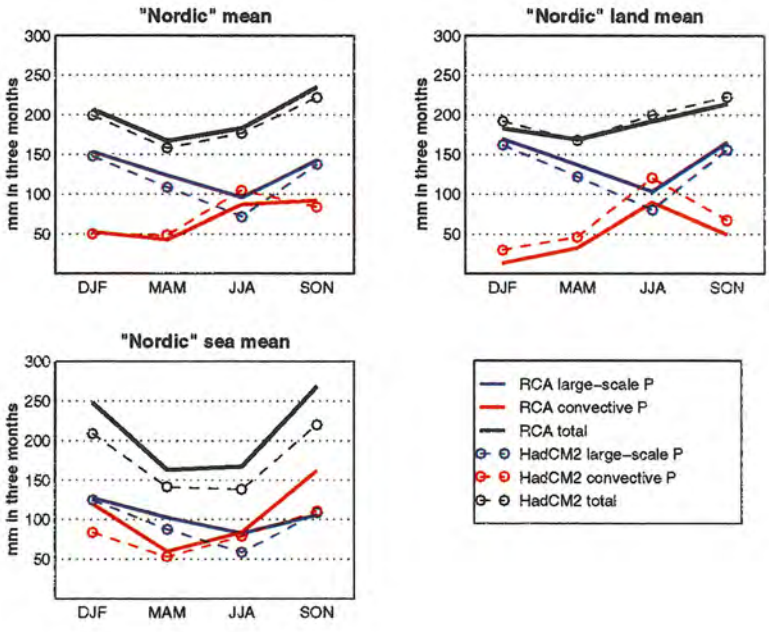

Figure 23. *Mean 10-year seasonal precipitation statistics [mm in three months] in the Nordic area (means over 1521 grid points, of which 945 are "land" and 576 are "sea").*

In this sub-domain, RCA gives some more precipitation in all seasons than HadCM2. At the same time, there is less seasonal variation in the partitioning between large-scale and convective precipitation as the summer minimum in the former and the summer maximum in the latter are attenuated. The most obvious of these domain-averaged differences is that there is more precipitation over sea in RCA than in HadCM2 (c.f. also Table 10). In winter and fall, this difference is present in the convective part and in spring and summer, in the large-scale part of precipitation. Over land, RCA simulates almost one third less convective precipitation than HadCM2 and the absolute difference is largest in summer. The reduction in the convective precipitation over land in RCA is almost compensated by an increase in its large-scale precipitation and the land totals in the two models are rather similar (758 mm in RCA and 783 mm in HadCM2). Over sea the intermodel difference is quite large (847 mm in RCA and 709 mm in HadCM2). For the whole domain, the majority of which is land, the totals are 792 mm in RCA and 756 mm in HadCM2.

5.4.7 Cloudiness

Another important issue in climate modeling is the simulation of clouds. It is closely connected with the hydrological cycle and the transfer of radiation. It is also notoriously sensitive to model parameterizations. A commonly used (although somewhat simplistic) diagnostic of cloud simulation is the total cloudiness. Figure 24 shows the simulated seasonal mean total cloudiness in Northern Europe in both RCA and in HadCM2. The observational estimate for land areas from Hulme et al. (1995) is also shown.

The RCA simulation is in good agreement with the observed climatology in summer: both the general level of cloudiness and the spatial patterns (e.g. the maximum over the Scandinavian mountains) are realistic. The fairly good agreement also extends to fall, although, the orographic maximum appears somewhat too strong (provided that the observational data set is in this respect correct). In winter and spring, however, the modeled cloud cover in the Nordic area is above the observed values. The simulated 10-winter mean cloudiness exceeds 90 % in eastern Finland, whereas observations indicate mean cloudiness of only slightly over 75 %. In addition, the RCA wintertime north-south gradient in Sweden is opposite to that observed, with more cloudiness in the northern than in the southern part of the country in RCA.

RCA is not alone with its overestimate of wintertime and springtime cloudiness. In the HadCM2 simulation, the same feature is evident, although with differences in details (e.g. the very abundant wintertime cloudiness in eastern Finland is not present in HadCM2). Unlike RCA, HadCM2 also generally overestimates the cloud cover in summer and fall. The fact that the two models share some common biases compared with observations might indicate that these biases could stem partly from deficiencies in the large-scale atmospheric circulation. It is also possible that they are explained by problems in the respective cloud parameterizations. Of course, total cloudiness is not a quantity that is very well measured in nature, so it is difficult whether the models are too unrealistic.

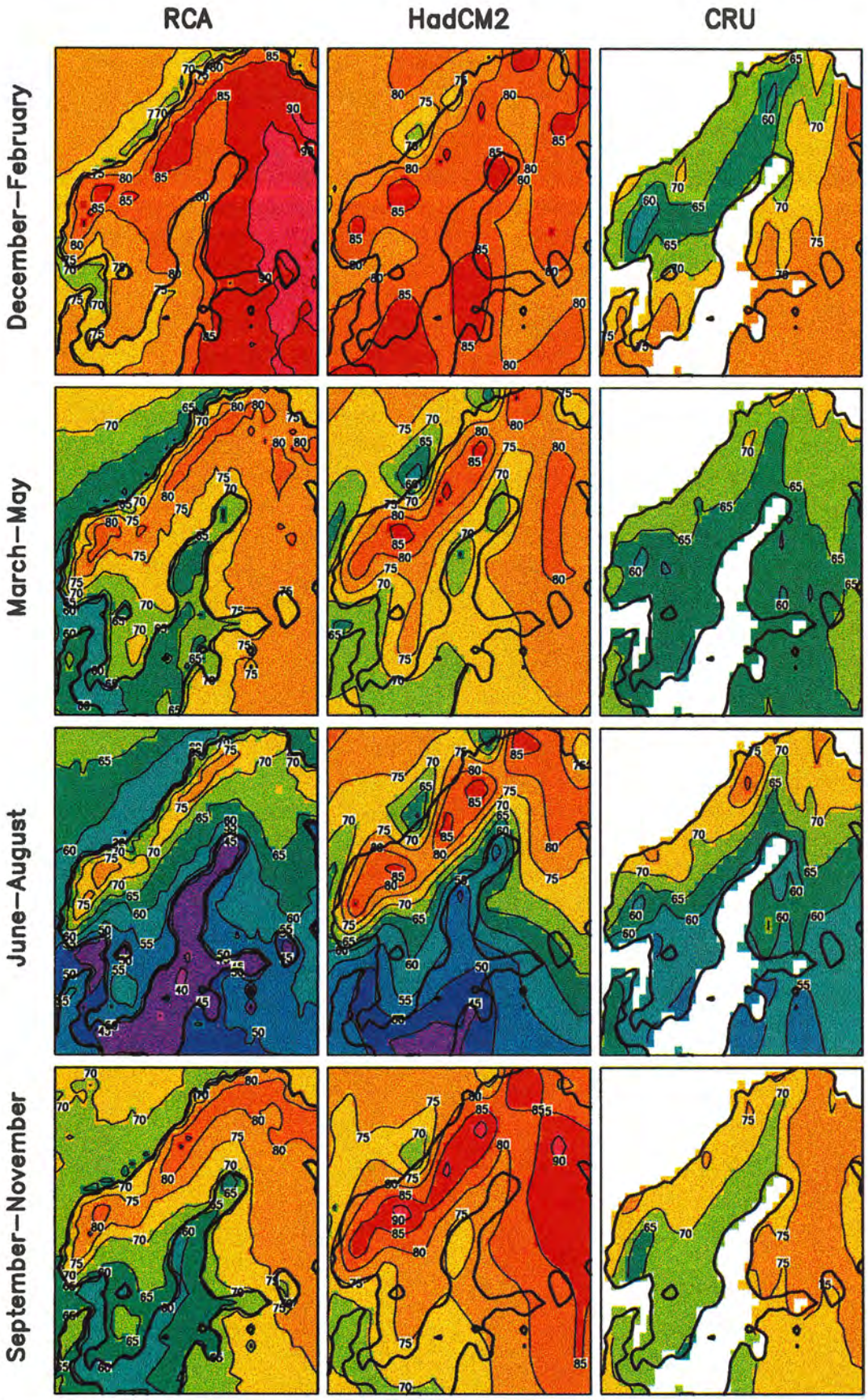

Figure 24. *The 10-year seasonal mean cloud cover [%] in RCA, in HadCM2 and according to the CRU climatology for 1961-1990 (Hulme et al. 1995).*

5.5 Local precipitation and temperature climate at selected stations in Sweden – comparison between RCA and HadCM2 simulations and station observations

Quantitative comparisons of means and qualitative comparisons of spatial distributions of the simulated and observed data give useful insight into the performance of the model. However, when the ability of the model to simulate climate at the smaller scales is examined, a relevant (but tough) test for the model is comparison of the model simulation to station observations. This is the case in particular with quantities like precipitation that show a strong spatial variability. In Figure 25, the 10-year monthly means of precipitation in RCA and HadCM2 are shown at nine Swedish sites, together with the 1961-90 observed precipitation statistics (Alexandersson et al., 1991). The stations are chosen to reflect the significance of topographic features (lee of the mountains, coasts, larger lakes) for the local climate. The values for RCA are from the grid box closest to the station; those for HadCM2 were interpolated to the same RCA grid box.

In general, there is considerable year-to-year variation in the simulated local precipitation in the models (not shown), just as in real life. For a given month and year, the local precipitation can be very different between HadCM2 and RCA. Over the simulated ten-year period, however, RCA gives a largely similar month-to-month precipitation behavior as does HadCM2. In the lee of the mountains the downscaling produces a general reduction in precipitation (see Jokkmokk, Karesuando, Hemavan and Frösön). At Vadstena, where the local climate is affected by the large lake Vättern, the precipitation in RCA is closer to the observed than the precipitation in HadCM2. As was already pointed out, the west coast maximum is underestimated (see Borås) in the model(s). The simulated seasonal cycle is at most stations flatter than the observed one, but this may be partly an artifact in the observational data. Although the magnitude of this bias depends on the rain gauge environment, the measured values of precipitation systematically underestimate the actual precipitation, with considerably larger bias for snowfall than for rain (e.g. Raab and Vedin, 1995). This factor is important even when comparing the simulated and observed annual totals. As estimated in Raab and Vedin (1995), the real Swedish mean annual precipitation in 1961-1990 was 727 mm, or 14 % larger than the directly measured value of 636 mm.

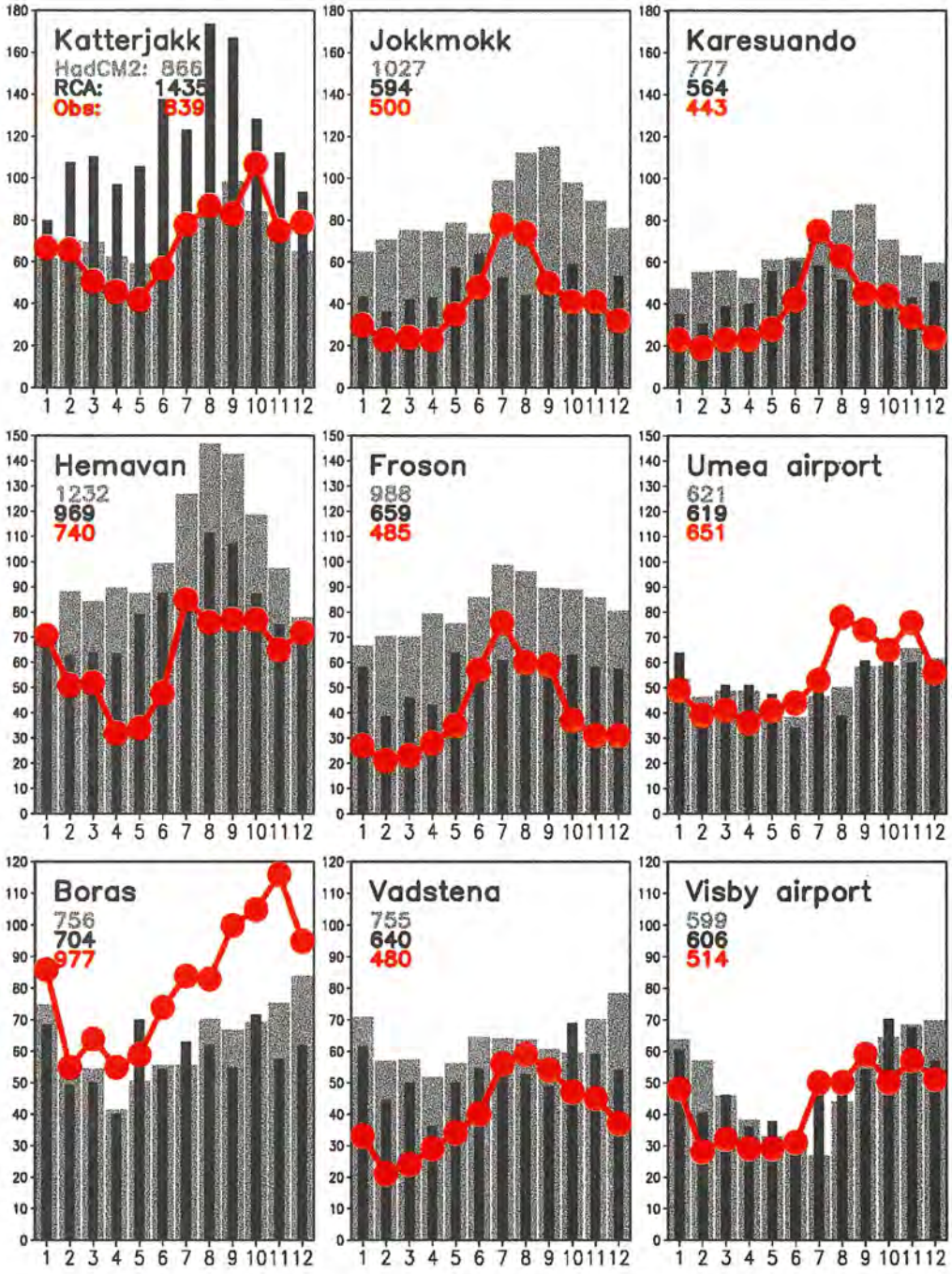

Figure 25. *Precipitation statistics at nine Swedish sites. Katterjåkk (68°N,18°E), Jokkmokk (67°N,20°E), Karesuando (68°N,22°E), Hemavan (66°N,15°E), Frösön (63°N,14°E), Umeå airport (64°N,20°E), Borås (58°N,13°E), Vadstena (58°N,15°E) and Visby airport (58°N,18°E). The gray bars are from HadCM2, the black bars are from RCA and the red lines are the 1961-90 observed means. The numeric values in the sub-panels are the mean annual totals [mm per year] for HadCM2, RCA and observations. The vertical axes have a different scaling in each row.*

In the Katterjåkk area, the spatial gradient in observed precipitation is very sharp. The 1435 mm given by the RCA exceeds the observed amount, but, on the other hand, in the adjoining grid box to the south-east, RCA gives only 657 mm of precipitation. In HadCM2, the precipitation distribution in the immediate surroundings of Katterjåkk is

(in the RCA grid scale) of course flat. The gridded distribution of precipitation at and around Katterjåkk in RCA and HadCM2 is shown in Figure 26.

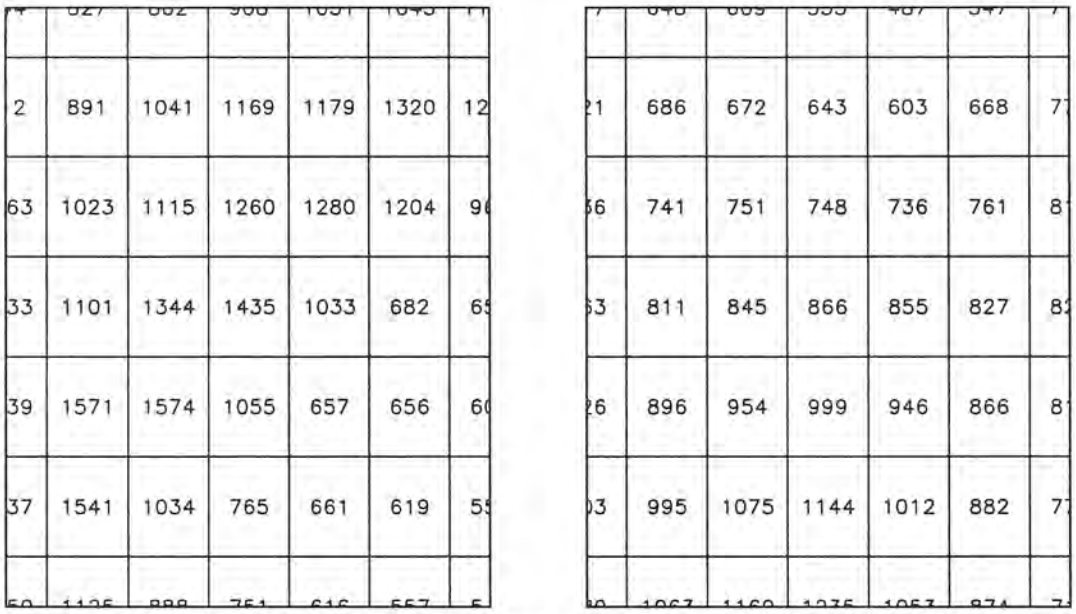

Figure 26. *RCA (left panel) and HadCM2 10-year mean annual precipitation totals in RCA grid boxes at and around Katterjåkk (Katterjåkk is in the middle in both panels). The HadCM2 precipitation was interpolated bilinearly to the RCA grid.*

A sample of two-meter temperature data at nine Swedish sites is shown in Figure 27 (Alexandersson et al., 1991). Except for Vadstena (where temperature has not been measured in 1961-90), the sites are as in the previous figure. In place of Vadstena, the data from Växjö are shown.

The earlier discussed models' summertime cold bias shows up at all sites. In addition, the observed seasonal cycle seems to be attenuated somewhat in the north, where the cold summer biases are accompanied by warm biases in winter. At the southern sites, the warm winter biases in HadCM2 have been reversed to generally smaller cold biases in RCA. The timing of the yearly temperature maximum is also generally better in RCA than in HadCM2. In HadCM2 most stations show a somewhat sluggish seasonal cycle. It is also noted that the impact of orography on the local temperature climate can be quite large, and the method of correction (constant lapse rate) used here is all but exact.

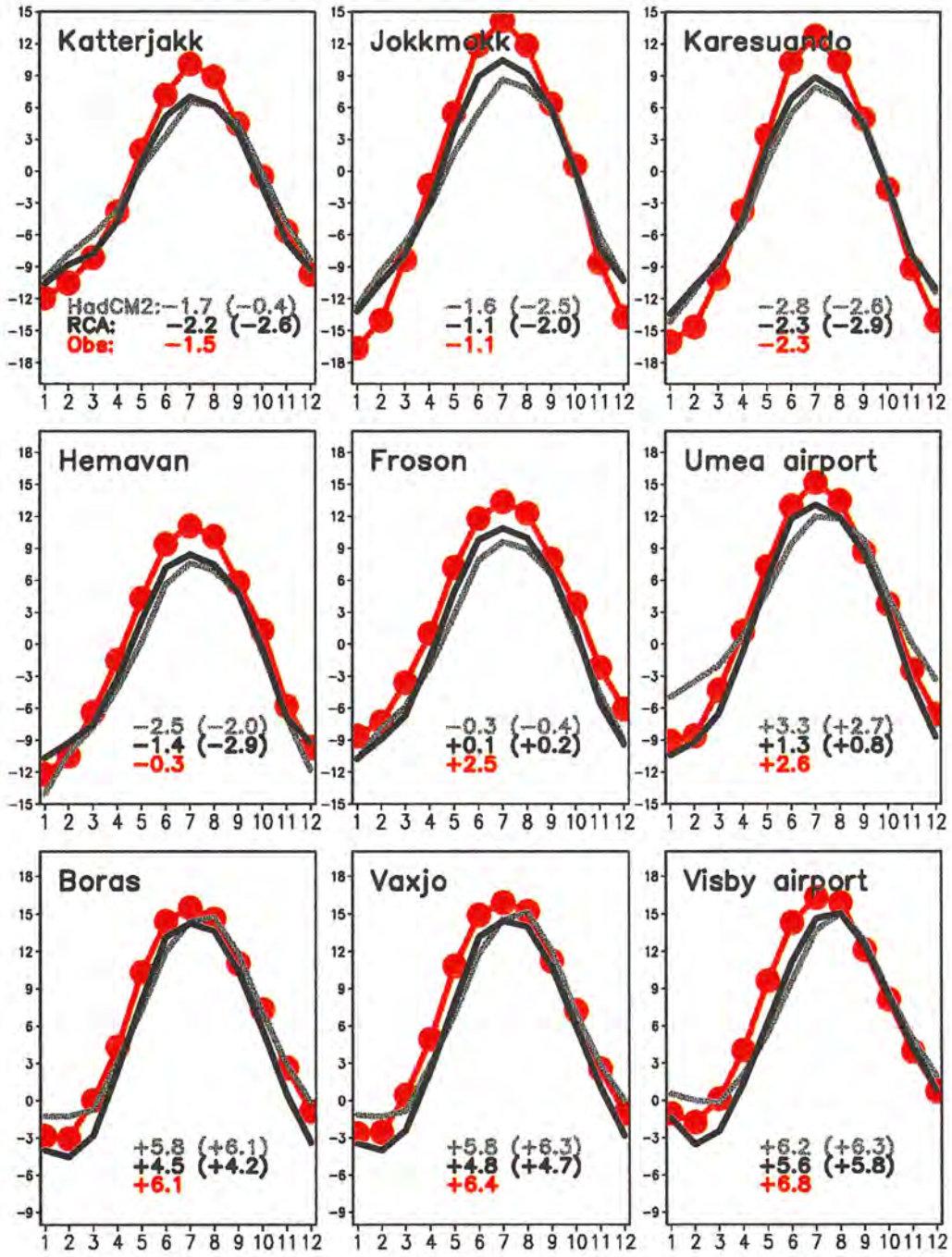

Figure 27. *Two-meter temperature statistics at nine Swedish sites. Katterjåkk (68°N,18°E), Jokkmokk (67°N,20°E), Karesuando (68 °N,22°E), Hemavan (66°N,15°E), Frösön (63°N,14°E), Umeå airport (64°N,20°E), Borås (58°N,13°E), Växjö (57°N,15°E) and Visby airport (58°N,18°E). The gray line is from HadCM2, the black one is from RCA and the red lines are the 1961-90 observed means. The numbers in the sub-panels are the mean annual temperatures for HadCM2, RCA and from the observations. The modeled temperatures are corrected for differences in orography between the models and nature with a lapse rate of 5.5°C km^{-1}. The uncorrected annual mean temperatures from HadCM2 and RCA are given in the parentheses. The vertical axis has a different scaling in each row.*

For a more complete overview of the simulated local temperatures and precipitation, a comparison between the seasonal means of these in RCA and according to the Swedish station observations is made in Figures 28-29. A total of 483 stations are included for the temperature comparison and 1248 for the precipitation one.

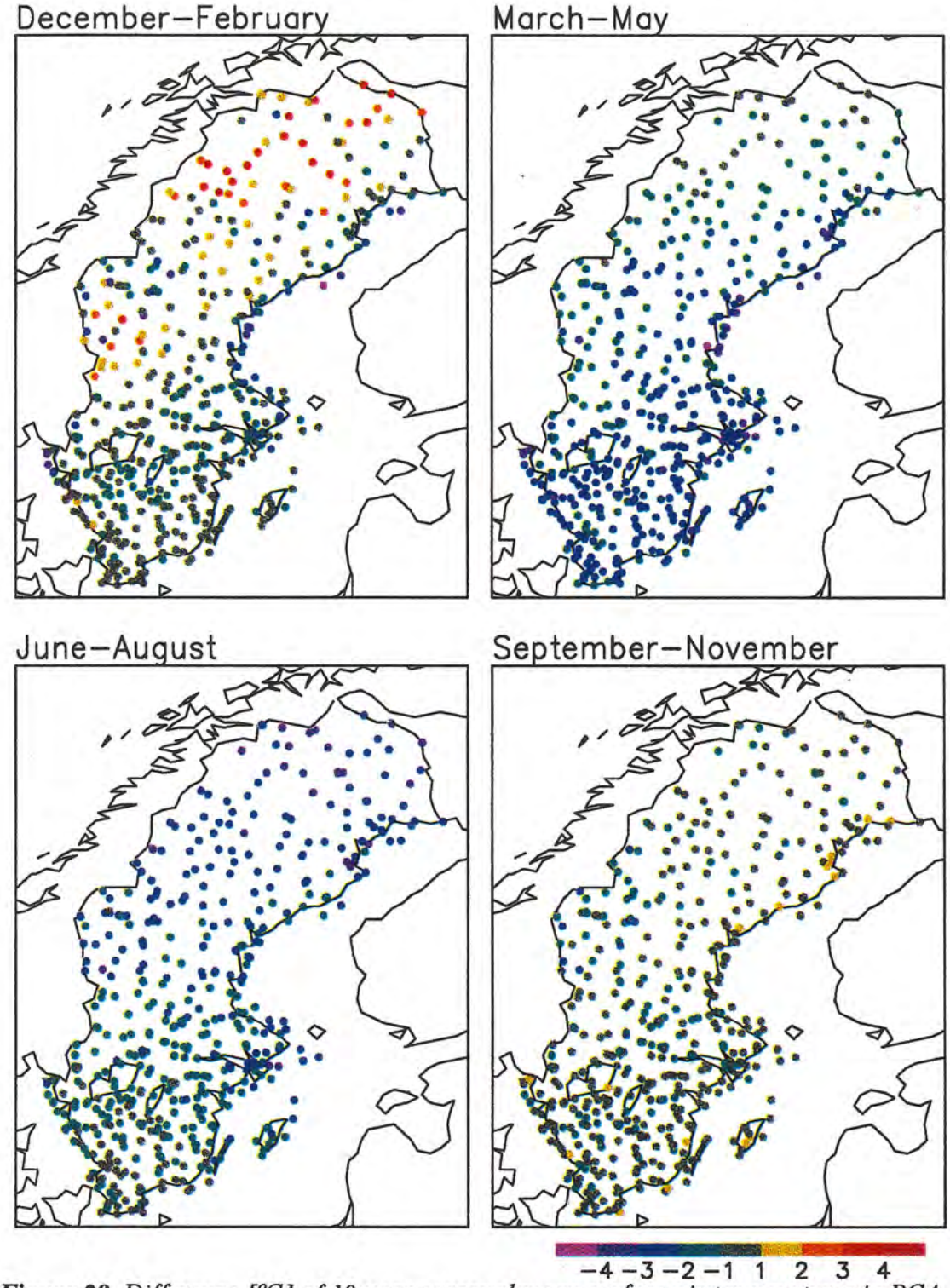

Figure 28. *Difference [°C] of 10-year seasonal mean surface air temperatures in RCA from station observations for 1961-1990. The simulated values are corrected for differences in orography with a lapse rate of 5.5°C km^{-1}.*

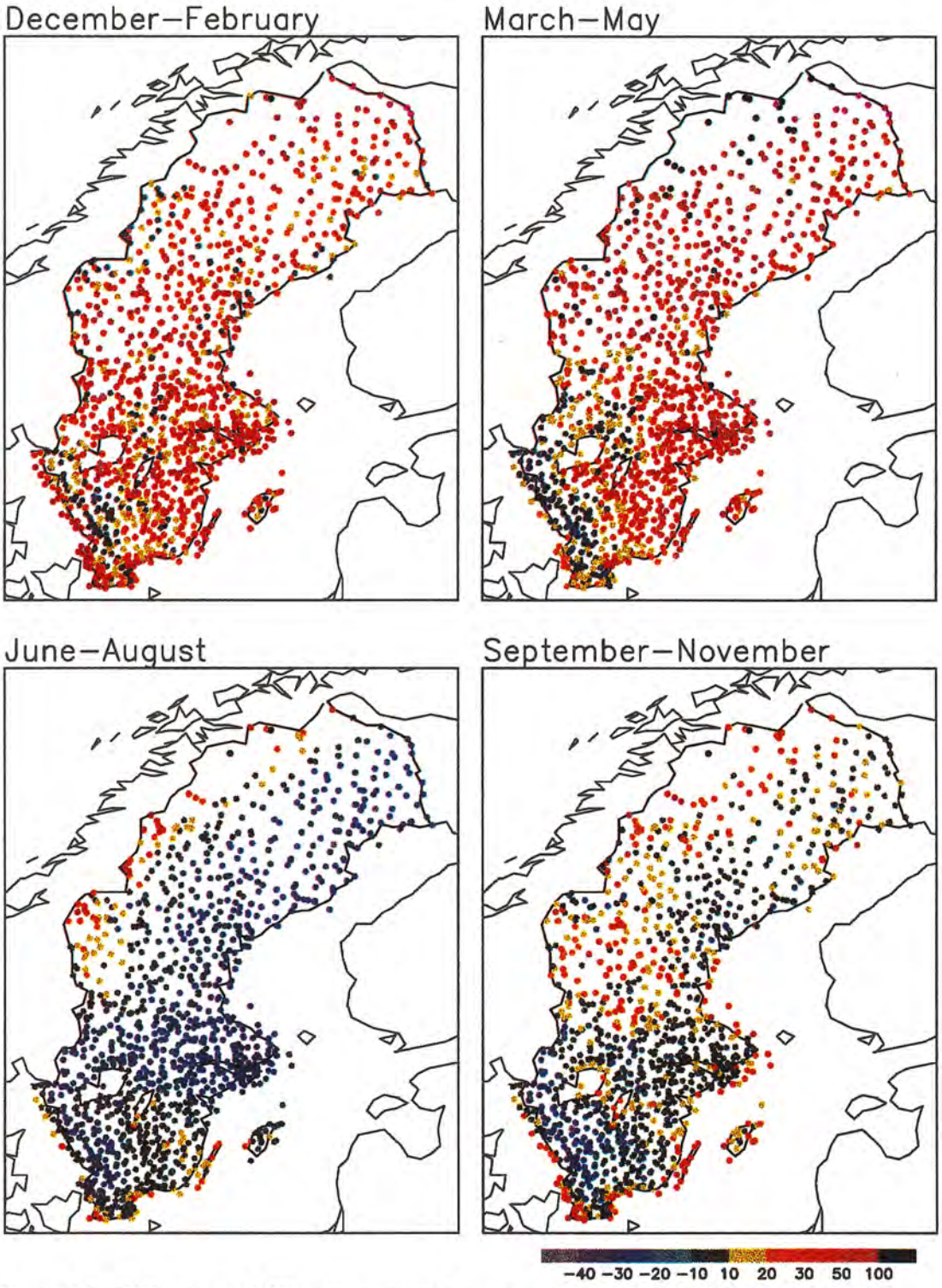

Figure 29. *Difference of 10-year seasonal mean precipitation in RCA from station observations for 1961-1990, given in [%] of the observed values.*

The main features have, of course, become obvious in the preceding discussion. The simulated winter temperatures in southern Sweden are close or slightly below those observed, whereas northern Sweden is dominated by positive biases. In the northern part of the country, there are quite large local variations in the bias. It is noted that the applied correction for orographic differences has little skill in this season as it in particular can not account for surface inversions. In both the spring and summer, the

simulated temperatures are generally below those observed, with largest biases in the south in spring and in the north in summer. In fall, the biases are mostly quite small.

Precipitation in RCA is well above the measured values at most stations in both winter and spring, although this may be significantly affected by the fact that the measurements underestimate the real precipitation. In spring, the ratio between the simulated and the observed precipitation exceeds two at several stations in the western- and northernmost parts of the country. An exception to the rule occurs slightly inland from the west coast, where there is a marked local maximum in the observed precipitation. In this area, the simulated precipitation is close or slightly below that observed in winter and spring, and more clearly below that observed in the other seasons. In summer, the model simulation underestimates the observed precipitation in most of Sweden, excluding only the western mountains and the southeastern part of the country. In fall, the differences between the model and the observations are less systematic and as whole somewhat smaller than in the other seasons.

Finally, the performance of RCA in simulating the local temperature and precipitation climate in Sweden is summarized statistically in Table 11. For comparison, the same statistics are also shown for the driving HadCM2 model.

Table 11. *Statistical comparison between modeled and observed seasonal and annual means of temperature and precipitation at Swedish meteorological stations. Bias gives the mean difference between the two models and observations as averaged over 483 (1248) sites with temperature (precipitation) data, rms the respective root-mean-square difference, and corr the correlation between the modeled and observed station values. Units for bias and rms are in [°C] for temperature and in [mm in 3 or 12 months] for precipitation. The precipitation biases are also given as percentages of the observed mean values. The simulated temperatures have been corrected for orography differences between the models and nature with a lapse rate of 5.5 °C km^{-1}.*

		DJF	MAM	JJA	SON	Ann
T (2 m)	Bias (RCA)	-0.4	-2.2	-1.8	-0.5	-1.2
	Bias (HadCM2)	1.9	-1.5	-2.4	0.4	-0.4
	Rms (RCA)	1.5	2.2	1.9	0.9	1.3
	Rms (HadCM2)	2.5	1.7	2.7	0.9	0.9
	Corr (RCA)	0.94	0.97	0.96	0.98	0.98
	Corr (HadCM2)	0.92	0.95	0.93	0.96	0.97
Precipitation	Bias (RCA)	37 (28%)	37 (32%)	-26 (-13%)	4 (2%)	52 (8%)
	Bias (HadCM2)	69 (52%)	52 (45%)	-7 (-4%)	23 (12%)	137 (22%)
	Rms (RCA)	44	46	45	39	117
	Rms (HadCM2)	78	71	62	70	242
	Corr (RCA)	0.74	0.21	0.44	0.49	0.55
	Corr (HadCM2)	0.29	-0.10	0.39	-0.06	0.10

In terms of temperature, there is no dramatic difference in the performance of the two models. The root-mean-square (rms) difference to observations is smaller in RCA than in HadCM2 in winter and summer, but slightly larger in spring and for the annual mean values. Spring temperatures are on the average more severely underestimated in RCA than in HadCM2, but the summertime cold bias is slightly reduced and the wintertime warm bias replaced with a smaller cold bias. As indicated by the correlation coefficients,

the geographic variations of temperature within Sweden are captured slightly better in RCA than in HadCM2, but they are basically realistic even in the latter.

The advantages of the higher resolution in RCA are more obvious in the simulation of precipitation. Both in terms of the rms differences and the correlation coefficients, RCA provides in all seasons and in the annual mean a better simulation than HadCM2. The correlations with the observed distribution are far from perfect even in the RCA simulation (in particular in spring), but HadCM2 shows in this respect very little skill. The all-station mean precipitation is in all seasons somewhat smaller in RCA than in HadCM2, basically because the maximum of precipitation associated with the Scandinavian mountains is shifted to a more realistic location on the western side of the border to Norway. RCA underestimates the mean precipitation in summer. The positive bias with respect to the observations in winter and spring is more difficult to interpret, given that the observations themselves underestimate the real precipitation. In addition, even more so than in the case of temperature, the large interannual variations in precipitation prevent deriving reliable statistics from just a 10-year sample. Thus, no perfect agreement with the observations would be expected even if the model were perfect.

5.6 Simulation of the variability of surface climate

With the exception of the daily variability of sea level pressure, only the time-mean characteristics of the RCA simulated climate have been discussed so far. However, just like the real nature, a climate model exhibits a large amount of variability on different scales. Some examples of this variability are now discussed.

5.6.1 The warmest and the coldest January and July in RCA

The simulated monthly mean temperatures vary very considerably in RCA from year to year in particular in winter (as in nature). The warmest and coldest January and July mean temperatures during the simulated 10-year period are shown in the upper part of Figure 30. As the coldest and warmest January and July did not occur in the same years in the whole area, these temperature distributions do not represent any individual years.

For Sweden, these 10-year extremes of monthly mean temperatures can be compared with the maps shown in Raab and Vedin (1995, p. 56). Keeping in mind that this kind of a statistic is prone to large random variability, the range from the coldest to the warmest January appears reasonable. In accordance with the 10-year mean biases in the simulated winter climate, though, the difference between southern and northern Sweden in the mean temperature of the coldest January is smaller than in the observations. In July, the overall cold bias in the model has a rather severe effect on the simulated extremes in particular in northern Sweden. Here, even the warmest simulated July is slightly cooler than the observed mean temperatures in 1961-1990, and the coldest July is probably totally outside of the variability of the present climate – the model is typically 3-4°C colder than the 10-year minima in the observations. In southern Sweden, the simulated 10-year maxima and minima are closer to the observations, but still both somewhat below them.

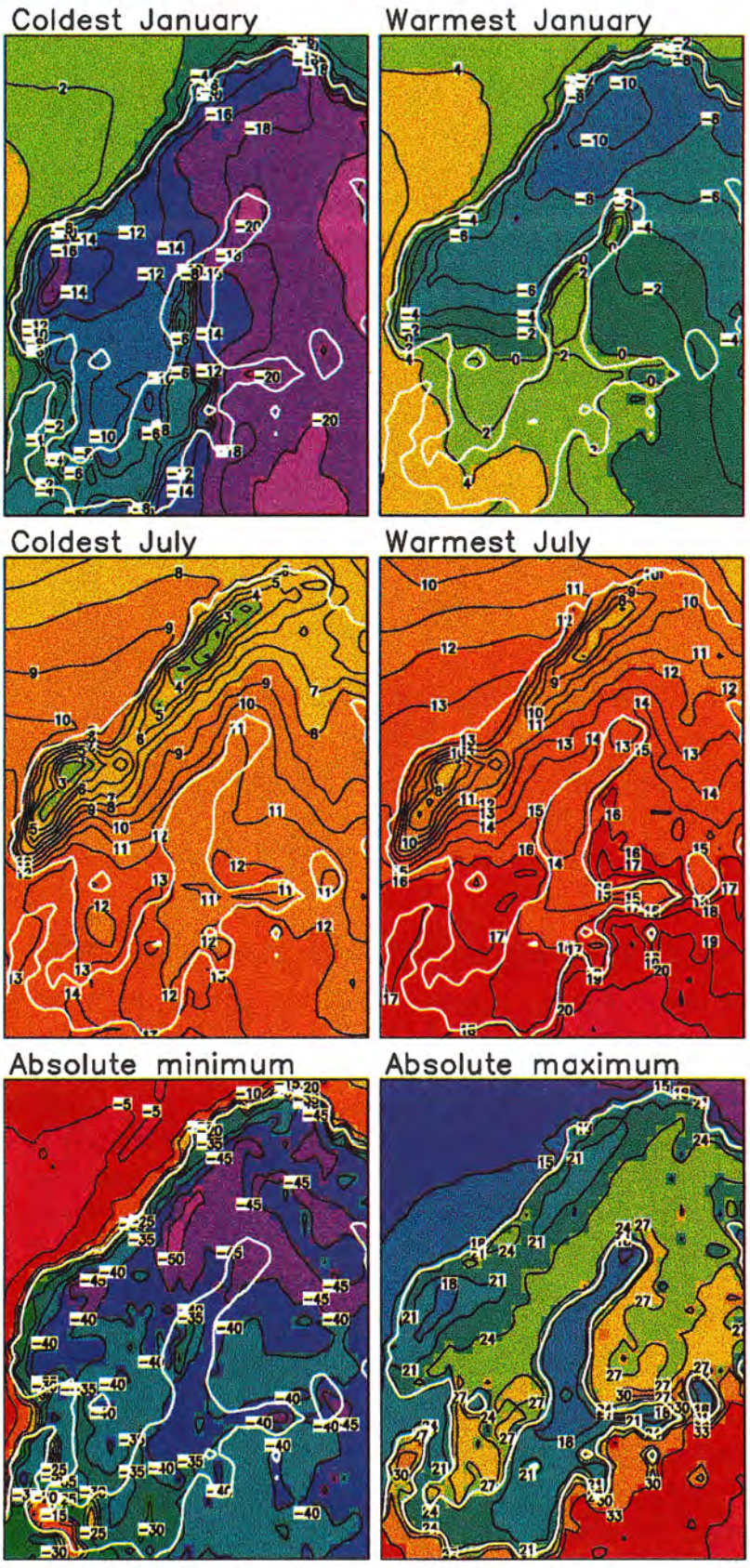

Figure 30. *The warmest and coldest January and July monthly mean temperatures in the RCA 10-year simulation, and the absolutely lowest and highest simulated temperatures during the same period.*

Compared to the driving HadCM2 model (not shown), RCA has a reduced wintertime interannual standard deviation of monthly mean temperatures in northern Sweden (in January, up to 40 % in the extreme north) and an increased one in southern Sweden (by over 50 % in January and February). In summer, the pattern is reversed and the RCA simulated interannual variability is larger than that in HadCM2 in northern Sweden and (in particular in July and in August) smaller than that in HadCM2 in southern Sweden and in the Baltic States. While the short simulation period makes it difficult to draw conclusions from these differences, the decrease in variability in late summer in southern Sweden and the Baltic States in RCA appears to be an improvement over HadCM2, which clearly overestimates the summertime interannual variability in this area (Räisänen 1998, manuscript in preparation).

At the lower part of Figure 30, the absolute lowest and highest RCA-simulated two-meter temperatures during the whole 10-year period are shown. As expected from the overall cold bias in the Nordic area, the absolute summer maxima are modest. Even in southern Sweden, the simulated temperature never rises above +29°C. Somewhat more disturbing is that the simulated absolute 10-year minima are generally very cold. Typical values in southern Finland and Sweden are between -35°C and -40°C. A few locations in southern Swedish Lapland were simulated to experience temperatures down to -51°C. These values are broadly similar to the observed minima for the 85-year period 1911-1995 (Tveito et al., 1998). Moreover, in one grid point in Denmark the simulated 10-year minimum is -40°C, substantially below their national record of -31.2°C – in spite of the fact that the average simulated winter temperatures in Denmark are very close to those observed (not shown). The origin of these very cold minimum temperatures requires further investigation, but apparently, the model creates unrealistically sharp surface inversions in some rare weather situations.

5.6.2 Diurnal variability of temperature in RCA

Another contributor to the relatively low absolute summer maximum temperatures is an underestimate in the simulated diurnal variability (see Figure 31). While the observed average summertime diurnal range in July is in most of Sweden close or slightly over 10°C, that simulated by RCA is 8-9°C in southern and central Sweden and only 6-8°C in northern Sweden. The summertime diurnal range is also somewhat underestimated in Finland, but it is close to that observed in the Baltic States. In winter, the interpretation of this diagnostic (defined as the difference between the daily maximum and minimum temperatures) is more difficult, since at least in northern Scandinavia the main contribution to it comes from synoptic-scale weather variability rather than from genuine day-night differences. Apart from the somewhat underestimated variability in northern Sweden and Finland, the simulated diurnal variability is in January relatively close to the observations.

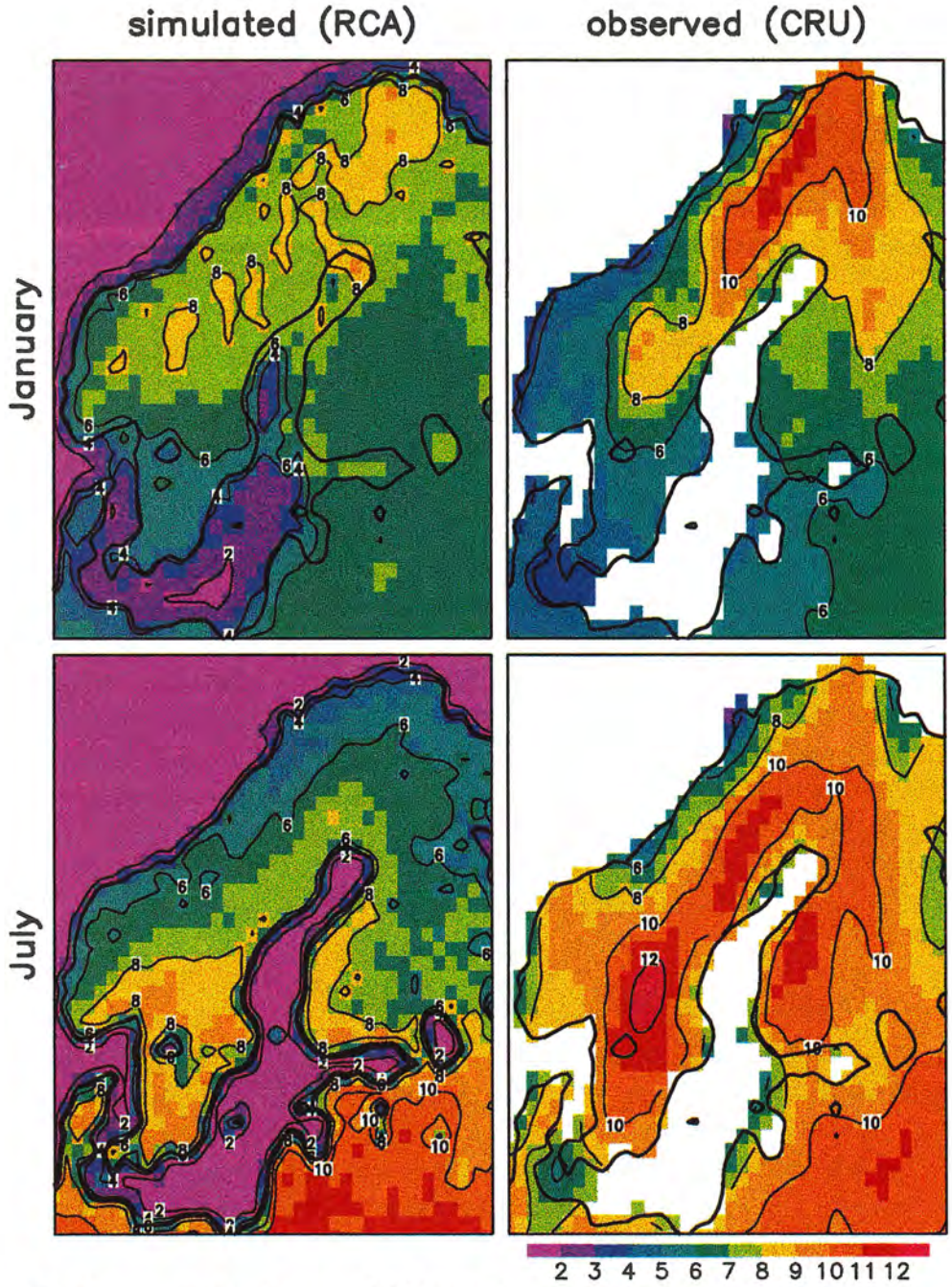

Figure 31. *Average diurnal range (difference between daily maximum and minimum) in surface air temperature [°C] in January and in July in the RCA 10-year control simulation and according to the observational data set of Hulme et al. (1995).*

5.6.3 Daily precipitation classes in RCA

A useful statistics for the variability of precipitation is the mean annual number of days with precipitation above a given threshold. In Figure 32, the results using three thresholds are shown. The thresholds are 0.1, 1.0 and 10 mm precipitation per day. In addition, the simulated mean annual maximum one-day precipitation is given. For the area of Sweden, all four maps can be compared with the observed distributions shown in Raab and Vedin (1995, p. 84).

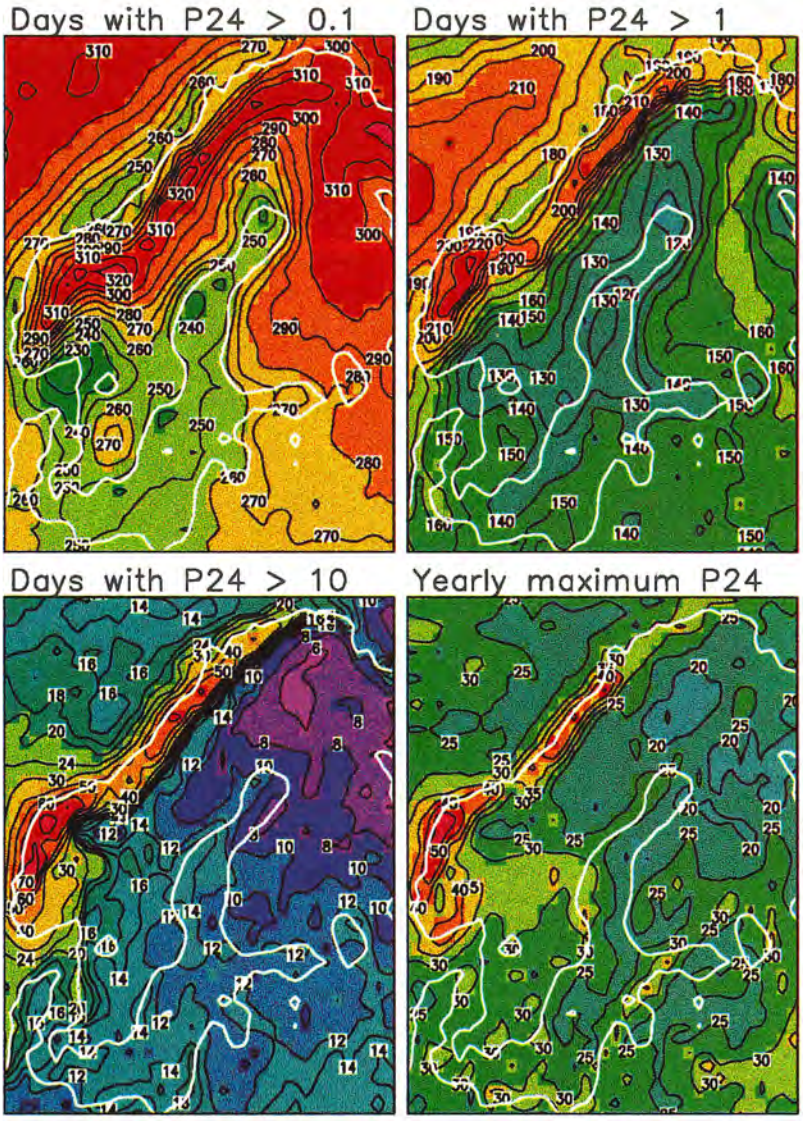

Figure 32. *Statistics of daily precipitation in the RCA 10-year control simulation. The first three panels show the average yearly number of days in which precipitation exceeds 0.1, 1.0, and 10 mm, respectively. In the last panel, the mean annual maximum one-day precipitation is depicted.*

Evidently, the model simulates more (less) days with weak (heavy) precipitation than what observations indicate. The observed maximum in the number of days with at least 0.1 mm of precipitation in south-western Sweden is just slightly over 200, but in the model the maximum over the southern highlands exceeds 270. Over the Scandinavian mountains and in eastern and northern Finland the simulated number is as high as 300-320, and even at the east coast of Sweden where the observational estimate is near 150, it is close to 250. These differences may be in part due to the fact that the model simulates grid box means rather than point precipitation. What the model interprets as weak precipitation in the whole grid box, might therefore be a single stronger shower in part of the grid box in nature. In addition, evaporation and adhesion losses may cause the observations to lose some days with weak precipitation. Nevertheless, a large part of the overestimate is probably real (this might stem from, for example, from an underestimation of the evaporation of falling precipitation, and/or from an overestimation of boundary layer stratus cloudiness in RCA).

The threshold of 1 mm is also exceeded slightly more often in the model than according to the observations, but for days with at least 10 mm of precipitation, the situation is reversed. The simulated (observed) frequencies are roughly 20 (30) days close to the west coast of Sweden, 12-14 (both sides of 15) days in eastern Sweden, and around 8-10 (10-15) days in northern Sweden excluding the western mountains. The difference between the model and the observations is at least qualitatively explained by the fact that the largest local precipitation events in nature frequently take place at scales below the 44-km grid scale of the model. Consequently, the mean annual maxima of one-day precipitation in the model are also slightly below the observed values, in southern Sweden around 30 mm (observed values 30-40 mm) and in northern Sweden 20-25 mm (observed ca. 30 mm). The absolutely largest one-day grid-box total in Sweden during the 10-year simulation was 76 mm.

5.6.4 10-meter wind speed statistics in RCA

The discussion of the model results is finally closed with a look at the wintertime and summertime statistics of wind speed at 10 metre height. These are shown in Figure 33. Compared with the observational estimate of Hulme et al. (1995), the simulated land area mean wind speeds in summer appear broadly realistic. In winter, however, the model does not capture the observed very low mean wind speeds in the inland of northern Sweden. This suggests that the frequency of inversion situations in this area is underestimated (c.f. the positive temperature bias, see Figure 28) and/or that the inversion situations are not calm enough. Over sea areas, the annual cycle is qualitatively correct with stronger winds in winter than in summer, and the overall magnitude of the wind speeds appears reasonable. However, the model clearly underestimates wind speeds over sea ice. This is reflected by the local wind speed minima in the most frequently ice-covered areas. The variability of the simulated winds is characterized in the lower part of Figure 33 with the frequencies of wind speeds exceeding two different threshold speeds (10 and 14 m s^{-1}). As in observations (e.g. Raab and Vedin 1995, pp. 59-63), such strong winds in land areas are very rare in the model as well. However, they actually appear somewhat too rare, since even in winter, many inland areas never experience a wind speed of 10 m s^{-1}. Winds above 14 m s^{-1} occur in Finland, Norway and Sweden almost exclusively at the coast, but they are slightly more common in Denmark and in the western part of the Baltic countries. As expected, strong winds over sea are much more common in winter than in summer. It is worth noting, though, that the model in principle simulates mean winds for the 0.4° gridboxes. This may be acting to smooth out the local extremes. The RCA results for the winter might also be affected by the way that roughness lengths are modeled over snow-covered ground.

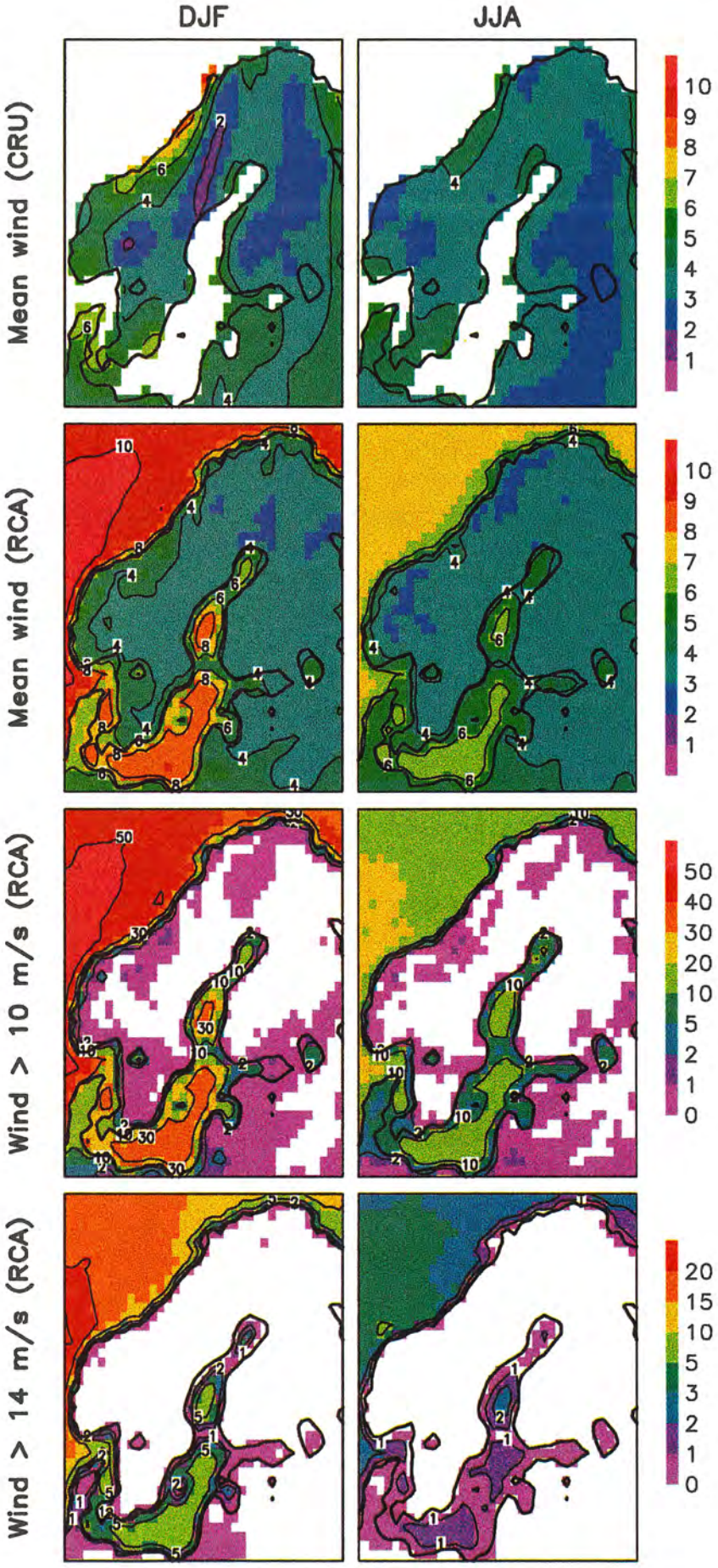

Figure 33. *Wintertime (DJF) and summertime (JJA) statistics of wind speed at 10 m height. The first two rows show the CRU observational estimate (Hulme et al. 1995) and the RCA simulated mean wind speed in [m s^{-1}]. The last two rows give the simulated frequencies in [%] of wind speeds exceeding 10 m s^{-1} and 14 m s^{-1}, respectively.*

6 Continuation of the regional modeling development

6.1 Surface and soil scheme

In the short range, some additional tuning and modifications are considered for the surface-soil-snow scheme (in the treatment of snow and ice, in specifying vegetation effects and in the soil moisture simulation). The physiography database (Bringfelt et al., 1995) might be imported in more detail. In the longer perspective, some incorporation of ISBA ("Interactions Soil Biosphere Atmosphere" scheme) or parts of it (Noilhan and Planton, 1989; Mahfouf and Jacquemin, 1989; Douville et al., 1995; Mahfouf and Noilhan, 1996) is being considered. However, if further testing shows that carefully formulated deep-soil temperature (for soil moisture, some other approach is likely to be necessary) provide a well-behaving driver for the regional model, a modified form (see e.g. Savijärvi (1992) for ideas on numerical techniques) of the present scheme can be used even in the future work.

6.2 Vertical diffusion

The specification of the Charnock constant, as well as the separation of the roughness lengths used for calculating the momentum, sensible heat and moisture fluxes will be considered. More realistic treatment of roughness lengths for snow cover and ice will also have to be considered. The use of Holtslag scheme is to be reexamined and the work in the HIRLAM project on even other formulations will be followed.

6.3 Radiation

The capability of the present scheme to respond to the conditions in the climate scenario time slice needs assessing. The present scheme incorporates explicitly the two main greenhouse agents (water vapor and clouds). The contributions from CO_2 and O_3 are fixed at a constant level. In addition, the driving GCM has worked in, with a more explicit radiation scheme, changes in the forcing to the lateral and sea surface data, which drive the regional model. The need for a more explicit radiation parameterization is therefore not outspoken. Eventually, the parameterization could be tuned for another level of equivalent carbon dioxide.

6.4 Convection and condensation

Apart from doing some tuning of present convection and condensation schemes in RCA, other schemes are considered as alternatives (for example the microphysics parameterization from Rasch and Kristjánsson. 1998; the STRACO coding by Sass, 1997; see also Bister, 1998, for a review of other alternatives).

6.5 Boundary treatment

The interface to the driving GCM is an important component in the regional model. The boundary relaxation has to allow the large-scale driving information to smoothly, as well as possible, enter and leave the regional domain. Generation of gravity waves in the boundary relaxation process should be avoided. The suitability of the present Davies-type relaxation in RCA is to be evaluated with modifications to the width of the boundaries, the relaxation weights and the inclusion of orography-relaxation and the inflow/outflow moisture treatment.

The work on the boundary treatment is coupled with the nesting strategy, some of the noise apparent (in MSLP and in precipitation, for example) inside the current RCA lateral boundaries can be due to the large transition from the driving data to the regional model. The double nesting technique should, for example, reduce such effects. In any case, the integration area(s) for the regional model need to be optimized so that the large-scale information in the driving model applies also in the interior of the regional model, but still leave room for the regional model to develop the desired regional-to-local scale details.

6.6 Coupling to the regional ocean model and/or hydrology

Perhaps the biggest challenge in the Rossby Centre regional model development is the coupling of the atmosphere, ocean and hydrological models. At present, the atmospheric model is given simplified ocean surface conditions and deep-soil moisture content as boundary conditions and the atmospheric model results can provide time series of meteorological forcing for the ocean and hydrological models. The first improvement towards coupling of these climate components is to include a lake thermodynamics package of the type by Ljungemyr et al. (1996) and a regional ocean model (Omstedt and Nyberg, 1996) to the atmospheric modeling.

To couple the atmospheric model, the ocean model and the hydrological component is seen as imperative for the production/provision of high quality regional climate change scenarios. Such a coupling of the atmospheric and land surface models and a regional 3-dimensional ocean model is the next major venture at the regional climate modeling work at the Rossby Centre.

Acknowledgements

The SWECLIM program and the Rossby Centre are funded by MISTRA and by SMHI. The HadCM2 time slice data were provided by the Hadley Centre. The testing and running of RCA has been done on the Cray T3E at the Swedish National Supercomputing Centre (NSC) in Linköping.

References

Alexandersson, H., Karlström, C. And Larsson-McCann, S., 1991. Temperaturen och nederbörden i Sverige 1961-90 referensnormaler (Temperature and precipitation in Sweden 1961-90 reference normals). *SMHI Meteorologi, 81,* 87 pp.

Bister, M., 1998. Cumulus parameterisation in a regional forecast models: A review. *HIRLAM* Technical *Report, No. 35,* 32 pp.

Blackadar, A. K., 1962. The vertical distribution of wind and turbulent exchange in a neutral atmosphere. *J. Geophys. Res., 67,* 3095-3102.

Blondin, C., 1988. Research on land surface parameterization schemes at ECMWF. In: *Parameterization of fluxes over land surface.* Proceedings of a workshop held at ECMWF 24-26 October 1988, 285-330.

Brandt, M., Bergström, S., Gardelin, M. and Lindström, G., 1987. Modellberäkning av extrem effektiv nederbörd. *SMHI, Hydrologi, 14,* Norrköping, 136 pp.

Bringfelt, B., Gustafsson, N., Vilmusenaho, P. and Järvenoja, S., 1995. Updating of the HIRLAM physiography and climate data base. *HIRLAM Technical Report No.19,* 42 pp.

Budyko, M. I., 1956. Heat balance at the earth's surface. Girometeoizdat, Leningrad, 225 pp.

Chen, D. and Hellström, C., 1998. The North Atlantic Oscillation and Swedish temperature variability from 1865 to 1994. Manuscript.

Christensen, J. H., Christensen, O. B., Lopez, P., van Meijgaard, E. and Botzet, M., 1996. The HIRHAM4 Regional Atmospheric Climate Model. *Scientific Report 96-4,* Danish Meteorological Institute, Copenhagen, Denmark, 51 pp.

Christensen, O. B., Christensen, J. H., Machenauer, B. and Botzet, M., 1998. Very-High-Resolution Regional Climate Simulations over Scandinavia. Present Climate. Manuscript.

Clapp R. B. and Hornberger, G. M., 1978. Empirical equations for some hydraulic properties. *Water Resources Res., 14,* 601-604.

Cosby, B. J., Hornberger, G. M., Clapp, R. B. and Ginn, T. R., 1984. A statistical exploration of the relationships of soil moisture characteristics to the physical properties of soils. *Water Resources Res., 20,* 682-690.

Cullen, M. J. P. and Davies, T., 1991. A conservative split explicit integration scheme with fourth order horizontal advection. *Quart. J. Roy. Meteor. Soc., 117,* 993-1002.

Davies, H. C., 1976. A lateral boundary formulation for multi-level prediction models. *Quart. J. Roy. Meteor. Soc., 102,* 405-418.

Deardorff, J. W., 1978. Efficient Prediction of Ground Surface Temperature and Moisture, With Inclusion of a Layer of Vegetation. *J. Geophys. Res., 83,* 1889-1903.

Douville, H., Royer, J.-F. and Mahfouf, J.-F., 1995. A new snow parameterization for the Météo-France climate model. *Clim. Dyn., 12,* 21-35.

ECMWF, 1991. Research Manual 3 ECMWF forecast model physical parameterization. *Meteorological Bulletin M1.6/2.* ECMWF Research Department, ECMWF, Reading, U.K.

Eerola, K., 1996. Experiences with the analysis of sea surface temperature, ice coverage and snow depth. In *HIRLAM 3 Workshop on Soil Processes and Soil/Surface Data Assimilation,* 27-29 November, 1995, 33-36.

Eerola, K., Salmond, D., Gustafsson, N., Garcia-Moya, J.-A., Lönnberg, P. and Järvenoja, S., 1997. A parallel version of the HIRLAM forecast model: Strategy and results. In Hoffmann, G.-R. and Kreitz, N. (eds): *Making its mark. Proceedings of the seventh ECMWF Workshop of the use of Parallel Processors in Meteorology.* Reading, UK, November, 1996,134-143.

FAO-Unesco, 1981. Soil map of the world: Vol 5, Europe. Unesco-Paris, 91 pp.

Geleyn, J. F., 1987. Use of a modified Richardson for parameterizing the effect of shallow convection. *J. Meteor. Soc. Japan, Special NWP Symposium issue,* 141-149.

Giorgi, F., Marinucci, M. R. and Bates, G. T., 1993a. Development of a Second-Generation Regional Climate Model (RegCM2). Part I: Boundary-layer and radiative transfer processes. *Mon. Wea. Rev., 121,* 2794-2813.

Giorgi, F., Marinucci, M. R., Bates, G. T. and De Canio, G., 1993b. Development of a Second-Generation Regional Climate Model (RegCM2). Part II: Convective Processes and Assimilation of Lateral Boundary Conditions. *Mon. Wea. Rev., 121,* 2814-2832.

Graham, L. P. 1998. Modeling runoff to the Baltic Sea. Ambio, in press.

Gray, D. M. and Male, D. H., (eds.) 1981. *Handbook of snow.* Toronto, 776 pp.

Gregory, D. and Allen, S., 1991. The effect of convective scale downdraughts upon NWP and climate simulations. *9th Conf. Numerical Weather Prediction,* Denver, CO, Am. Meteorol. Soc., 122-123.

Gregory, D. and Rowntree, P. R., 1990. A mass flux convection scheme with representation of ensemble characteristics and stability dependent closure. *Mon. Wea. Rev., 118,* 1483-1506.

Gustafsson, N. (ed.), 1993. HIRLAM 2 final report. *HIRLAM Technical Report, 9,* SMHI, Norrköping, Sweden, 126 pp.

Holtslag, A. A. M. and Boville, B. A., 1993. Local versus nonlocal boundary layer diffusion in a global climate model. *J. Climate, 6,* 1825-1842.

Hulme, M., Conway, D., Jones, P. D., Jiang, T., Zhou, X., Barrow, E. M. and Turney, C., 1995. *A 1961-90 Gridded Surface Climatology for Europe.* Available from Climatic Research Unit, Norwich, 51 pp. (plus maps).

Hurrel, J. W. and van Loon, H., 1997. Decadal variations in climate associated with the North Atlantic Oscillation. *Clim. Change, 36,* 301-326.

IPCC (Intergovernmental Panel on Climate Change), 1996. *Climate Change 1995. The science of climate change.* Houghton, J. T., Meira Filho, L. G., Callander, B. A., Harris, N., Kattenberg, A., and Maskell, K. (eds.). Cambridge University Press, 572 pp.

Johansson, Å., Barnston, A., Saha, S. and van den Dool, H., 1998. On the level and origin of seasonal forecast skill in Northern Europe, *J. Atm. Sci., 55,* 103-127.

Johns, T. C., Carnell, R. E., Crossley, J. F., Gregory, J. M., Mitchell, J. F. B., Senior, C. A., Tett, S. F. B. and Wood, R. A., 1997. The second Hadley Centre coupled ocean-atmosphere GCM: model description, spinup and validation. *Clim. Dyn., 13,* 103-134.

Jones, R. G., Murphy, J. M. and Noguer, M., 1995. Simulation of climate change over Europe using a nested regional-climate model. I: Assessment of control climate, including sensitivity to location of lateral boundaries. *Quart. J. Roy. Meteor. Soc., 121,* 1413-1449.

Kuo, H. L., 1965. On the formation and intensification of tropical cyclone through latent heat release by cumulus convection. *J. Atmos. Sci., 22,* 40-63.

Kuo, H. L., 1974. Further studies of the parameterization of the influence of cumulus convection on large-scale flow. *J. Atmos. Sci., 31,* 1232-1240.

Kållberg, P., 1977. Test of a lateral boundary relaxation scheme in a barotropic model. *ECMWF research department internal report no. 3,* 21 pp.

Källén, E. (ed.), 1996. *HIRLAM documentation manual. System 2.5.*

Ljungemyr, P., Gustafsson, N. and Omstedt, A., 1996. Parameterization of lake thermodynamics in a high-resolution weather forecasting model. *Tellus, 48A,* 608-621.

Louis, J. F., 1979. A parametric model of vertical eddy fluxes in the atmosphere. *Bound. Lay. Met., 17,* 187-202.

Louis, J. F., Tiedtke, M. and Geleyn, J. F., 1981. A short history of the PBL parameterization at ECMWF. *Proc. ECMWF Workshop on Boundary-Layer Parameterization,* ECMWF, 59-79.

Machenhauer, B. (ed.), 1977. On dynamics of gravity oscillations in a shallow water model with applications to normal mode initialization. *Beitr. Phys. Atmosph, 50,* 253-271.

Machenhauer, B., 1988. HIRLAM final report. *HIRLAM Technical Report, 5,* DMI, Copenhagen, Denmark, 116 pp.

Mahfouf, J.-F. and Jacquemin, B., 1989. A study of rainfall interception using a land surface parameterization for mesoscale meteorological models. *J. Appl. Meterol., 28,* 1282-1302.

Mahfouf, J.-F. and Noilhan, J., 1996. Inclusion of gravitational drainage in a land surface scheme based on the force-restore method. *J. Appl. Meteorol.,* 35, *987-992.*

Maidment, D. R. (ed.), 1992. *Handbook of Hydrology.* McGraw-Hill, Inc.

Makin, V. and Perov, V., 1997. On the wind speed dependence of momentum, sensible heat and moisture exchange coefficients over sea in the HIRLAM model – a case study. *HIRLAM newsletter, 29,* 26-31.

McCumber, M. and Pielke, R., 1981. Simulation of the effects of surface fluxes of heat and moisture in a mesoscale numerical model. I. Soil layer. *J. Geophys. Res., 86,* 9929-9938.

McDonald, A., 1995. The HIRLAM two time level, three dimensional semi-Lagrangian, semi-implicit, limited area, grid point model of the primitive equations. *HIRLAM Technical Report No. 17,* 25 pp.

McDonald, A., 1996. Further discussion on the influence of the soil scheme on minimum 2m temperatures on calm clear nights. *HIRLAM Newsletter, 23,* 46-51.

Mesinger, F., 1981. Horizontal advection schemes on a staggered grid, an enstrophy and energy conserving model. *Mon. Wea. Rev., 109,* 467-478.

Mitchell, J. F.B ., Johns, T. C., Gregory, J. M. and Tett, S. F. B., 1995. Climate response to increasing levels of greenhouse gases and sulphate aerosols. *Nature, 376,* 501-504.

Mitchell, J. F. B. and Johns, T. C., 1997. On modification of global warming by sulfate aerosols. *J. Clim., 10,* 245-267.

Noilhan, J. and Planton, S., 1989. A simple parameterization of land surface processes for meteorological models. *Mon. Wea. Rev., 117,* 536-549.

Omstedt, A. and Nyberg, L., 1996. Response of Baltic Sea to seasonal, interannual forcing and climate change. *Tellus, 48A,* 644-662.

Perov, V. and Gollvik, S., 1996. A new expression for the eddy viscosity in the Holtslag's scheme of vertical diffusion. HIRLAM Newsletter, 23, 29-32.

Raab, B. and Vedin, H. (eds.), 1995. *Climate, Lakes and Rivers, National Atlas of Sweden.* SNA Publishing, 176 pp.

Rasch, P. J. and Kristjánsson, J. E., 1998. A comparison of the CCM3 model climate using diagnosed and predicted condensate parameterizations. J. Climate, in press.

Rontu, L., 1995. One-dimensional study of a clear nights temperature. *HIRLAM Newsletter, 22,* 35-37.

Räisänen, J., 1994: A comparison of the results of seven GCM experiments in Northern Europe. *Geophysica, 30,* 3-30.

Räisänen, J., 1997. Climate response to increasing CO_2 and anthropogenic sulphate aerosols – Comparison between two models. *Report No. 46,* Department of Meteorology, University of Helsinki, 80 pp.

Sass B. H., Rontu, L. and Räisänen, P., 1994. HIRLAM-2 Radiation Scheme: Documentation and Tests. *HIRLAM Technical Report No. 16,* Norrköping, 43 pp.

Sass, B. H. and Christensen, J. H., 1995. A Simple Framework for Testing the Quality of Atmospheric Limited-Area Models. *Mon. Wea Rev., 123,* 444-459.

Sass, B. H., 1995. Inclusion of cloud liquid water in the vertical diffusion scheme. *HIRLAM Newsletter, 22,* 25-28.

Sass, B. H. and McDonald, A., 1995. A possible contributor to the problem of minimum 2-metre temperatures being too high on calm clear nights. *HIRLAM Newsletter, 22,* 38-43.

Sass, B. H. and Järvenoja, S., 1996. Improvement of the surface temperature prediction in the HIRLAM model. *HIRLAM Newsletter, 23,* 33-45.

Sass, B. H., 1997. Reduction of numerical noise connected to the parameterization of cloud and condensation processes in the HIRLAM model. *HIRLAM Newsletter, 29,* 37-45.

Savijärvi, H., 1990. Fast radiation parameterization schemes for mesoscale and short-range forecast models. *J. Appl. Meteor., 29,* 437-447.

Savijärvi, H., 1992. On surface temperature and moisture prediction in atmospheric models. *Beitr. Phys. Atmosph., 65,* 281-292.

Sigg, R. and Kjellström, 1995. Predicting snowfall with HIRLAM: Call for a better utilization of existing model output. *HIRLAM Newsletter, 22,* 29-34.

Simmons, A. J. and Burridge, D. M., 1981. An energy and angular momentum conserving vertical finite-difference scheme and hybrid vertical coordinates. *Mon. Wea. Rev., 109,* 758-766.

Slingo, A. and Wilderspin, R. C., 1986. Development of a revised longwave radiation scheme for an atmospheric general circulation model. *Quart. J. Roy. Meteor. Soc., 112,* 371-386.

Slingo, A., Wilderspin, R. C. and Smith, R. N. B., 1988. The effect of improved parameterizations on simulations of cloudiness and the Earth's radiation budget in the tropics. *J. Geophys. Res., 94,* 2281-2301.

Slingo, A., 1989. A GCM parameterization for the shortwave radiative properties of water clouds. *J. Atmos. Sci., 46,* 1419-1427.

Smith, R. N. B., 1990. A scheme for predicting layer clouds and their water content in a general circulation model. *Quart. J. Roy. Meteor. Soc., 116,* 435-460.

Sundqvist, H., 1988. Parameterization of condensation and associated clouds in models for weather prediction and general circulation simulation. In: M. E. Schlesinger (ed.), *Physically-based modelling and simulation of climate and climatic change.* Reidel, Dordrecht, 433-461.

Sundqvist, H., Berge, E. and Kristjánsson, J. E., 1989. Condensation and cloud parameterization studies with a mesoscale numerical weather prediction model. *Mon. Wea. Rev., 117,* 1641-1657.

Sundqvist, H., 1993. Inclusion of ice phase of hydrometeors in cloud parameterization for mesoscale and largescale models. *Beitr. Phys. Atmosph., 66,* 137-147.

Tett, S. F. B., Johns, T. C. and Mitchell, J. F. B., 1997. Global and regional variability in a coupled AOGCM. *Clim. Dyn., 13,* 303-323.

Tveito, O. E., Heino, R. and Vedin, H., 1998. Nordic Atlas of Climatic Extremes. Norwegian Meteorological Institute, *Report 15/98 Klima,* 45 pp.

Viterbo, P., 1996. *The representation of surface processes in general circulation models.* European Centre for Medium-Range Weather Forecasts, Reading, UK, January 1996, 201 pp.

Woetmann-Nielsen, N., 1996. On the performance of the first order nonlocal vertical diffusion scheme in HIRLAM2.5. In: *HIRLAM Workshop on Physical Parameterizations,* 14-16 October, 1996, Helsinki, 27-39.

Woetmann-Nielsen, N. and Amstrup, B., 1997. Field verification measures of the impact of nonlocal versus local first order closure turbulent diffusion in HIRLAM 2.5. *HIRLAM Newsletter, 29,* 17-25.

Related www-sources (September, 1998)

HIRLAM

http://www.knmi.nl/hirlam/

NSC

http://www.nsc.liu.se/

SMHI and Rossby Centre

http://www.smhi.se/
http://www.smhi.se/sgn0106/rossby/index.htm

MISTRA

http://www.mistra-research.se/

HADLEY CENTRE

http://www.meto.govt.uk/
http://www.meto.govt.uk/sec5/sec5pg1.html

SMHIs publications

SMHI publishes six report series. Three of these, the R-series, are intended for international readers and are in most cases written in English. For the others the Swedish language is used.

Names of the Series	**Published since**
RMK (Report Meteorology and Climatology)	1974
RH (Report Hydrology)	1990
RO (Report Oceanography)	1986
METEOROLOGI	1985
HYDROLOGI	1985
OCEANOGRAFI	1985

Earlier issues published in serie RMK

1 Thompson, T., Udin, I., and Omstedt, A. (1974)
Sea surface temperatures in waters surrounding Sweden.

2 Bodin, S. (1974)
Development on an unsteady atmospheric boundary layer model.

3 Moen, L. (1975)
A multi-level quasi-geostrophic model for short range weather predictions.

4 Holmström, I. (1976)
Optimization of atmospheric models.

5 Collins, W.G. (1976)
A parameterization model for calculation of vertical fluxes of momentum due to terrain induced gravity waves.

6 Nyberg, A. (1976)
On transport of sulphur over the North Atlantic.

7 Lundqvist, J.-E., and Udin, I. (1977)
Ice accretion on ships with special emphasis on Baltic conditions.

8 Eriksson, B. (1977)
Den dagliga och årliga variationen av temperatur, fuktighet och vindhastighet vid några orter i Sverige.

9 Holmström, I., and Stokes, J. (1978)
Statistical forecasting of sea level changes in the Baltic.

10 Omstedt, A., and Sahlberg, J. (1978)
Some results from a joint Swedish-Finnish sea ice experiment, March, 1977.

11 Haag, T. (1978)
Byggnadsindustrins väderberoende, seminarieuppsats i företagsekonomi, B-nivå.

12 Eriksson, B. (1978)
Vegetationsperioden i Sverige beräknad från temperaturobservationer.

13 Bodin, S. (1979)
En numerisk prognosmodell för det atmosfäriska gränsskiktet, grundad på den turbulenta energiekvationen.

14 Eriksson, B. (1979)
Temperaturfluktuationer under senaste 100 åren.

15 Udin, I., och Mattisson, I. (1979)
Havsis- och snöinformation ur datorbearbetade satellitdata - en modellstudie.

16 Eriksson, B. (1979)
Statistisk analys av nederbördsdata. Del I. Arealnederbörd.

17 Eriksson, B. (1980)
Statistisk analys av nederbördsdata. Del II. Frekvensanalys av månadsnederbörd.

18 Eriksson, B. (1980)
Årsmedelvärden (1931-60) av nederbörd, avdunstning och avrinning.

19 Omstedt, A. (1980)
A sensitivity analysis of steady, free floating ice.

20 Persson, C., och Omstedt, G. (1980)
En modell för beräkning av luftföroreningars spridning och deposition på mesoskala.

21 Jansson, D. (1980)
Studier av temperaturinversioner och vertikal vindskjuvning vid Sundsvall-Härnösands flygplats.

22 Sahlberg, J., and Törnevik, H. (1980)
A study of large scale cooling in the Bay of Bothnia.

23 Ericson, K., and Hårsmar, P.-O. (1980)
Boundary layer measurements at Klockrike. Oct. 1977.

24 Bringfelt, B. (1980)
A comparison of forest evapotranspiration determined by some independent methods.

25 Bodin, S., and Fredriksson, U. (1980)
Uncertainty in wind forecasting for wind power networks.

26 Eriksson, B. (1980)
Graddagsstatistik för Sverige.

27 Eriksson, B.(1981)
Statistisk analys av nederbördsdata. Del III. 200-åriga nederbördsserier.

28 Eriksson, B. (1981)
Den "potentiella" evapotranspirationen i Sverige.

29 Pershagen, H. (1981)
Maximisnödjup i Sverige (perioden 1905-70).

30 Lönnqvist, O. (1981)
Nederbördsstatistik med praktiska tillämpningar.
(Precipitation statistics with practical applications.)

31 Melgarejo, J.W. (1981)
Similarity theory and resistance laws for the atmospheric boundary layer.

32 Liljas, E. (1981)
Analys av moln och nederbörd genom automatisk klassning av AVHRR-data.

33 Ericson, K. (1982)
Atmospheric boundary layer field experiment in Sweden 1980, GOTEX II, part I.

34 Schoeffler, P. (1982)
Dissipation, dispersion and stability of numerical schemes for advection and diffusion.

35 Undén, P. (1982)
The Swedish Limited Area Model. Part A. Formulation.

36 Bringfelt, B. (1982)
A forest evapotranspiration model using synoptic data.

37 Omstedt, G. (1982)
Spridning av luftförorening från skorsten i konvektiva gränsskikt.

38 Törnevik, H. (1982)
An aerobiological model for operational forecasts of pollen concentration in the air.

39 Eriksson, B. (1982)
Data rörande Sveriges temperaturklimat.

40 Omstedt, G. (1984)
An operational air pollution model using routine meteorological data.

41 Persson, C., and Funkquist, L. (1984)
Local scale plume model for nitrogen oxides. Model description.

42 Gollvik, S. (1984)
Estimation of orographic precipitation by dynamical interpretation of synoptic model data.

43 Lönnqvist, O. (1984)
Congression - A fast regression technique with a great number of functions of all predictors.

44 Laurin, S. (1984)
Population exposure to SO and NO_x from different sources in Stockholm.

45 Svensson, J. (1985)
Remote sensing of atmospheric temperature profiles by TIROS Operational Vertical Sounder.

46 Eriksson, B. (1986)
Nederbörds- och humiditetsklimat i Sverige under vegetationsperioden.

47 Taesler, R. (1986)
Köldperioden av olika längd och förekomst.

48 Wu Zengmao (1986)
Numerical study of lake-land breeze over Lake Vättern, Sweden.

49 Wu Zengmao (1986)
Numerical analysis of initialization procedure in a two-dimensional lake breeze model.

50 Persson, C. (1986)
Local scale plume model for nitrogen oxides. Verification.

51 Melgarejo, J.W. (1986)
An analytical model of the boundary layer above sloping terrain with an application to observations in Antarctica.

52 Bringfelt, B. (1986)
Test of a forest evapotranspiration model.

53 Josefsson, W. (1986)
Solar ultraviolet radiation in Sweden.

54 Dahlström, B. (1986)
Determination of areal precipitation for the Baltic Sea.

55 Persson, C. (SMHI), Rodhe, H. (MISU), De Geer, L.-E. (FOA) (1986)
The Chernobyl accident - A meteorological analysis of how radionucleides reached Sweden.

56 Persson, C., Robertson, L. (SMHI), Grennfelt, P., Kindbom, K., Lövblad, G., och Svanberg, P.-A. (IVL) (1987)
Luftföroreningsepisoden över södra Sverige 2 - 4 februari 1987.

57 Omstedt, G. (1988)
An operational air pollution model.

58 Alexandersson, H., Eriksson, B. (1989)
Climate fluctuations in Sweden 1860 - 1987.

59 Eriksson, B. (1989)
Snödjupsförhållanden i Sverige - Säsongerna 1950/51 - 1979/80.

60 Omstedt, G., Szegö, J. (1990)
Människors exponering för luftföroreningar.

61 Mueller, L., Robertson, L., Andersson, E., Gustafsson, N. (1990)
Meso-γ scale objective analysis of near surface temperature, humidity and wind, and its application in air pollution modelling.

62 Andersson, T., Mattisson, I. (1991)
A field test of thermometer screens.

63 Alexandersson, H., Gollvik, S., Meuller, L. (1991)
An energy balance model for prediction of surface temperatures.

64 Alexandersson, H., Dahlström, B. (1992)
Future climate in the Nordic region - survey and synthesis for the next century.

65 Persson, C., Langner, J., Robertson, L. (1994)
Regional spridningsmodell för Göteborgs och Bohus, Hallands och Älvsborgs län. (A mesoscale air pollution dispersion model for the Swedish west-coast region. In Swedish with captions also in English.)

66 Karlsson, K.-G. (1994)
Satellite-estimated cloudiness from NOAA AVHRR data in the Nordic area during 1993.

67 Karlsson, K-G. (1996)
Cloud classifications with the SCANDIA model.

68 Persson, C., Ullerstig, A. (1996)
Model calculations of dispersion of lindane over Europe. Pilot study with comparisons to measurements around the Baltic Sea and the Kattegat.

69 Langner, J., Persson, C., Robertson, L., and Ullerstig, A. (1996)
Air pollution Assessment Study Using the MATCH Modelling System. Application to sulfur and nitrogen compounds over Sweden 1994.

70 Robertson, L., Langner, J., Engardt, M. (1996)
MATCH - Meso-scale Atmosperic Transport and Chemistry modelling system.

71 Josefsson, W. (1996)
Five years of solar UV-radiation monitoring in Sweden.

72 Persson, C., Ullerstig, A., Robertson, L., Kindbom, K., Sjöberg, K. (1996)
The Swedish Precipitation Chemistry Network. Studies in network design using the MATCH modelling system and statistical methods.

73 Robertson, L. (1996)
Modelling of anthropogenic sulfur deposition to the African and South American continents.

74 Josefsson, W. (1996)
Solar UV-radiation monitoring 1996.

75 Häggmark, L., Ivarsson, K.-I. (SMHI), Olofsson, P.-O. (Militära vädertjänsten). (1997)
MESAN - Mesoskalig analys.

76 Bringfelt, B, Backström, H, Kindell, S, Omstedt, G, Persson, C, Ullerstig, A. (1997)
Calculations of PM-10 concentrations in Swedish cities- Modelling of inhalable particles

77 Gollvik, S. (1997)
The Teleflood project, estimation of precipitation over drainage basins.

78 Persson, C., Ullerstig, A. (1997)
Regional luftmiljöanalys för Västmanlands län baserad på MATCH modell-beräkningar och mätdata - Analys av 1994 års data

79 Josefsson, W., Karlsson, J.-E. (1997)
Measurements of total ozone 1994-1996.

80 Rummukainen, M. (1997)
Methods for statistical downscaling of GCM simulations.

81 Persson, T. (1997)
Solar irradiance modelling using satellite retrieved cloudiness - A pilot study

82 Langner, J., Bergström, R. (SMHI) and Pleijel, K. (IVL) (1998)
European scale modelling of sulfur, oxidized nitrogen and photochemical oxidants. Model development and evaluation for the 1994 growing season.

SMHI
Swedish Meteorological and Hydrological Institute
SE 601 76 Norrköping, Sweden.
Tel +46 11-495 80 00. Fax +46 11-495 80 01

ISSN 0347-2116